UiT
NORGES
ARKTISKE
UNIVERSITET

FACULTY OF SCIENCE AND TECHNOLOGY

Department of Geology

Time-lapse seismic analysis of focused fluid flow on the Vestnesa Ridge

—

Lena Myreng Mathisen

EOM-3901 Master`s Thesis in Energy, Climate and Environment

June 2016

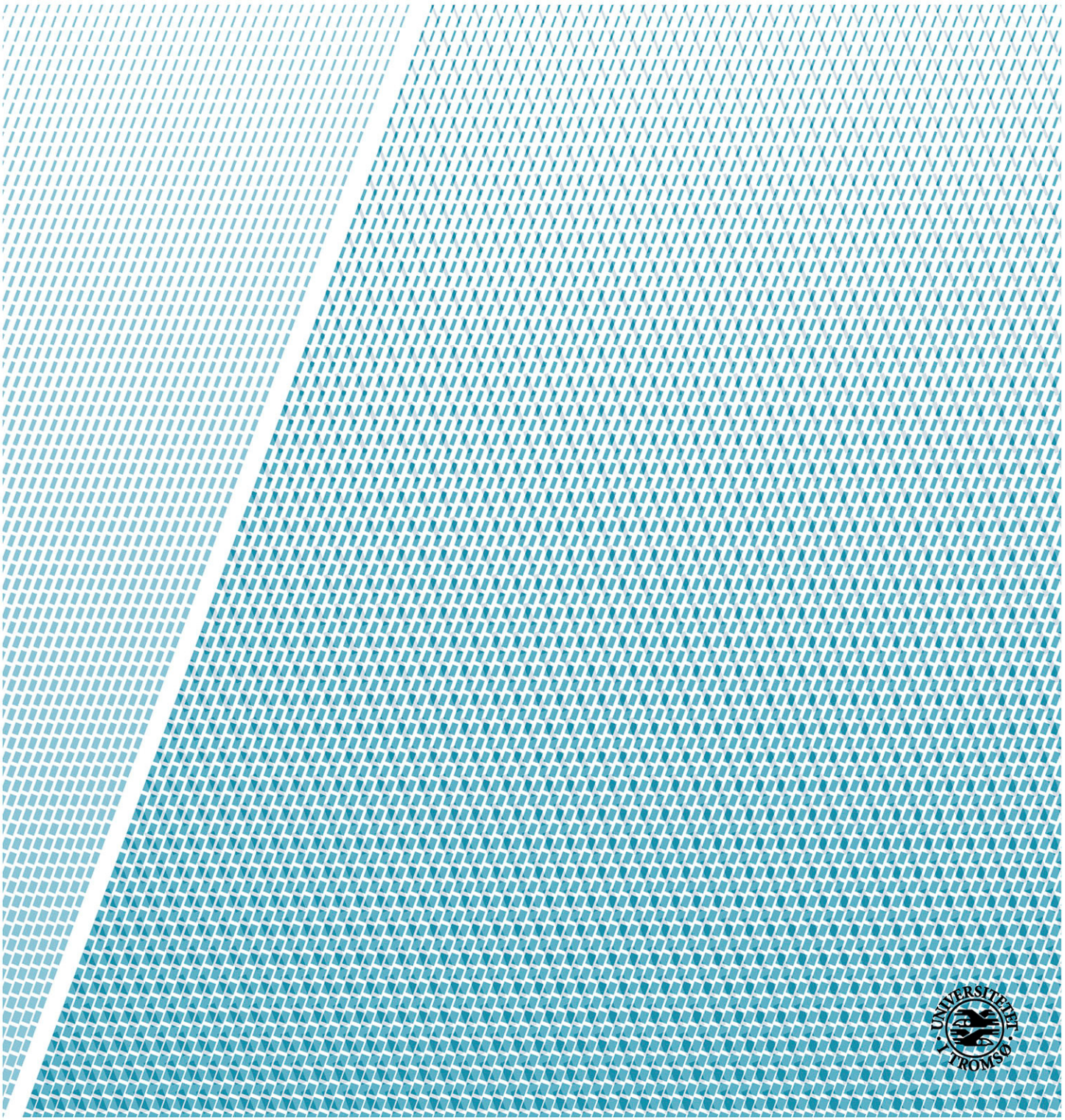

UiT / THE ARCTIC UNIVERSITY OF NORWAY

FACULTY OF SCIENCE AND TECHNOLOGY

Department of Geology

Time-lapse seismic analysis of focused fluid flow on the Vestnesa Ridge

—

Lena Myreng Mathisen

EOM-3901 Master`s Thesis in Energy, Climate and Environment

June 2016

Abstract

The Vestnesa Ridge is a large sediment drift at water depths of 1200-1300 meter and is the northernmost known gas hydrate province that exists along the Arctic continental margin. Several pockmarks connected to vertical fluid flow features are present at the crest of the Vestnesa Ridge. The fluid flow pierce through the gas hydrate stability zone and interrupt the bottom simulating reflection (BSR) originating from the transition zone between stable gas hydrates and free gas. Gas seeps into the water column from several pockmarks demonstrating that the fluid flow system is very active. The abundance of fluid-flow structures and the activity of this system make this an excellent area to study the genesis and mechanisms of focused fluid flow and their related geological processes. A unique approach to gain new knowledge about fluid flow systems in the subsurface is by use of 4D time-lapse seismic data that may help to better understand how these systems develop over relatively short periods of time. The feasibility of high-resolution 3D seismic data with a broad frequency bandwidth of up to 350 Hz for time-lapse studies has not yet been established. High resolution P-Cable 3D seismic data has been acquired over the eastern segment of the ridge in 2012 and repeated in 2013 and 2015. These three seismic surveys have been 4D processed side-by-side in order to highlight subsurface fluid-induced changes. In this thesis, a 4D processing workflow is developed in order to match the seismic data from the three surveys. The 4D processing steps included re-binning of geometry, time and phase matching, shaping filter, shallow statics correction and time-variant shifts. Several 4D attributes are used to quantify the repeatability of the 4D seismic data, the two main attributes being normalized root mean square (NRMS) and predictability (PRED). The NRMS value, for both of the repeats (2015-2012 and 2013-2012), improved significantly during the full processing workflow, while the PRED only changed minimal. PRED is more sensitive to noise and distortion than to time-shift, so the reason for the minimal change here is believed to be due to residual noise in the 4D data. The poorest NRMS values of up to 1.5 are observed over the areas of the gas chimneys, while outside of these structures the NRMS measures lower than 0.4 showing very good repeatability.

The overall NRMS values obtained after 4D processing were not as low as anticipated. Several geological and non-geological factors contribute to this. The Vestnesa Ridge with its fluid flow structures presents a challenging and complex setting for the 4D processing in regards to achieving a reliable and confident 4D match and interpretation. The high-resolution 3D seismic data allows the mapping of small structures in the sub surfaces, but it is also very sensitive to

noise and other non-geological factors like weather or acquisition effects. Nonetheless, the 4D seismic interpretation shows a clear brightening of amplitudes in the 4D data from 2012 to 2013 and from 2013 to 2015. The most evident brightening occurs in the zones beneath the BSR and may be interpreted as a consequence of increased gas accumulation beneath the BSR. Also chimney conduits show 4D changes with the larger changes associated with actively seeping chimneys. Gas migration pathways can be clearly imaged on the data and show a complex path both vertically and laterally and likely self-enhanced by hydraulic fracturing. However, the 4D interpretation is less confident because chimneys represent very inhomogeneous structures where seismic energy rapidly attenuates or is scattered away, which manifests itself in poorer repeatability measures. The time-span of 3 years, from 2012 to 2015, might prove to be too short to detect any major structural changes in the architecture of the chimney conduits. And it might also be too short to recognize and document any substantial fluid changes along the chimney conduits. Additional repeat surveys might help to further shed lights on the mechanisms of gas migration along focused fluid flow structures.

Acknowledgement

Da er 5 år på skolebenken over og tiden har gått så alt for fort. Etter et friår i Australia og et godt avbrekk fra skole var det tøft å starte på han igjen, men nå er jeg ferdig utdannet og det har gått over all forventning!

Jeg vil takke alle i klassen som har bidratt til et flott klassemiljø og spesielt nøye vil jeg takke «squaden» min, eller firkløveren som vi liker å kalle oss, Lisa Myreng Mathisen, Nils Andreas Løvås Karlsen og sist men ikke minst John Sverre Løvaas. Uten et fantastisk bra samarbeid og motivasjon fra dere hadde jeg aldri kommet meg gjennom dette på en så fin måte som jeg har.

Jeg vil også gi en stor takk til Stefan Bünz, som til tross for å være en veldig opptatt mann, har hjulpet meg masse med å få til en veldig interessant og spennende masteroppgave. Og en stor takk til mamma og pappa som har hjulpet til for at jeg skulle få en bra studenttilværelse her i Tromsø.

Jeg har lært sykt mye og ser nå framover mot nye eventyr!

Lena Myreng Mathisen

Juni 2016

Table of Contents

1 Introduction and fundamental theory

1.1 Objective

The Vestnesa Ridge is a large sediment drift located on the western Svalbard continental margin. Several pockmarks occur along the crest of the ridge in water depths of approximately 1200 to 1300 m (Vogt et al., 1994; Bunz et al., 2012). Active seepage of natural gas was first discovered in 2008 from one of the pockmarks on the eastern segment of the Vestnesa Ridge (Hustoft et al., 2009). Later, several additional gas plumes have been discovered on hydro-acoustic data (Bunz et al., 2012; Smith et al., 2014). Pockmarks are connected to vertical fluid-flow features, so-called chimneys. High-resolution P-Cable 3D seismic data provides significantly improved details of internal chimney structures (Bunz et al., 2012; Plaza-Faverola et al., 2015). Petersen et al. (2010) and Bünz et al. (2012) documented the variable nature of these chimney structures, many of which are characterized by a disturbance of strata and generally weak seismic amplitudes. However, numerous amplitude anomalies exist within the upper part of the chimneys indicating large impedance contrasts possibly due to the presence of free gas, gas hydrates and/or carbonate accretions formed at a paleo seafloor.

Fluid flow in this region is mostly topographically controlled as leakage occurs only at the crest of the slope (Bunz et al., 2012). Plaza-Faverola et al. (2015) showed evidence for a link between extensional faults and chimney distribution along the ridge, suggesting that seepage periodicity since the last 2.7 Ma has been modulated to some extent by the tectonic stress field. In addition, several other authors have tried to identify the duration and periodicity of seepage since the last glacial maximum using foraminifera and chemosynthetic proxies from sedimentary cores (Panieri et al., 2014; Consolaro et al., 2015; Ambrose et al., 2015). However, the mechanisms, duration and periodicity of leakage through chimneys are still poorly understood.

One way to better understand amplitude anomalies within the chimney structures could be to employ time-lapse seismic studies. The main objective of this thesis is to use repeated P-Cable 3D seismic surveys on the Vestnesa Ridge and develop a 4D seismic processing sequence that can highlight subsurface changes due to changes in fluid content. The secondary objective subsequently is to use the time-lapse seismic data in order to better understand the genesis and processes of focused fluid flow through chimney structures. The baseline P-Cable 3D seismic

data has been acquired in 2012 and repeated in 2013 and 2015. The 4D processing in this thesis has been done side by side between both repeat surveys and the baseline survey.

1.2 Fluid systems in the subsurface

Fluid flow occurs in sedimentary basins either as slow diffusive flow through the pore space of the sediments or as focused, advective and fast flow (Berndt, 2005; Huuse et al., 2010). Whereas the former is very well understood, very little is known about the latter. These focused fluid flow pathways often result from bypassing a seal and examples include sand injections, sill intrusions or so-called chimneys and pipes (Cartwright et al., 2007). Of these aforementioned structures, the focus will be on chimneys and pipes that cut almost vertically across sedimentary strata providing pathways for the rapid ascend of gas-charged fluids from deep or shallow hydrocarbon accumulations to the seafloor where these gas-charged fluids seep into the water column (Leifer et al., 2006; Løseth et al., 2009; Reilly and Flemings, 2010; Bunz et al., 2012). Fluid release at the seafloor often leads to the formation of small depressions known as pockmarks (Hovland and Judd, 2007). Such focused fluid flow structures vary in size from few hundreds to several km in diameter (Hovland and Judd, 2007; Cartwright and Santamarina 2015; Vadakkepuliyambatta et al., 2013) and exist on almost all continental margins on Earth. They may in fact be much more widespread than previously assumed (Cartwright and Santamarina 2015).

Most of the focused fluid flow structures are induced by pressure difference in the subsurface causing fluids to flow towards a lower pressure regime as all substances seek to obtain equilibrium. Especially if the fluids are under overpressure it can lead to fracturing of the overburden (Cosgrove, 2001). To obtain an overpressure in the subsurface there must be loading of overburden sediments or generation of biogenic or thermogenic gas, and these processes must add a pressure that is higher than the pressure dissipates, such that the pore pressure becomes higher than the hydrostatic pressure, yielding an overpressure. This occurs if the hydraulic conductivity of the overlaying rock does not allow flux rates equal to or in excess than the fluid pressure generation rate (Hart, Flemings and Deshpande, 1995).

The information we have about such fluid systems are through seismic data and as most of seismic data are acquired in relation to the petroleum industry, and some exceptions acquired

by research cruises, the knowledge represent fluid systems in petroliferous basins (Cartwright & Santamarina, 2015). Fluid pipes in the subsurface manifest on seismic data as sub-vertical columns with weak seismic energy or almost complete wipe-out in otherwise layered sediments. This is due the energy loss when seismic waves travel through fluids, and possibly also due to scattering of seismic energy at irregular boundaries smaller than the wavelength of the seismic signal. Bright spots can occur at the side margins of several pipes; this may indicate accumulation of gas (Andreassen, 2009). However, an exact understanding of the internal structure and the genesis of these chimneys is lacking.

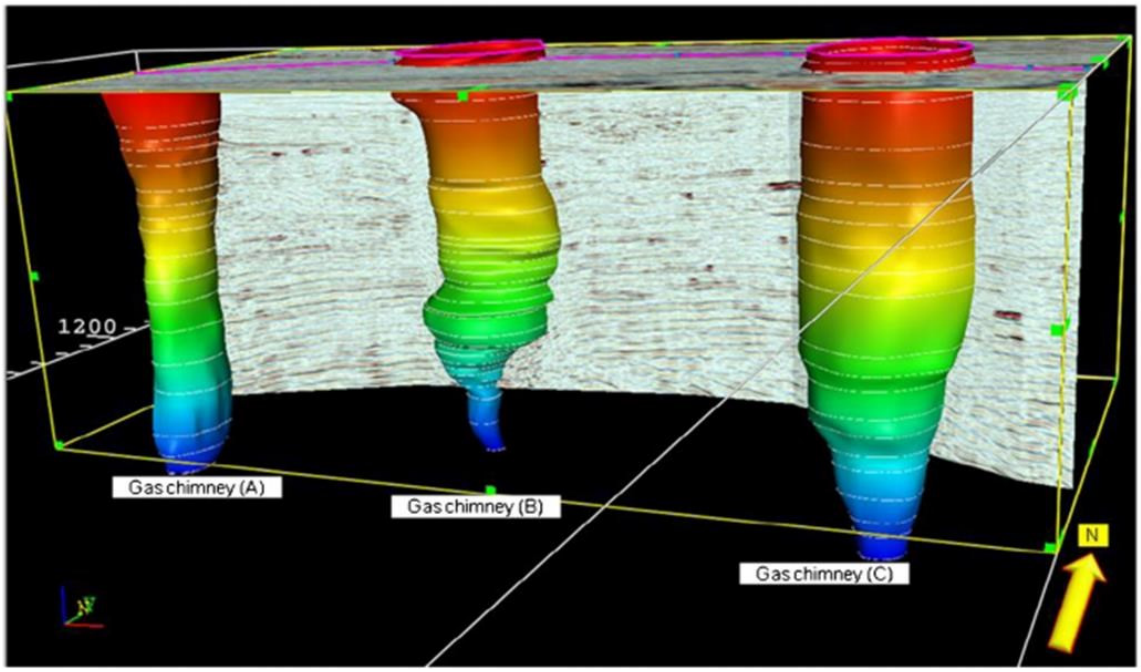

Figure 1 sketch illustrating the shape of different fluid systems. A) Parallel side margins. B) Stack of varying diameter, with a widening in diameter towards the seafloor. C) Widening in diameter towards the seafloor. (Helal, et al. 2015)

1.2.1 Gas chimneys

A gas chimney is a vertical/sub-vertical column of rising natural gas, mainly methane. In a seismic image gas chimneys are often characterized by the vertical noise and almost wipe-out of signals (Andreassen, 2009). This is due to the contrast of physical properties, impedance contrast, between the rising gas and the surrounding sediments or because gas accumulations further up in the system are masking or absorbing all the seismic energy. Gas chimneys are often associated with faulting as a small tectonic or mechanical collapse can contribute to the migration pathways (Plaza-Faverola et al., 2015), releasing the gas from where it otherwise would have been sealed by the surrounding sediment/rock. Several local accumulation of HC`s can collect in the nearby sediments of gas chimneys, the accumulations are represented by bright spots or anomalously high seismic amplitudes with reversed polarity with respect to the seafloor (Vadakkepuliyambatta, 2014). A bright spot is a seismic amplitude anomaly or strong amplitude that can indicate the presence of HC`s (Schlumberger glossary) as they result due to high acoustic impedance contrast. Gas chimneys are often associated with pockmarks, craters at the seafloor, above the chimney. These pockmarks are created by and manifest the fluid flow in the chimneys (Hovland and Judd, 1988).

By use of seismic data the geometry of different chimneys have been studied. They have the shape of a vertical columnar geometry in three dimensions. The size can vary with tens to hundreds of meter in diameter and from hundreds to over thousands of meter in height (Cartwright and Santamarina, 2015). The size of the chimneys are often defined by the slenderness ratio, this is the ratio of height divided by diameter, and the value can vary between 0.8 to over 20 (Cartwright and Santamarina, 2015). Most pipes are semi-vertical, but pipes with a tilt of up to 60 degrees from vertical have been observed trough seismic data (Cartwright & Santamarina, 2015). The side margins, or the “walls”, of the pipes are semi parallel or have a upward or downward tapering, meaning their diameter increases or decreases towards the surface (Figure 1).

1.3 Why is it important to study

It is important to study the subsurface fluid systems for several reasons. Fluid systems may be a potential geohazard in the petroleum industry as they are the reason for accumulation of shallow gas near the seafloor (Bryant og Roemer, 1983; Prince 1990; Tjelta et al., 2007; Hovland and Judd, 2007). It is important to be aware of this when drilling a well or when putting heavy installations on the seafloor as an increase in pressure can cause sudden blow outs on the seafloor. Fluid systems may also represent secondary migration routes for hydrocarbons out of reservoirs further down in the subsurface (Heggeland, 1998; O'Brien et al., 2005). Vents on the seafloor also contribute to putting methane into the ocean; methane is then being oxidized into carbon dioxide in the water column. Fluid flow in the subsurface, and potentially release into the water columns, may not only have an impact on global climate change, but also create rich ecosystems on the seabed, as several organism actually feed on methane (Kennicutt et al., 1985; Greinert et al., 2010). However these structures and their governing processes are poorly understood (Bunz et al., 2012).

Information gained about natural fluid systems can be used as an analogue for the future behavior of the carbon injected into the ground today through CCS (carbon capture storage), as this carbon are expected to behave in somehow similar ways as the natural fluid systems. It is therefore important to get knowledge on how these systems grow and develop by time. In the Sleipner field carbon are being stored in a saline aquifer above the Sleipner reservoir. The injection of carbon started in 1996 being one of the first CCS projects offshore of this size (Chadwick et al., 2009). In the image below (Figure 2) we can see the development of the carbon plume since 1994 to 2006, and detect that several gas chimney structures have begun to form.

Identifying the processes controlling seepage distribution, duration and timing related to other geological mechanisms is important for understanding these systems and to understand their potential as a contributor to global warming (Plaza-Faverola et al., 2015).

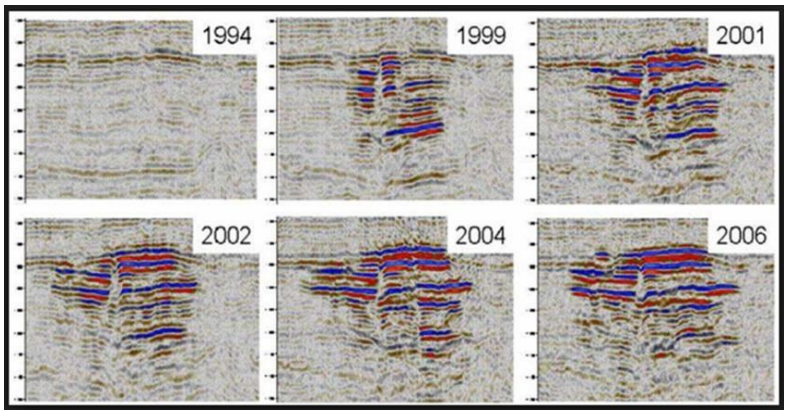

Figure 2 seismic example from the sleipner field where carbon are being stored in a saline aquifer above the reservoir, Snapshot from 1994 to 2006. The injection of carbon started in 1996. (Arts, et al. 2008)

1.4 Source and root zone

The root zone is the lowest point of the pipe and a link to the source region. Important information lies in the root zone in regards of which fluids that flow through the systems (Hustoft et al., 2010; Moss et al., 2010) and how the pressure build up has occurred.

Shallow root zones can indicate hosting within aquifers and to venting of over pressured pore fluids or potentially in situ generation of biogenic gas (Cartwright and Santamarina, 2015). While deeper root zones might involve evolution of organic rich matter and generation of thermogenic hydrocarbons, mud slurry or water expelled during mechanical or chemical compaction (Cartwright & Santamarina, 2015).

The seismic resolution decreases with depth, it is therefore difficult to map/detect the root zone of fluid pipes that penetrate deep into the subsurface, neither does all fluid pipes have one single horizon source, but can consist of a larger zone from where the systems draw their fluid supply from (Cartwright and Santamarina, 2015).

1.5 Termination

The termination is the endpoint of the focused fluid flow, where the flow, for one or another reason, stops flowing or where fluids are being vented on the seafloor. Fluid pipes can terminate in different ways. The termination can occur at the seafloor as a pockmark or a mound, where in some cases gas bubbles can be observed piercing through the seafloor. Stacked paleo pockmarks or mounds in the subsurface may indicate episodic pipe growth at earlier stages (Cartwright & Santamarina, 2015). In general, the termination can occur within sedimentary layers where the permeability is not sufficient, the capillary entry pressure is too high, due to a major changes in lithology (Van Rensbergen et al., 2007) or if the source does no longer feed fluids to the pipe system.

1.6 Gas hydrates and hydrate formation

Gas hydrates, known as the burning ice, are crystalline, ice-like compounds composed of water and gas; the gas molecules are trapped within a cage-like framework of hydrogen bonded water molecules (M. Hovland, 2005). Gas hydrates only form under specific conditions related to temperature and pressure and are dependent on the right amount of flux of water and free gas present to from. The right condition are found on land in polar regions or in the subsurface of oceans with water depth exceeding 300-500m (Figure 3) and where temperature are adequately low (<10℃) (M. Hovland, 2005). It has been estimated that 99% of the global occurrence of gas hydrates are within marine sediments along continental margins worldwide (Ruppel, 2011).

The zones where stable gas hydrates can form and remain stable are referred to as the gas hydrate stability zone (GHSZ). The end-point of the GHSZ are often marked with a BSR (bottom simulating reflector) on seismic data and represent the transition zone between the region where stable gas hydrates can form above and where free gas can accumulate underneath. Since both the temperature and pressure increases with depth in the subsurface the GHSZ are limited to an area where the pressure + temperature combined have the right values to keep gas hydrates stable (Figure 3).

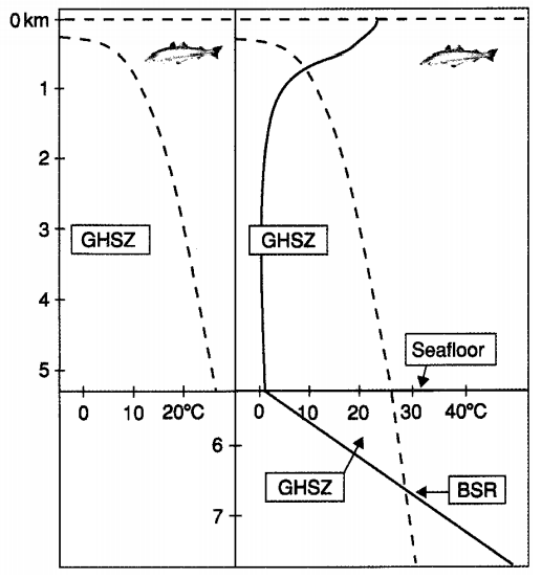

Figure 3 Methane hydrate stability zone diagram. Gas hydrates will usually not form at water depths less than 300 m, neither will it form in open seawater due to seawater circulation and the high solubility of methane in seawater. Where the temperature gradient curve (dotted line) intersects the hydrate stability curve (bold line) is often marked with a bottom simulating reflector, BSR, and is the endpoint of where stable gas hydrates can from and remain stable. The area between these two curves represent the gas hydrate stability zone, GHSZ (M. Hovland 2005).

In the process of hydrate formation heat and salinity are being released: gas hydrates only bound fresh water so salt is being excluded and since the water molecules goes from fluid to solid form heat is being released in the process (M. Hovland, 2005).

Gas hydrates can be permeable or complete barriers to flow. Gas hydrates may from rapidly when the supply of gas is sufficient, but they may also dissolve rapidly when the pressure/temperature condition changes (M. Hovland, 2005). Early work on gas hydrates suspected that the entire column within the GHSZ was cemented by gas hydrates and that this zone then was impermeable to flow, this has proven to be incorrect (M. Hovland, 2005).

A widespread destabilization of the climate sensitive gas hydrate deposits trapped in marine and permafrost-associated sediments can cause for large quantities of methane release into the atmosphere (Ruppel, 2011). The potency of CH_4 (methane) as a greenhouse gas (GHG), as it is 20 times more potent than carbon dioxide, and the oxidation of methane into CO_2 (carbon dioxide) will contribute to the increased global warming and may cause further release of these substances into the atmosphere (Ruppel, 2011).

Methane emissions are dominated by wetlands, ruminants, fossil fuel production and rice cultivation, and as these sources fluctuate with season and human behavior and the fact that the atmosphere consists of a mixture of gases, it is difficult to detect methane signals that is directly linked with dissociation of gas hydrates (Ruppel, 2011). There is a need to better understand gas hydrates and their sensitivities to temperature changes, it is also important due to their potential as a future cleaner energy source since gas hydrates contain more carbon than any other global reservoir (Kvenvolden et al., 2000).

1.6.1 Changes in BSR depth

The bottom simulating reflection (BSR) occurs at the base of gas-hydrate stability and results from a strong impedance contrast between hydrate-bearing sediments with high seismic velocity situated above gas-charged sediments with low seismic velocity (Hyndman and Spence 1992; Holbrook et al. 1996). The prerequisite for the formation of stable gas hydrates are explained above. These prerequisite can change over limited areas due to a change in temperature, gas supply or due to advective heat flow piercing through the GHSZ and hence cause a shift in the BSR depth. The shifting of the BSR can also originate from pull up or push down in seismic reflections due to high or low seismic velocity above the BSR, and does not represent actual shifts. If gas occurs locally above the BSR, it will cause a shift in time of events below since seismic waves travel slower trough gas than trough sediments, causing a push-down of reflectors below. Another case is if there have been carbonate build ups or formation of gas hydrate within a pipe conduit, this will then pull the BSR up since carbonate/hydrate have higher velocity than surrounding sediments and hence seismic waves travel faster trough carbonate/hydrate than trough other sediments.

1.7 Authigenic carbonate precipitation

Precipitation of carbonates are restricted to the sulfate reduction Zone, which is only a few meters below the seafloor (Petersen et al., 2010). Methane originating from the free gas zone below the BSR or from dissociation of gas hydrates may dissolve in pore waters, be trapped in sediments or flow up towards the seafloor as gas bubbles (Consolaro et al., 2015). Up to 90% of the rising gas can be consumed by anaerobic oxidation of methane (AOM) (equation 1.7.1) by a consortium of methanotrophic archaea and sulfate-reducing bacteria within the sulfate-methane transition zone (SMTZ) (Consolaro et al., 2015, Boetius et al., 2000).

$$CH_4 + SO_4^{-2} \rightarrow HCO_3^- + HS^- + H_2O \qquad \textit{equation 1.7.1}$$

$$Ca^{2+} + 2HCO_3^- \rightarrow CaCO_3 + CO_2 + H_2O \qquad \textit{equation 1.7.2}$$

The production of bicarbonate from AOM can induce the precipitation of calcium carbonate (equation 1.7.2) (Consolaro et al., 2015). These methane derived authigenic carbonates (MDAC) can precipitate in different shapes and sizes; slabs, crusts, nodules, chimneys or pipes (Consolaro et al. 2015).

Methane-derived authigenic carbonates (MDAC) are indicative of fluid seepage (Magalhaes et al., 2012). Large abundant and widespread discoveries of MDAC can be a direct evidence of extensive episodic methane seepage.

On seismic images MDAC is often marked, if seismic resolution allow it to be displayed, with bright, strong reflections as it is cemented tight together compared with adjacent sediments, yielding strong impedance contrast and anomalously high seismic amplitudes. As precipitation of carbonates are restricted to the sulfate reduction zone, which is only a few meters below seafloor, deeper MDAC reflections may originate from earlier stages of seepage.

Results collected from a sediment core from a pockmark field on the Vestnesa Ridge (~80°N) was used in order to reconstruct past changes in emissions of methane in the area (Consolaro et al. 2015). The result, extracted from $\delta^{13}C$ record measurement on the benthonic foraminiferal species *cassidulina neoteretis* shows two distinct intervals with negative values termed carbon

isotope excursion, indicating two episodes of increased emissions of methane; at the end of and shortly after the last glaciation, respectively 13-14 and 10 kyr (Consolaro et al., 2015)

1.8 Pockmarks

Pockmarks are often associated with subsurface structures such as gas chimneys and are present where fluid flow breaches the seafloor (Hovland and Judd, 2007; Bunz et al., 2012).

Pockmarks are seafloor craters formed in soft, fine-grained sediments where localized fluid flow of gas and pore fluids occur (Consolaro et al., 2015). They are nearly circular depressions and their length to breadth ratio generally varies from 1 (circular) to 1.25. The depth range from 1 to 80 m deep, but most pockmark are shallower than 10 m, and the diameter ranges between a few meters to over 300 meters wide (Cathles et al., 2009). In some cases the geometry of the pockmarks will reflect the geometry of the fluid flow that caused the depression (Cathles et al., 2009).

A model for the formation of pockmarks where thermogenic gas is being generated is the one articulated by (Hovland and Judd, 1988). Gas generated at depths migrate upwards and creates domes on the seafloor. The gas continues to put pressure on the dome until small cracks and fractures are created. As gas venting enlarges these fractures the flow velocity increases until a burst of gas occurs breaching the seafloor, creating a unit pockmark. Unit pockmarks continue to form around the dome until a fully grown pockmark has been created (Hovland and Judd, 1988).

Vertical stacks of paleo pockmarks in the subsurface suggest that pockmarks may be reactivated by later pulses of gas, but the repeat time of this process remains unknown (Hovland and Judd, 2007).

1.9 Mechanisms for pipe genesis

There are many different geological, geochemical and geophysical methods to get information about the fluid systems in the subsurface. Examples are geochemical analysis of sediment cores and seawater, side-scan sonar surveys, heat flow measurement, pore pressure measurements and many other (Berndt, 2005). Still, the best way to get a three dimensional image over larger areas are by use of reflection seismology as it provides high resolution imaging in all directions, which is crucial for imaging structures of limited lateral extent such as fluid pipes (Berndt, 2005).

Most knowledge available about fluid systems in the subsurface has been inferred from high resolution seismic data, which have much better resolution of shallow subsurface structures than conventional seismic (Cartwright & Santamarina, 2015). There are still several limitations to seismic characterization of such structures: small structures may be partially or fully hidden due to not sufficient vertical and horizontal resolution, strata reflection in the host succession may be offset, attenuated or have their amplitudes enhanced within the vertical zone, seismic artifacts can result in poor seismic migration, distortion due to pull-up or push-down, scattering and attenuation, low signal to noise ratio, reflected refractions, uncollapsed diffractions and complex multiples, near incident ray paths are particularly distorted, so the imaging must rely on wide-angle ray paths that could be affected by anisotropy in the host layers (Cartwright & Santamarina, 2015).

Even so the knowledge about fluid systems have developed a lot due to better seismic imaging, and as it is the best tool available for interpreting such structures we are dependent on relying on it. By use of seismic data there have been suggested several methods for the development of fluid systems in the subsurface.

There must be an initial starter mechanism and a driving force for the fluids to move from the root zone to the termination, end point. Hypothetical mechanism for pipe genesis must be able to explain the geometry, seismic expression, the root zone and the terminations that are observed in the fluid systems (Cartwright and Santamarina, 2015). Different mechanisms have been suggested to explain different fluid systems, different mechanisms also fails to explain parts of the formation. It is therefore unlikely that a single mechanism alone can explain the pipe genesis, but rather a combination of trigger and driver mechanism must be applied to explain these systems (Cartwright and Santamarina, 2015).

In the following text six different mechanism for pipe genesis are being shortly explained, the six mechanism are as followed: hydraulic fracturing, erosional fluidization, capillary invasion, localized collapse by volume loss, syn-sedimentary flow localization and multiphase flow as a mechanism for the development of fluid systems through Gas hydrate stability zone. The first 5 mechanisms is extracted from (Cartwright & Santamarina, 2015) and the last mechanism from (Smith et al., 2014).

1.9.1 Hydraulic fracturing

Hydraulic fracturing is frequently proposed to explain pipe formation (Løseth, et al. 2001, 2011; Cartwright et al., 2007; Hustoft et al., 2007, 2009; Moss and Cartwright, 2010; Davies et al., 2010; Plaza-Faverola et al., 2010, 2011). If fluids accumulate in the subsurface in such a way that the fluid pressure exceeds the sum of the minimum stress in the overburden plus the tensile strength this may cause fracturing into the overburden (Cosgrove, 2001). When the first fracture is generated it give the fluids migration pathways towards the surface and a network of fractures (Figure 4) start building due to further pressure from the flowing fluids. The fluids can then flow up towards a lower pressure regime.

Since a significant pressure build up is required for the generation of fractures this will most likely occur where you have root zones at stratigraphic highs, as in these areas the gas or fluid column can grow to sufficient height to exceed the acquired amount of pressure. The source for such a pressure build up can be due to basinal hydrodynamics, evolution of organic rich matter, accumulation of free gas underneath the gas hydrate stability zone (Flemmings et al., 2003) or due to in situ biogenic gas generation (Cartwright & Santamarina, 2015).

Hydraulic fracturing as a trigger and driver mechanism for fluid flow fails to explain areas where pipes originate from stratigraphic lows as the fluids would rather flow towards higher areas instead of building up a pressure. Where fluid pipes are high and relatively narrow fracturing as a driver mechanism also fails as a mechanism as a network of fractures build in horizontal direction as well and often widens up towards the seafloor (Cartwright and Santamarina, 2015).

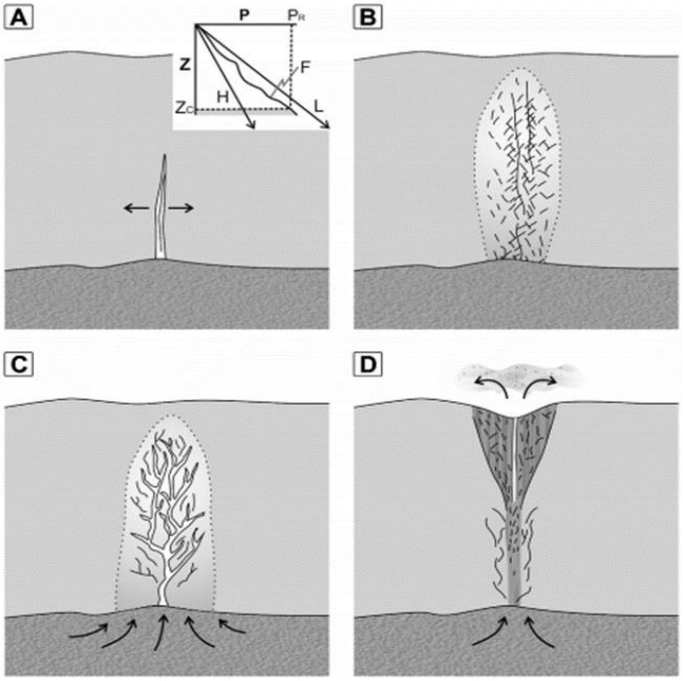

Figure 4 Basic sketch illustrating how a network of fractures cause fluids to flow up towards the seafloor. A) Overpressure in the root zone, fluid pressure exceed minimum stress in the overburden and the first fracture is generated. B) Fluids are able to flow upward, creating a network of fractures. C) Migration routes for the flow cause drainage of the overpressure root zone. D) A venting route for fluids have been created, letting fluids flow into the water Column. (Cartwright and Santamarina 2015)

1.9.2 Erosive fluidization

Fluidization is the movement of granular material due to fluid flow forces (Kunii et al. 1969). Hydraulic fracturing as an initial trigger is needed to create a migration pathway for the fluids entering otherwise sealing rock.

Fluidization can explain the widening of pipes towards the seafloor and the clustering pattern and exclusion distance between the pipes (Moss and Cartwright, 2010), as the lateral effect from the over pressured zone decreases radially from the root (Cartwright & Santamarina, 2015). Since granular material is being displaced, fluidization will ruin the internal structure within the pipe (McCallum, 1985; Nermoen et al., 2010), so in high resolution seismic where we can detect the internal structure, other mechanism must be used to explain the fluid flow. It also fails to explain the areas where pipe distribution are in a clear and sorted pattern or where the root zone are located at a stratigraphic low for the same reason as for hydraulic fracturing (Cartwright & Santamarina, 2015).

This mechanism can explain the formation of pockmarks since grains are being pushed upward by forces from the fluid flow and transported to the side of the pipe (Figure 5), leaving a depression, or a pockmark, on the seafloor (Cartwright and Santamarina, 2015).

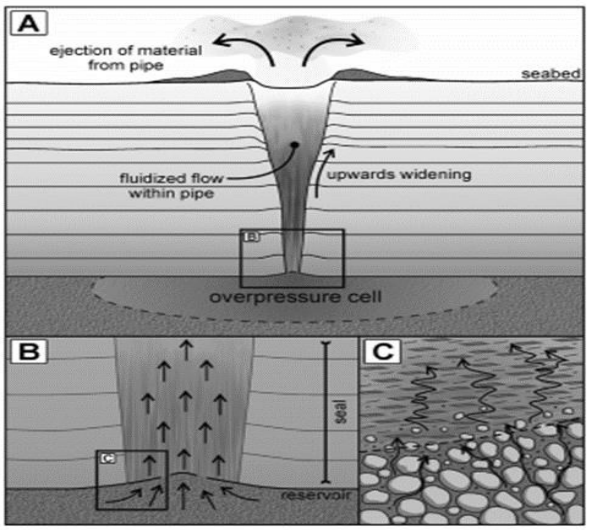

Figure 5 Simple sketch illustrating how erosive fluidization generates a fluid pathway towards the surface and ruins the internal structure of the sediments in which it is flowing through, A) over pressured cell in the subsurface are feeding fluids towards the surface. B) Zoomed in area showing the flow from source to overburden sediments. C) Zoomed in area showing how the flowing fluids pass through sediments displacing the smallest grains, ruining the internal structure of the pipe. (Cartwright and Santamarina 2015)

1.9.3 Capillary invasion

Fluids expel a pressure on water when it travels through water-saturated sediments. If the difference between the pressure from the gas (P_g) and the pressure from the surrounding water (P_w) in opposite direction exceeds the capillary entry pressure, given by equation (equation 1), the gas are then able to penetrate into the formation creating an upward migration route (Showalter, 1979; Watts, 1987; Berg, 1975). This mechanism can only occur in sediments that have effective/permeable pores.

$$(p_g - p_w) \geq \frac{\gamma\, Cos\theta}{r} \qquad \text{Equation 1}$$

$p_g = density\ gas$ $p_w = density\ water$ $\gamma_g = unit\ weight\ gas$

$\gamma_w = unit\ weight\ water$ $H_g = height\ of\ continous\ gas\ column$

$\gamma = interfacial\ tension$ $\theta = contact\ angle$ $r = effective\ pore\ throat$

$$p_g - p_w = (\gamma_w - \gamma_g) \qquad \text{Equation 2}$$

Capillary invasion is suggested as a mechanism when the root zone can generate free phase gas (Liu and Flemings, 2006, 2007). Capillary invasion as an explanation for fluid flow can actually explain the shape of the pipe, that it is round/oval, assuming every sedimentary layer have somehow homogenous thickness in a relatively small area. However, considering that different stratigraphic layers have different physical properties, meaning that the pressure needed to exceed the capillary entry pressure will vary, yielding a stack of different diameter (Figure 6), instead of the more parallel side margins that have been detected on several fluid pipes on seismic data. Since capillary invasion is dependent on such a pressure build up for the gas to push away the water, this mechanism fails to explain pipes that originate from stratigraphic lows. The required height (H_g) of the gas column to overcome the capillary entry pressure is given by equation 2 (Cartwright and Santamarina, 2015).

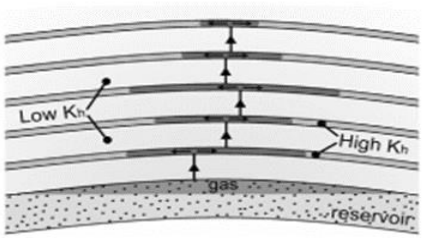

Figure 6 sketch illustrating how different sedimentary layers have different permeability's, K, causing a stack of different diameters rather than uniform side margins for the fluid pipe. (Cartwright and Santamarina 2015)

The viscosity of methane gas under shallow subsurface condition is about 60 times less than water, meaning it moves more easily through a medium (Cathles et al., 2009). So the main problem for the development of fluid pipes due to capillary invasion is not that the fluids, often gas, has to pass through the pores, but in fact that the gas has to push away the water first.

This mechanism have a theory for the development of pockmarks, which is often a clear sign and manifest fluid flow in an area. When the fluid flow towards the seafloor is fast enough to make the sediments above quick, meaning the grains loose contact with each other, a pockmark can be created if the ocean current along the seafloor is strong enough to transport away the quick sediments, leaving a depression, or a pockmark (Figure 7), on the seafloor (Cathles et al., 2009).

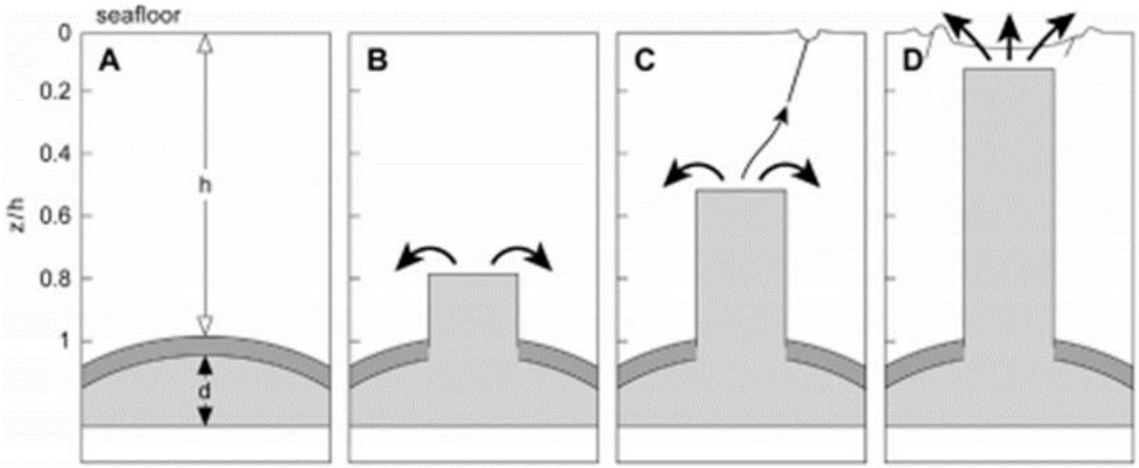

Figure 7 Basic model of how a fluid system move towards the seafloor due to capillary invasion. A) Gas column of height d builds up. B) When the pressure from the gas exceeds the capillary entry pressure + the water pressure the gas starts flowing into the formation, displacing water. C) When the gas flow is about halfway to the seafloor a pockmarks starts to form. D) When the gas flow breaches the seafloor sediments are being transported to the sides and a pockmark with similar size as the internal structure of the pipe is being formed. (Cartwright and Santamarina 2015)

1.9.4 Localized subsurface volume loss

Localized subsurface volume loss is the process in which a void in the subsurface is being replaced by the local sediments above, this happens by a collapse of the overburden. The void can originate from dissolution of carbonates or evaporates (Bertoni and Cartwright, 2005; Cartwright et al., 2007; McDonnel et al., 2007; Qiliang et al., 2013), degradation of organic matter or due to hydrate dissociation (Cartwright and Santamarina, 2015). The collapse causes migration routes through otherwise sealing sediments (Figure 8), since all layer above the void will be shifted downward. This shift in sedimentary layers will enhance the permeability, letting fluids escape towards the surface.

Since this mechanism is not dependent on a pressure build up for the fluids being able to flow towards the surface, it can explain fluid pipes with root zones at stratigraphic low.

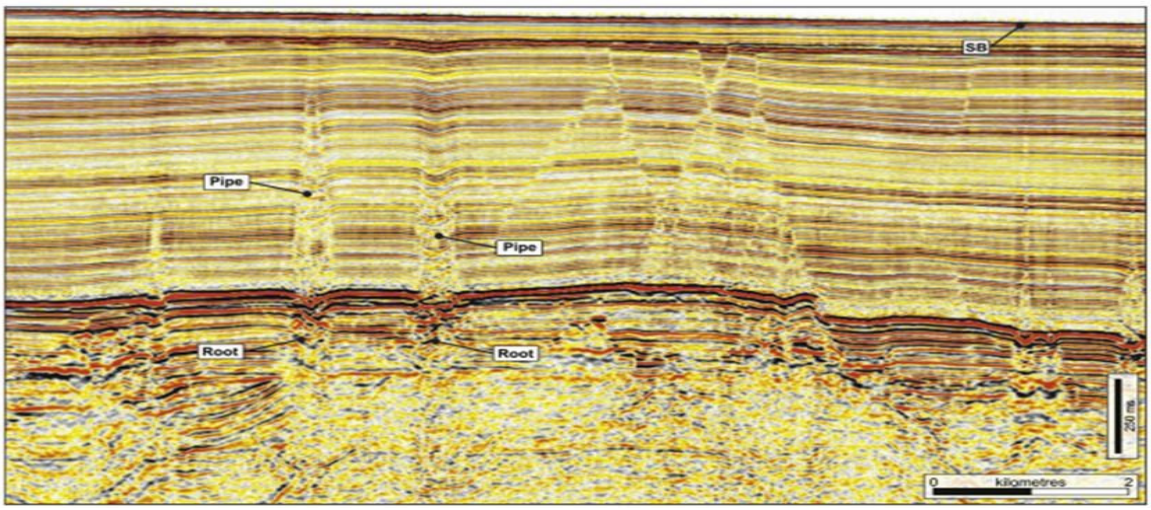

Figure 8 seismic line showing an area where two fluid pipes have been generated due to localized collapse by volume loss. We can see in the internal structure of the pipes that the layers are shifted downward compared to adjacent areas. (Qiliang et al., 2013)

1.9.5 Syn-sedimentary formation

Syn-sedimentary formation of fluid pipes occurs during sedimentation (Figure 9). Fluids are being "pushed" upward as new sediments increases the pressure underneath. This process must occur in unconsolidated sediments for the fluid being able to flow through. One prerequisite for the formation of such a fluid system is that the sediments are heterogenic, that there are finer and coarser grains available, the finer grains are being pushed away by the fluid flow and the coarser grains remains in the flow pathway (Cartwright & Santamarina, 2015). In areas where the sediments are homogenous distributed a flow originated from such a mechanism is unlikely, since homogenous sediments are packed tighter together and may seal off the flow.

These kinds of fluid systems can start by the development of a short fluid pipe and then by time as new sediments are deposited on top, grow higher. Fluid pipes with this generation mechanism often terminate at stratigraphic layers where the supply by fluids from below is not sufficient to push away the finer grains or where the sediments are very homogenous, sealing off the flow (Cartwright and Santamarina, 2015).

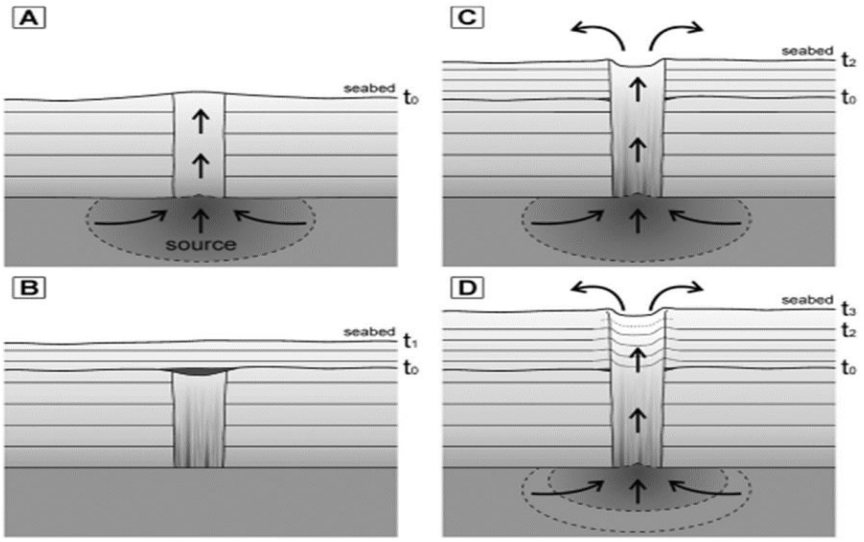

Figure 9 Simple sketch illustrating an episodic pipe growth during sedimentation. A) Fluids flow up due to pressure from overburden sediments. B) New sediments are deposited on top and puts pressure on the source region. C) The fluid pipe continue to grow towards the seafloor. D) The same process continuous to occur until the source region is drained or the flow is being sealed for some reason. (Cartwright and Santamarina 2015)

1.9.6 Multiphase flow through gas hydrate stability zone

Multiphase flow is a mechanism explaining how fluid pipes can develop through the gas hydrate stability zone. The gas hydrate stability zone is defined by a zone where the temperature and pressure condition is sufficient for the formation/crystallization of stable gas hydrates, if the right amount of flux of free gas and water are present (Ruppel, 2011). The transition zone between stable gas hydrate above and free gas underneath is often marked with a bottom-simulating reflector (BSR) on seismic data. This reflector has the name BSR because it parallels the seafloor as the specific temperature and pressure condition is reach at a specific depth below the seafloor. When hydrate crystalizes the salinity and temperature increases due to release of latent heat and exclusion of salt in the crystallization process. This increase in temperature and salinity make a three-phase equilibrium possible. This means that a propagating substance of free gas/hydrate reaction moves towards the seafloor, shifting the BSR upward (Figure 10). After the gas chimney breaches the seafloor the temperature gradient dissipates and an increase in salinity occurs to maintain the three-phase equilibrium (Smith et al., 2014).

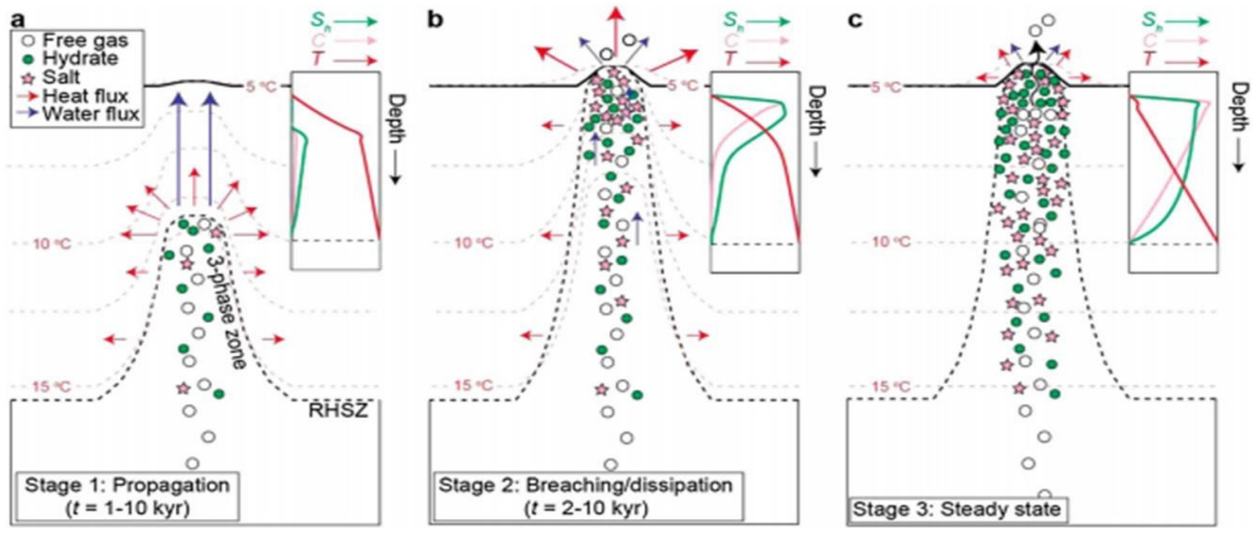

Figure 10 Sketch illustrating how a 3-phase flow propagates towards the seafloor through the gas hydrate stability zone. a) Crystallization of gas hydrates give of latent heat and increased salinity, making a multiphase flow possible. b) The BSR continues to shift towards the seafloor if flux of free gas and water is sufficient to continue the crystallization and release of latent heat and increased salinity. c) After the gas chimney breaches the seafloor the temperature gradient dissipates and an increase in salinity occurs to maintain the three-phase equilibrium. (Smith, et al. 2014b)

2 Area of investigation

The area of investigation is the eastern part of the 100 km long hydrate bearing Vestnesa ridge on the West-Svalbard margin (Figure 11), Fram strait, South West Barents sea. Active and inactive chimney structures have been detected through use of High resolution 3D seismic data and single-beam echo sounding (Bunz et al., 2012). These chimney structures indicate the presence of free gas, which is also supported by the discovery of a BSR 200 ms (twt) bsf (beneath seafloor) interpreted to originate from a stability zone between gas hydrate & free gas (Bunz et al., 2012). The 3D seismic data also reveal that the seepage zones are closely related to faults and fractures that reflect the influence of nearby tectonic stress (Plaza-Faverola et al., 2015).

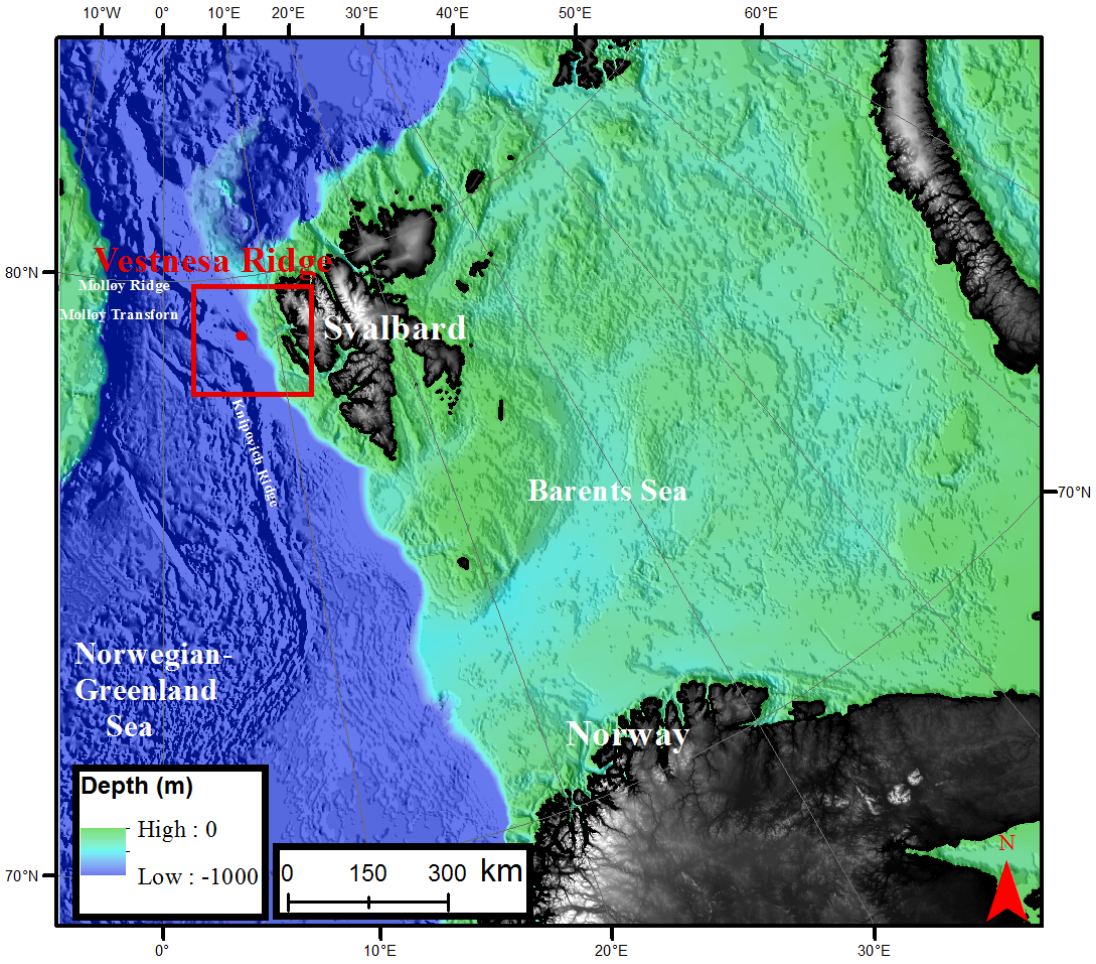

Figure 11 overview picture of the area of investigation, The Vestnesa Ridge in relation to Norway, Svalbard, the Barents Sea and The Norwegian-Greenland Sea.

2.1 Geology in The Vestnesa Ridge

The Vestnesa Ridge is a >2km thick contourite drift deposit at water depths of 12-1300 m and are located on the west Svalbard passive margin, closely to the ultraslow-spreading ridges of the northern North Atlantic (Eiken and Hinz, 1993; Howe et al., 2008; Hustoft et al., 2009; Sarkar et al., 2011). The Ridge stretches in SE-NW direction. South of the Vestnesa Ridge the Knipovich Ridge extends in S-N direction at a water depth of 2300m, the Ridge offsets westward due to the Molloy Transform fault, and continues within the Molloy Ridge, located NW of The Vestnesa Ridge (Bunz et al., 2012).

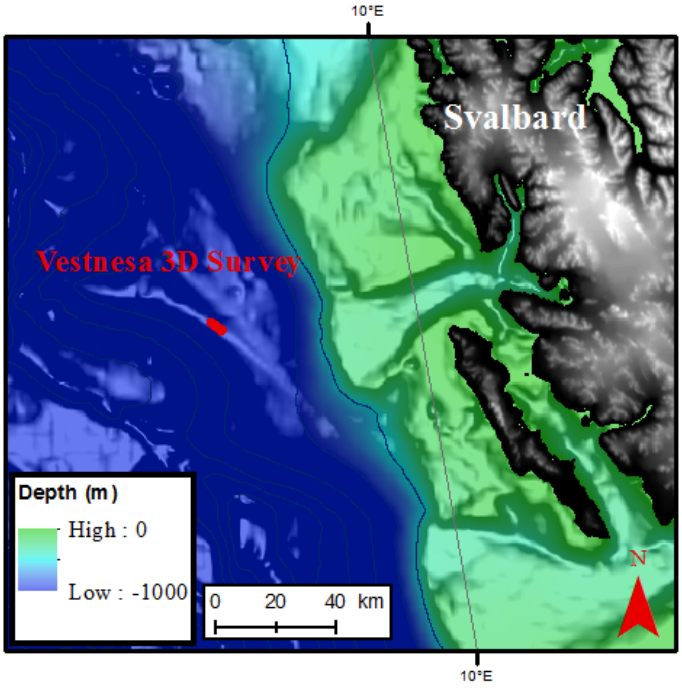

Figure 12 Zoomed in are of the location of the 3D survey area along the Vestnesa Ridge, west of Svalbard.

Small scale (>10 m width) semi-vertical faults and fractures detected on high resolution 3D seismic data shows correlation between these structures and the seepage distribution along the Vestnesa Ridge (Plaza-Faverola et al., 2015). Plaza-Faverola et al. (2015) hypothesize that stress associated with the Molloy and Knipovich spreading ridges play a major role in the seepage evolution along this hydrate system.

The main stratigraphic units at the Vestnesa Ridge can be divided into three main sequences: YP1 is the oldest sequence, it consists of syn-rift deposits over >20 Ma old oceanic crust, YP2 is a result of migrating contour currents with a main sedimentary depocenter striking parallel to the west Svalbard margin & YP3 is dominated by margin-parallel contour currents and has two depocenters separated by a thin sedimentary sequence (Eiken and Hinz, 1993). The YP2/YP3 boundary is dated to -2,7 Ma based on correlations with Ocean Drilling Program (ODP) (Knies et al., 2009).

The close proximity to the spreading center and the hydrothermal circulation systems influence the dynamics of the gas-hydrate and free-gas system (Bunz et al., 2012).

The Fram Strait is dominated by two main surface currents; the warm West Spitsbergen current (WSC) and the cold east Greenland current (EGC) (Consolaro et al., 2015). The WSC is the main contributor to heat and salinity to northern latitudes, while the EGC carries cold polar waters and sea ice from the Arctic Ocean (Consolaro et al., 2015).

The presence of a prominent BSR (Figure 13) is revealed on seismic profiles in several studies which indicate that gas hydrates and gas accumulation are common in the area, making the Vestnesa ridge one of the northernmost gas hydrates provinces that exist along Arctic continental margins (Bunz et al., 2012).

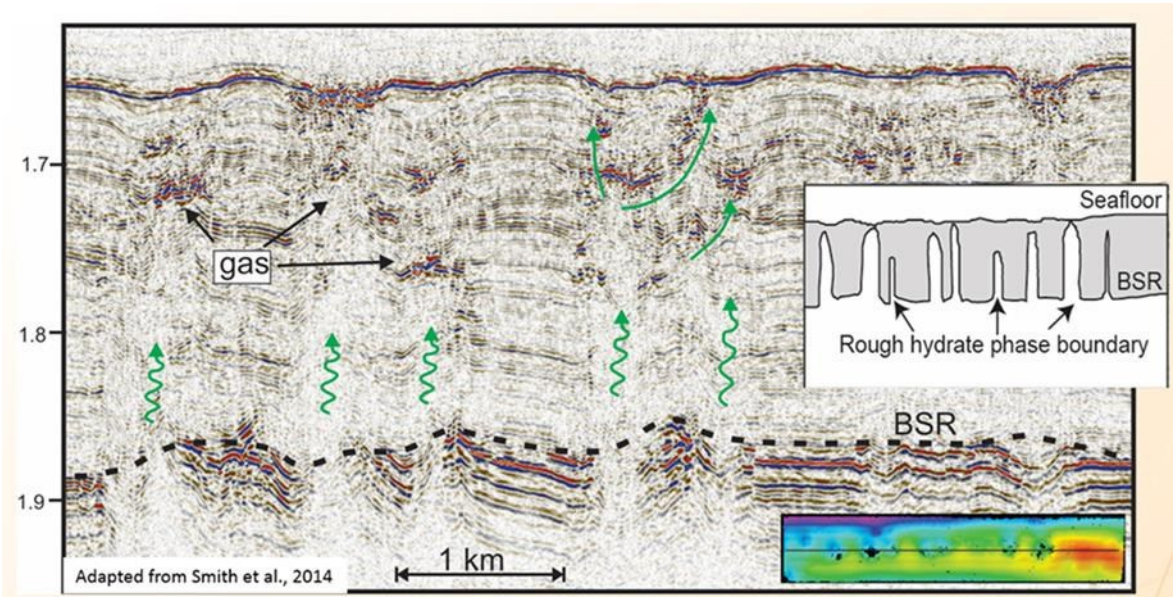

Figure 13 seismic line showing the profile of the eastern segment of the Vestnesa Ridge where several chimneys are present and piercing trough the gas hydrate stability zone. BSR indicated by black dotted line, fluid pathways indicated by green arrows. (Smith, et al. 2014a)

The Vestnesa Ridge can be divided into two main segments: The western passive segment and the eastern active segment where present seepage has been discovered in the water column (Figure 14) (Plaza-Faverola et al., 2015). The 3D surveys used in this thesis is over the active eastern segment of the Vestnesa Ridge. The eastern segment has a narrow (< 2 km wide) and rectilinear crest with active seepage (Plaza-Faverola et al., 2015). The internal geometry of the chimneys differ in the western and the eastern part of the Vestnesa ridge, indicating dissimilar seepage evolution. In the eastern part, our study area, the pockmark-stacks are nonconcentric, the chimneys have crooked geometry; they record syn-depositional deformation and their latest stage of deformation occurred such that truncation of reflections prograded along an oblique plane (Plaza-Faverola et al., 2015). The internal structure of the chimneys also contain buried mounds, which has been interpreted from studies on other margins to indicate carbonate precipitation during past seepage events (Plaza-Faverola et al., 2015). The distribution of the gas chimneys are controlled by 2 factors; that gas accumulation is morphologically controlled by the crest of the ridge and on the fault and fractures present, acting as a conductor for the gas to move upward (Plaza-Faverola et al., 2015).

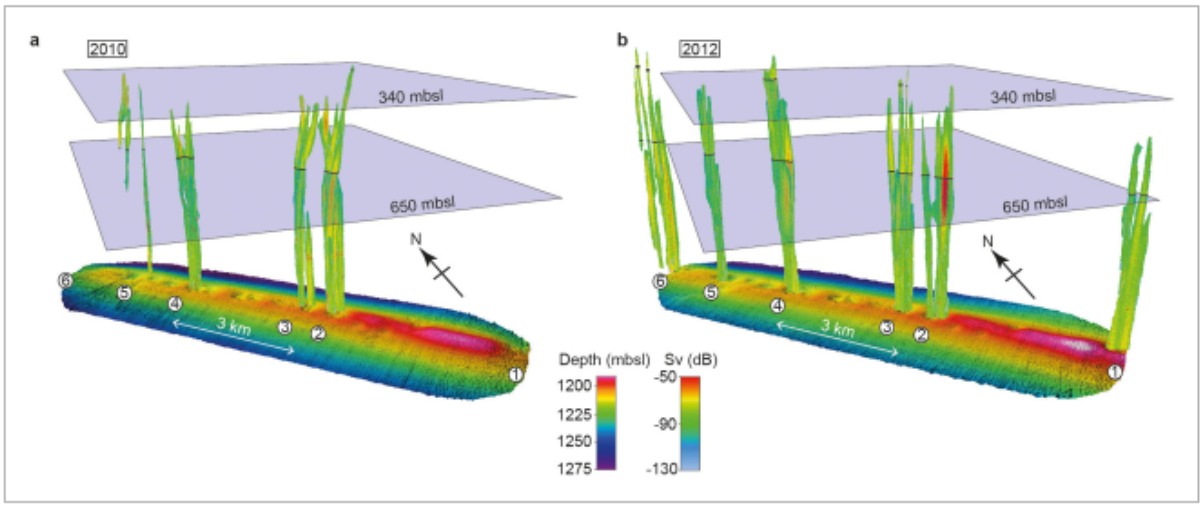

Figure 14 Flares above pockmarks at eastern segment of the Vestnesa Ridge in a) 2010 and b) 2012. (Smith, et al. 2014a)

3 Data and methods

3.1 Datasets

The datasets used in this thesis are the High resolution P-Cable seismic acquired over the crest of the eastern onset of the Vestnesa Ridge in june 2012, july 2013 & july 2015. The area covered are about $12km^2$ (6 x 2km), have a bin spacing of 6,25 m, sampling interval of 1 ms and have a dominant frequency of around 80 Hz. The migrated stack has a lateral resolution of 6.25 m and a vertical resolution of approximately 5m (Plaza-Faverola et al., 2015).

3.2 High frequent p-cable seismic

Most use of 3D seismic data are in relation to exploration of HC`s, the data then need to target greater depths, and hence the shallower structures are not well mapped. For mapping of subsurface shallow structures the University of Tromsø, in cooperation with volcanic basin petroleum research (VBPR), national oceanographic Centre Southampton (Southampton University) and IFM-GEOMAR (Kiel University) developed the lightweight high-resolution P-Cable system (Peterson et al., 2010). The P-Cable system offers full 3D seismic data acquisition using parallel streamers with high resolution which makes it great for academic research (Peterson et al., 2010). This P-Cable technology was used acquiring the seismic data from Vestnesa ridge and the purpose of this study is to use this high resolution seismic and process it into time-lapse seismic.

The datasets acquired over the area in 2012, 2013 and 2015 will be used in this project. The acquisition parameters used are:

- Mini-GI ($15/15in^3$), at 170-180 bar, 1.75 m water depth, frequency bandwidth: 30-350 Hz.
- Shot interval: 4-6 sec.
- 14 streamers, each with 8 rec. groups, at 1.5 m water depth.
- (This is the general settings, some deviations must be expected in the three different acquisitions).

3.3 Processing flow for the 3D data used in this thesis

The data processing of the three different 3D surveys was not conducted by the author of this thesis. The processing is divided into three main groups: navigation files, geometry and basic seismic data processing. The basic seismic processing-flow is applied to each line individually and consists of the following: cleaning for bad channels and traces with wrong geometry, band-pass filtering (20-40-500-800 Hz), geometry assignment and check, static correction. After merging all the lines into a single file the following flow was applied: amplitude correction and common depth point reflection binning at 6.25 x 6.25 m^2, normal moveout correction, stacking and 3-D stolt migration using 1500 m/s (Plaza-Faverola et al., 2015).

3.4 Short about 4D seismic

The concept of 4D seismic is to use repeated 3D seismic data over an area to monitor the changes in the subsurface. Changes in the subsurface due to fluid flow will change properties such as fluid saturation, temperature, porosity and pressure, and hence the elastic properties of the rock, which cause a change in seismic response (Johnston, 2013). Two or more seismic surveys are being repeated at different times, where the first one are considered the base and the following monitors.

By applying a fourth dimension, time, to 3D seismic data we can observe subsurface changes due to fluid flow or depletion of a reservoir in production. 4D, time-lapse data, have now been used as a monitoring tool for more than 20 years. Of the total in place reserves, on average, only 35% of the amount is being recovered, leaving 65% of the reserves in the ground (Eriksrud, 2014). This makes 4D seismic a very valuable tool for enhancing the total depletion of a reservoir, but also in use of research work on dynamic subsurface structures as changes over relatively short periods of time can give new insight into how different systems develop and grow by time.

By using qualitative 4D data one can gain knowledge about the complexity of a dynamic subsurface and reduce reservoir-model uncertainty. This will lead to reduced drilling costs since fewer dry holes are being drilled and a better understanding of the behaviors of different reservoirs and hence increased oil recovery (IOR) for producing fields (Eriksrud, 2014). Even if the cost of acquiring 4D time lapse is great, an increase in oil recovery of only a few percent (depending on the size and HC`s in place in the reservoir) will easily cover these costs. An

example is the Gullfaks field where use of 4D seismic has contributed with a net present value of around 1 billion dollars, while the total coast of the 4D seismic was estimated to be around 60 million dollars (Eriksrud, 2014). The time-lapse data itself will not add value to a field, but implemented with other data and good decision making, it can add significant value.

The reliability of 4D data technology continuous to evolve and hence the use of it has expanded from the North Sea to all over the world (Johnston, 2013). The importance of shearing experience and results of time-lapse data are an important factor for the growth of it.

3.5 Challenges with 4D processing

There are several technical issues that need to be addressed for the use of time-lapse to be as useful as possible. Since the aim is to image only the changes due to fluid flow, we need to limit the possibility of other factors altering the data. The most important factors to look at is repeatability.

3.5.1 Repeatability

As a time-lapse seismic survey aim is to compare two or more 3D seismic surveys at the same location, but at different times, it is important that the location is repeated thoroughly. Acquisition differences may hide the seismic response over time due to fluid flow/changes in reservoir (CGGVeritas, 2008).
Repeatability is about producing two or more images over the same location with a time interval between. Several factors contribute to whether the repeatability of time-lapse data is good or not. The most important factor is repeatability of the acquisition, hence that the source-receiver equipment and geometry remains the same during base and monitor survey. Only a small shift in position will alter the quality of the time-lapse data, difference in source receiver geometry imply different ray paths through the overburden and hence different illumination of target (Johnston, 2013). Also, that the acquisition takes place in the same direction and with similar offset ranges for monitor and base surveying. In most cases this is impossible. Several factors such as water currents, tidal, salinity, seasonal temperature changes, weather condition and topography makes it impossible to create a rerun of baseline acquisition during monitor acquisition (Oghenekohwo et al., 2013). Obstructions due to installation in a producing field

can make it impossible to run the vessel over the exact same area, several vessels may need to be used. Even though the acquisition repeatability is not obtained perfectly the repeatability of processing of the 3D data will, if done correctly, reduce noise and processing artifacts and enhance the time-lapse data (Johnston, 2013).
Repeatability is often measured in NRMS. The lower the NRMS value is, the better the match between base and monitor is, hence the better repeatability (Johnston, 2013). In acquiring the 3D data two main methods are being used, permanently installed seismic cables at the seabed (PRM) or by a towed streamer. Towed streamers normally achieve a NRMS above 20%, while PRM has shown to achieve lower than 5% (Eriksrud, 2014). It is important to state that these values are taken from conventional 3D seismic acquisition, in this case we will look at high frequency P-Cable data acquired by towed streamers, which has much wider frequency bandwidth than conventional seismic.

The NRMS is the rms (root mean square) amplitude of the difference, normalized by the average rms amplitudes of the base and monitor values. The following equation give us the NRMS (Johnston, 2013):

$$NRMS = \frac{2RMS(monitor - base)}{rms(monitor) + rms(base)} \qquad rms = \sqrt{\frac{\sum X_i^2}{N}}$$

$$N = number\ of\ samples \quad X_i = sample\ i$$

The output of the equation above is over a chosen time window in the seismic data and give out the mean NRMS value within this window.
The effort made during acquisition have a large impact on the work acquired to get the best result of the 4D data. A lot of time and effort during processing can be saved if the acquisition method used during base and monitor survey is consistent.

3.5.2 Detectability

How big are the changes in the elastic properties of rock that result from fluid flow? To answer this question we need to look at the physics of rocks (Johnston, 2013).

A source sends out a sound wave, this wave travels down towards the subsurface. When the wave hits a material with a different acoustic impedance than the overlaying, energy is being reflected back upward. This energy give off a signal with a specific amplitude that arrives at a specific time at a receiver, all these different signals that originate from different points in the subsurface combined give us the 3D seismic image. Off course the real case is a bit more complicated then explained here. When evaluating the time-lapse changes in the subsurface it is important to know how these signals change if fluid saturation change due to fluid flow (Johnston 2013).

$$I_p = pv_p \qquad v_p = \sqrt{\frac{K + \frac{4}{3}\mu}{p}}$$

$$I_p = impedance \qquad v_p = p - wave\ (compressional)\ velocity \qquad p = rock\ density$$

$$\mu = shear\ modulus\ or\ rigidity \qquad K = bulk\ modulus\ (resistance\ to\ compression)$$

The p-wave velocity, as given in the equation above, depends on the compressibility of both the rock and the fluids within the rock, and hence is dependent on changes of fluid saturation. The more compressible the rock matrix are, the more sensitive the p-wave velocity will be to changes in fluid saturation, type of fluid, temperature and pressure (Johnston, 2013). Hence compressional gas will have significant impact on the p-wave velocity. Increase in saturation of fluid will decrease the p-wave velocity and density, decrease in fluid saturation will increase p-wave velocity and density, and then decrease and increase the amplitude of the seismic signals, respectively. A change gas accumulation will not only alter the amplitude on the exact location where the changes has occurred, but also in the nearby areas as well.

3.5.3 Predictability

Predictability is a measurement of how closely the traces in each volume follow each other (Johnston, 2013). How similar they are. Several factors contribute to weather two surveys are similar or not. In areas where there have been movement of fluid the predictability is often poor and this needs to be corrected for by calibrating the phase- and time-shift needed to match the two datasets (System 2014).

Predictability is given as:

$$PRED = \frac{\sum Xcorr^2(base, monitor)}{\sum Acorr(base) x Acorr(monitor)}$$

$$Xcorr = crosscorrelation \quad Acorr = autocorrelation$$

The output value from the equation above is calculated over a chosen time window in the seismic data. If predictability equals 1 this mean that the traces are perfectly correlated (or anticorrelated, no match at all). If the value is 0 the two surveys are uncorrelated (Johnston, 2013). The predictability is more sensitive to noise and distortion than to time shift. So even if the time shift is big, the predictability can still be good (Johnston, 2013).
Big shifts in time can be produced by changes in fluid accumulation as these changes will decrease or increase the velocity of seismic waves, and then pull-up or push down reflectors, displace them in time.

3.5.4 Interpretability

How should we interpret the changes in a reservoir found by time-lapse data?

Repeatability of acquisition, a good predictability of the end-result and that the actual changes are detectable are all important factors, but without the ability to interpret the final time-lapse data no valuable information is gained. Several factors need to be considered to be able to read something valuable from the time-lapse data. How do we extract the datasets: monitor-base or base- monitor? Which changes are we expecting in the area? Is water replacing oil or have there been accumulation of gas? How is the rock physics in the area? Are any important signals being removed in the 4D processing?

In our study area, the Vestnesa Ridge, the fluid systems are present in over 50% of the seismic 3D data. The knowledge about these fluid systems and how fast they develop are not well understood.

3.6 Hampson-Russel, pro 4D

The 4D processing is done using the window based software Pro4D from CGG Hampson-Russell. Pro 4D management system helps organize the seismic data and offer several tools for analyzing and interpreting the time-lapse data. Leading edge survey calibration tools enables the user to match the different 3D datasets in regards of frequency, phase, amplitude and time of events in the base and monitor surveys in zones where fluid flow has not occurred (hence the data should in theory be the same for base and monitor). When the non-production induced variations have been removed the changes due to fluid flow can be analyzed. The software also offers a wide range of time-lapse attributes that highlight production related anomalies.

3.7 Essential elements of 4D processing

To get the best possible result from a 4D processing it is important to constantly evaluate and compare the monitor and base survey, and their similarities, during the different processing steps.

In a simple explanation the 4D processing is about forcing the data in the zones where fluid flow has not altered the seismic signals to become similar so that the fluid flow induced changes become evident. Several metrics are being used to decide which areas that been influenced by fluid flow and how to set the parameters in the different processes.

The processing is iterative, requires a lot of try-and-failing and may demand several re-runs before a desired result are accomplished.

Figure 15 shows a sketch of the different processes that can be done during a time-lapse processing workflow in the Hampson-Russel software, pro4D. Every processing case is unique so the steps applied in a workflow will vary from case to case. In the next couple of pages the different main processing steps used in this thesis will be briefly explained. The information is extracted from the Hampson-Russel pro4D help guide (System, 2014).

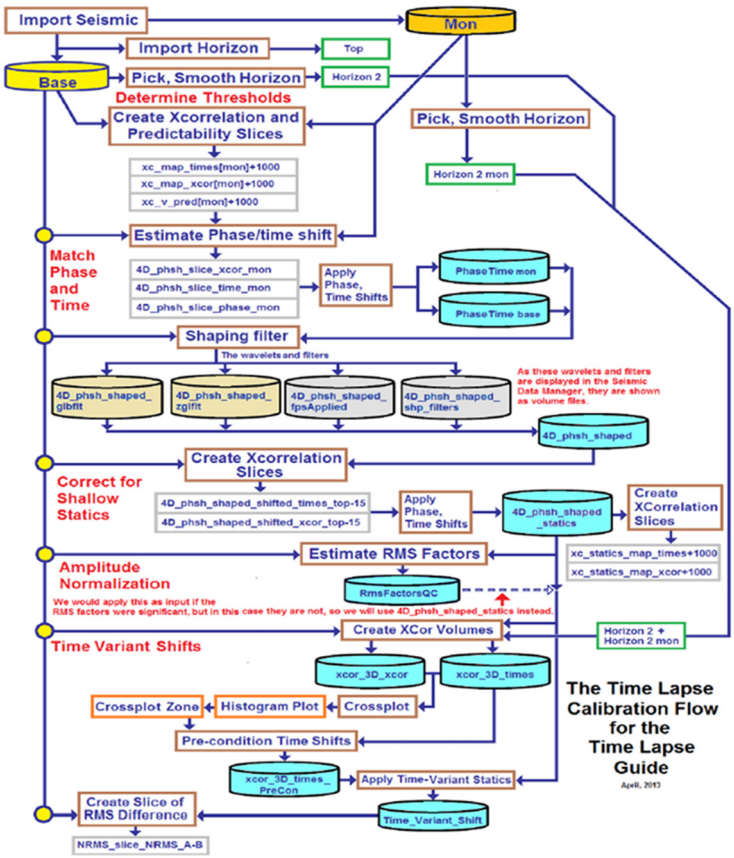

Figure 15 Sketch illustrating the full processing workflow for time-lapse calibration in Pro4D. (System 2014)

3.7.1 Re-binning

The survey regrid process in Pro4D let us regrid traces from the seismic volume so that the bins match the geometry of all the other volumes used in the processing. This is very important prior to as many functions require that the volumes have the same geometry. It is best to use the volume with the limiting extent as a reference for re-gridding as no interpolation is required (System, 2014).

3.7.2 Time- and phase-matching

When calibrating the time- and phase-shifts needed to match the datasets we leave out the areas where fluid flow has effected the seismic signals, this is done by setting the threshold values so strict that it excludes the affected areas. This process will be an iterative process and different shifts will be applied to get the best possible match.

3.7.3 Shaping filter

The shaping filter process adds a filter on the monitor data, the filter size are based on calculations comparing the base and the monitor surveys. This process will try to match frequency content, phase, time and amplitude of the datasets.

The shaping filter process will shape the traces in one or more monitor surveys so that they become more similar to the traces in the base. The process estimates a transfer function, or a filter that is being added to one or more monitors, to match the frequency content, frequency dependent phase, time and average power within the surveys (System 2014). The filters only affects the monitor surveys, as displayed below (Figure 16).

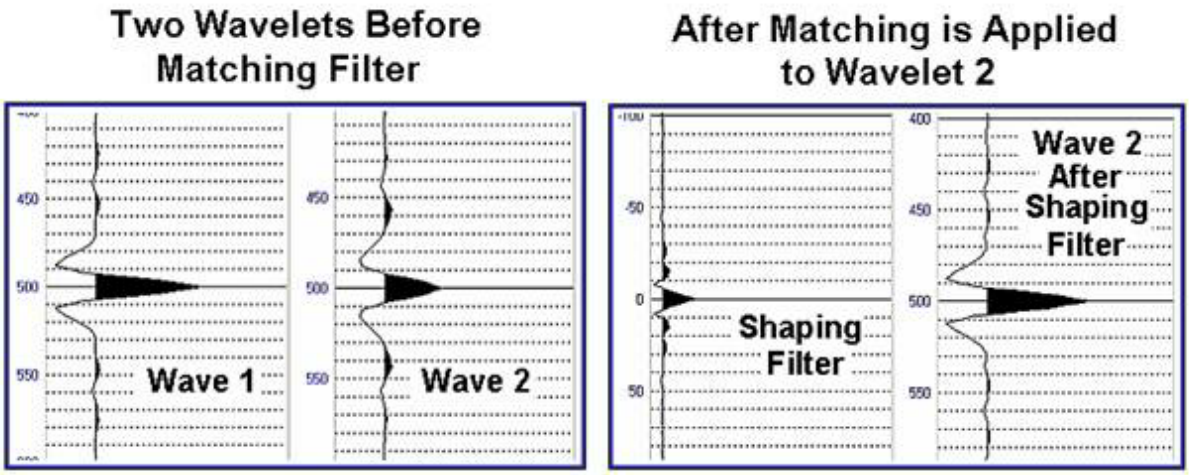

Figure 16 sketch illustrating the theory of shaping filter. Wave 1 and wave 2, from base and monito, are being compared, a shaping filter is being computed to match the amplitudes between the surveys. The shaping filter is then added to the monitor surveys to enhance the similarities between the surveys. (System 2014)

When applying the shaping filter it is important to set the cross-correlation and shift threshold so strict that the changes in signals due to fluid flow won't be lost, meaning that the shaping filter calculation is only based on areas that does not have fluid induced changes/differences. The zones that does not match well between the two volumes are being excluded from the filter calibration process.

3.7.4 Shallow statics

The shallow static correction is applied trace by trace instead of globally. Time delays due to sea state conditions during acquisition is being corrected for in this step. To improve the correction applied during this step it can be a good idea to pick a horizon along the seafloor reflector and use it to define a window when estimating the required static correction.

3.7.5 Normalizing the amplitudes

By estimating the relationship between the monitors and the base in regards of amplitudes the program calculates if the surveys are amplitude balance, the output of this calculation gives an RMS factor. If the RMS factor is close to 1, the surveys are amplitude balance and no amplitude correction is needed.

3.7.6 Correction for time-variant shift

Velocity changes due to movement of fluid/gas will affect the travel time of nearby events in the monitor surveys compared to base survey. By calculating the time-variant shifts between base-monitor surveys the adjustment needed to compensate for this is calibrated. Ideally this process requires a horizon picked beneath the reservoir/area beneath active gas leakage that is expected to have been shifted in the monitor surveys compared to base surveys due to fluid effects. In this case, the Vestnesa ridge, where the survey are dominated by several gas chimney, this is a challenge.

3.8 QC factors

Quality control factors are an essential part of checking that the processing workflow actually improves the quality and platform for comparison between the datasets used in the workflow. In the Hampson-Russel software, pro4D, there are 5 main QC factors that can be used to ensure that a progress is made during the processing workflow, these 5 factors will be briefly explained below. The information below is extracted from the Pro4D help guide (System 2014).

3.8.1 Amplitude spectrum

The amplitude spectrum plots the overall frequencies that are present in the different surveys, it displays frequency distribution in relation to amplitude value. This plot gives a visual impression of the similarities between average energy in the different surveys used in the workflow, the plots for each survey should ideally be quite similar and the graphs should follow each other fairly good.

3.8.2 Cross-correlation coefficient

Both cross-correlation coefficient and time-shift plots are a good way to highlight the difference between the two datasets.

Correlation coefficients is a tool to help determine threshold parameters to use for calibration. The program compares the base and the monitors in regards of phase, frequency and time of events to estimate the common signals between traces. This will help when deciding which areas that has been affected by fluid flow in the subsurface, and hence which areas to avoid when calibrating/correcting the “dead-areas”/making the signals in the surveys as similar as possible.

The cross-correlation value is calculated over a chosen time-window in the seismic data. Traces from the base and the monitor surveys, where the reference trace being from the base survey, are being multiplied with each other. Multiplying two identical traces will give high/good cross-correlation value as two positive amplitudes, peaks, or two negative amplitudes, troughs, give the maximum values. On the other hand if two traces with opposite signal or if the signals are shifted compared to each other, this will give out a poor cross-correlation value (System 2014). The image below illustrate how this works (Figure 17).

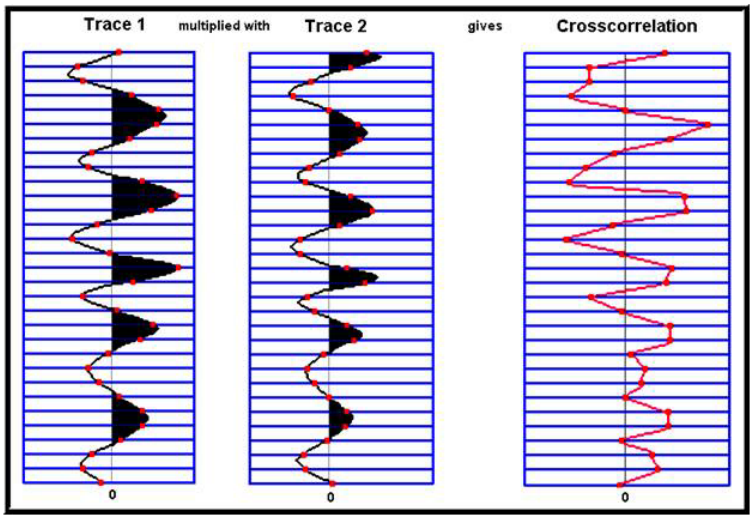

Figure 17 Sketch illustrating how the x-correlation value is calculated between base and monitor (trace 1 and trace 2) survey. The wavelet amplitude value at specific points in base and monitor surveys are being multiplied with each other giving out a cross-correlation value. + + and - - add up and give good/high correlation values, while opposite signals give out poor x-correlation values. (System 2014)

The correlation slices created will help decide which areas to leave out of the calibration during data matching. In areas where the correlation coefficients are very low are expected to be due to fluid flow or other degrading factors, and hence is being excluded in the calibration of the processing.

3.8.3 Time-shifts

The calculated time-shifts is also applied over a chosen time window within the seismic data.

By assessing the time shift between two volumes a correlation window length is defined, this window means that we allow the program to look for similar amplitudes in the monitor survey compared to base within a specific range (System 2014). A simple sketch of this process is shown below (Figure 18).

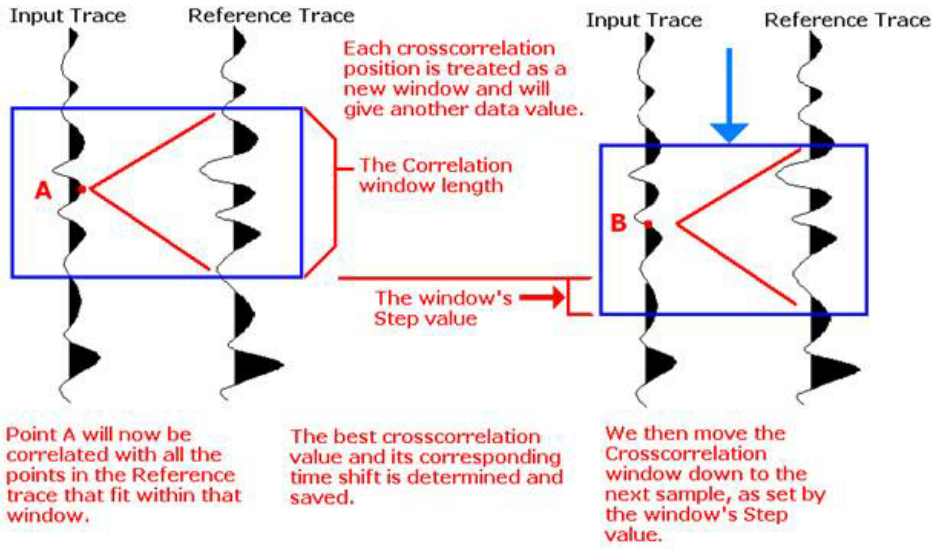

Figure 18 Sketch illustrating how the program calculates the time-shift between base and monitor surveys. The program looks for best match between signals in base compared to signals in the monitor survey within a chosen correlation window. (System 2014)

3.8.4 Predictability

Predictability is a measure of how closely the traces of two volumes follow each other. The statics from the maps created in this step will tell us the trends in matching between the two volumes. The theoretical span is from 0 to 1, where 1 means perfect match. In areas where there have been movement of fluid the predictability is often poor. The predictability is more sensitive to noise and distortion than to time shift, so even if the time shifts are significant, the predictability can still be good.

3.8.5 NRMS

The NRMS is the rms (root mean square) amplitude of the difference, normalized by the average rms amplitudes of the base and monitor values and can be used as a control check measurement for time-lapse data. The NRMS value is especially sensitive to acquisition geometry repeatability (Johnston, 2013). The goal for many processing workflows (assuming that no changes are expected in the earth response) is to get the NRMS value as close to zero as possible, this is significantly more difficult using high frequency bandwidth compared to conventional. The wide frequency bandwidth in p-cable seismic will result in an increase of the overall NRMS.

3.9 What 4D seismic actually measures

4D seismic records changes in seismic amplitude and travel time (Johnston, 2013). These changes is not only dependent on the change in fluid type/saturation, but is also very much dependent on the host rock in which the changes occur in. It is important to be aware of that the changes due to fluid flow in the Subsurface will not only change the seismic signals in the area where the actual changes occur, but also change the seismic signals of events below. Factors that influence the seismic property of sedimentary rocks, and hence their seismic signals are: compaction, consolidation history, age, cementation, texture, bulk density, clay content, anisotropy, fractures, porosity, lithology and pore shape (Johnston, 2013).

3.10 Pitfalls

The aim for 4D processing should not be to create nice images or to achieve the lowest possible NRMS Value, but instead to measure meaningful and actual changes (Johnston 2013).

When processing for 4D it is important that the surveys used are acquired properly with 4D in mind, hence that some work has been put into getting the geometry, tow depth of source, receiver-array positioning and other conditions that may affect the data as similar as possible in each repeat. Also, that the 3D processing flow is being done with 4D in mind, that the processing workflow are as similar as possible for each repeat and that multiples, noise and other non-geological artefacts are being removed, so that the ground for comparison is good. Noise in one of the surveys, especially the base survey which is used as a reference for the processing, can damage the repeatability of the different repeats.

Lateral differences between the different datasets can be the reason for a poor platform for comparison between the different surveys, only a small lateral shift will yield big differences, especially when using high frequency data.

When employing time-lapse to monitor the depletion of a reservoir wells are used to make reservoir models. It is then possible to predict the expected behavior based on production rates and other controlled factors. In this case, processing of the high frequent seismic over the Vestnesa Ridge, there are no well data available, the knowledge of the fluid systems in the subsurface and the rate of development are not well understood, this will be a challenge as we do not have any models to compared the observations with.

3.11 Petrel interpretation tool

The interpretation of the final time-lapse seismic will be done using Schlumberger`s interpretation and visualization platform Petrel E&P, 2014 edition. This includes the Multi-volume compare plug-in which allows comparison between different seismic surveys.

3.11.1 RMS-amplitude as a volume attributes

RMS is the square root of the sum of the squared amplitudes. By calculating the RMS over a chosen time/depth-window or over an entire volume the strongest/brightest amplitudes, which can be a good indicators of hydrocarbons, are highlighted independently of signal (negative/positive).

4 Results

4.1 3D interpretation

In this part a short 3D seismic interpretation of the 2013 survey will be given. The aim will be to map out and display BSR characteristics, fluid pathways, internal structure, bright spots and seafloor expressions within the 3D survey area. The interpretation of this area has been presented in Bünz et al. (2012) and Plaza-Faverola et al. (2015). It is nonetheless important to give a short overview and summary of the main observations as these structures might potentially show changes in the 4D time-lapse seismic data, which are presented in subsequent chapters 4.2 and 4.3.

There are several chimney structures within the survey area of the Vestnesa Ridge. Figure 19 shows 8 of these structures with characteristic pockmark expressions on the seafloor where the conduits terminate. The chimneys appear to mostly originate from a zone of high-amplitude reflections which are located beneath the gas-hydrate related BSR (Bünz et al., 2012). All of the chimney structures seem to be piercing through the gas hydrate stability zone and interrupting the continuity of the BSR reflector; causing a pull-up or push-down of the BSR, locally causing a pull-up or push-down of the BSR.

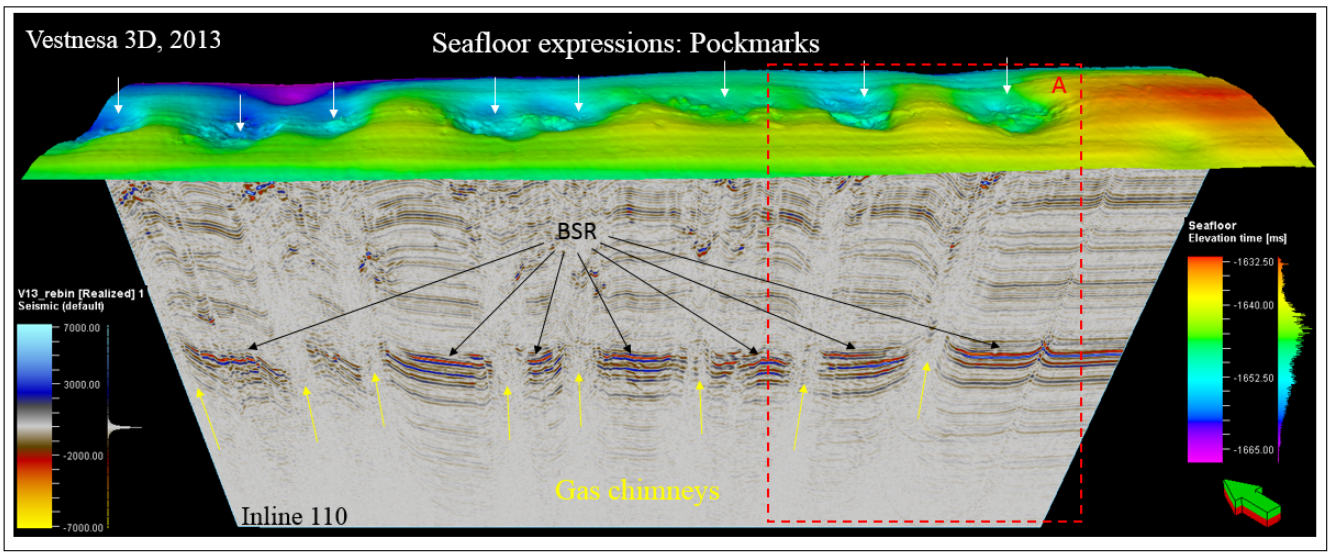

Figure 19 overview picture of a seismic Inline with seafloor surface over the Vestnesa 2013 surveys. BSR, Gas chimney pathways and pockmarks are highlighted on the picture, respectively black, yellow and withe arrows. Red box A indicate an area that are being examined closer in the next section.

The pockmarks on the seafloor are oriented on a straight line along crest of the Vestnesa Ridge and measure up to 700 m in diameter and 10 m in depth (Bunz et al., 2012). They are spaced closely together and in some areas it seems like two or more pockmarks are connected.

The internal structure of the chimneys vary along the Vestnesa 3D survey; some show clear stratigraphic layering, either pushed downward or upward, while some have more chaotic reflections.

The size of the chimneys, interpreted to be in total 8 larger ones that connects to a pockmark on the seafloor, and some smaller fluid structures within this survey area, vary in size and seismic expression.

In the next section the focus will be on the eastern part of 3D survey area, area A (Figure 19) which consist of two chimney structures (Figure 20), both of which have proven to be active during previous studies on this segment (Bunz et al., 2012).

The seismic sections 1, 2 and 3 (Figure 20, c) display the development of the two easternmost chimneys which both pierce trough the BSR and terminate at a pockmark on the seafloor. In otherwise layered and continuous reflectors, some seismic signals stands out; the interruptance of the BSR reflector and the spurious bright amplitudes along the chimney conduit, indicating the complex dynamic of these chimney structures.

In the easternmost pipe the BSR appear to be shifted up and down within the same conduit (Figure 20, c), as we can see on line 1, inline 90, that there is a push-down while on 2 and 3, inline 120 and inline 150, the BSR are pulled up (Figure 20). Whether these are actual shifts of the BSR boundary or whether they are due to pull-up and push-down effects of free gas accumulation or gas hydrate further up in the conduit is yet unknown.

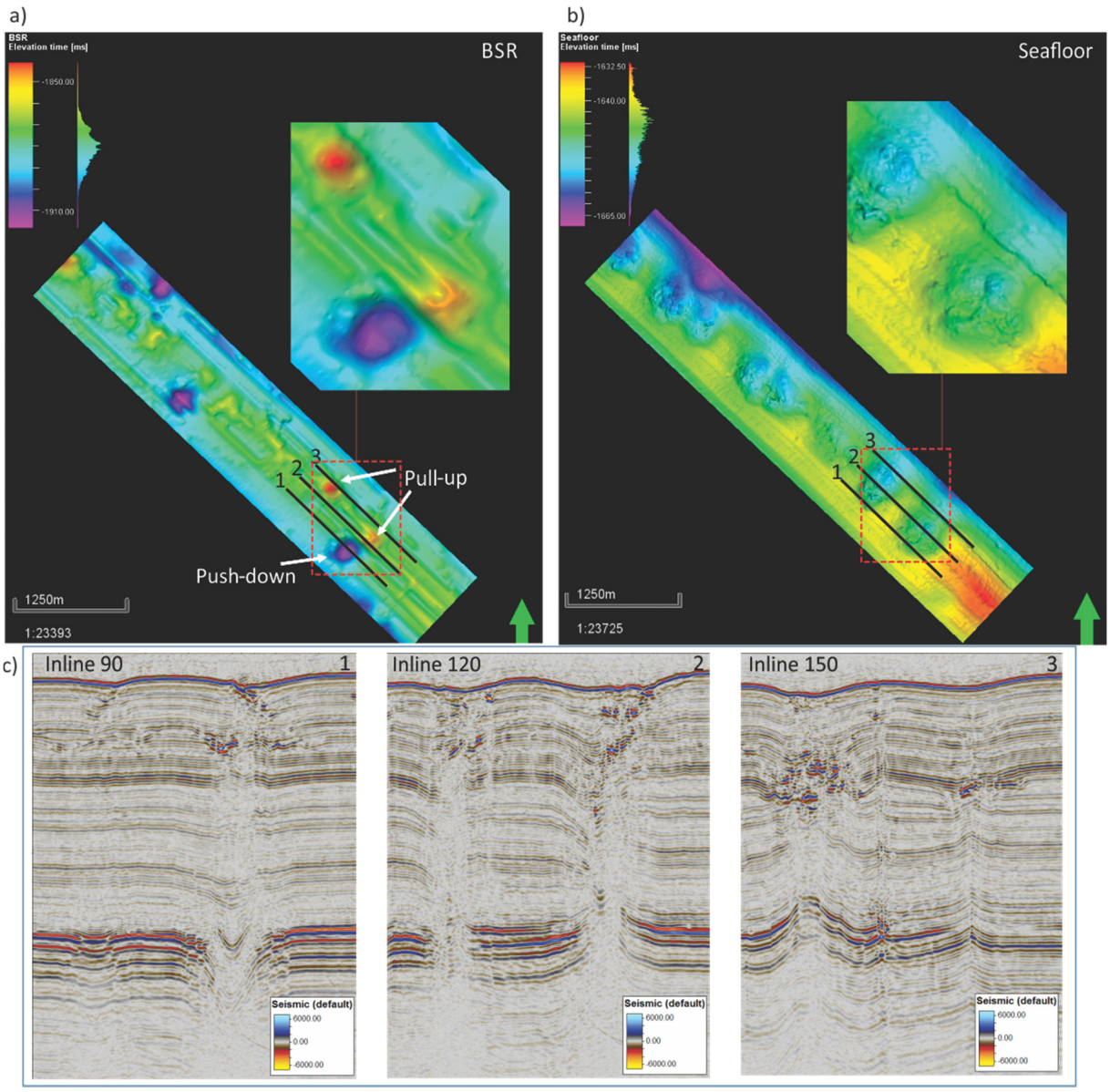

Figure 20 a) Surface interpreted along the BSR reflector. B) Surface interpreted along the seafloor reflector. C) Seismic slices 1, 2 and 3, highlighted on the two surfaces. Show two chimney conduits which pierce trough the BSR and terminate at a pockmark on the seafloor.

In both seismic sections, inline 120 and x-line 824, amplitude blanking within the chimney conduit occurs. The weak amplitudes can originate either due to masking of amplitudes if gas have accumulated above or due to gas present in the conduit. The bright spots detected within the chimney conduits can be interpreted to be accumulation of gas, gas is also likely the only substance that can yield such high impedance contrast towards sediments and give such strong reflections in the seismic data. The fact that some of the bright amplitude anomalies can appear to be peaks, positive reflections, may be explained by thin events of gas charge, tuning effects

and interference with nearby events. However, Petersen et al (2010) and Bünz et al. (2012) speculate that the bright spots might also result from gas hydrates and/or carbonates formed at a paleo seafloor.

In the easternmost chimney (Figure 21) there are several amplitude anomalies, bright spots that are crossing the disrupted, stratigraphic layerings. These amplitude anomalies can be traced upward at small angles, splitting up and terminating beneath small depressions on the seafloor (Figure 21, a, b). The small depressions on the seafloor are the places where gas seeps from the subsurface (pers. communication S. Bünz, UiT) making it likely that amplitude anomalies are indeed related to free gas. It is very likely that these amplitude anomalies resemble the pathway for gas within the shallow part of the chimney.

Dissociation of gas hydrates is not expected to occur in the subsurface in the area covering the 3D seismic survey, because pressure is high, and bottom water temperature is stable at about -1°C (Ferrè et al. 2012).

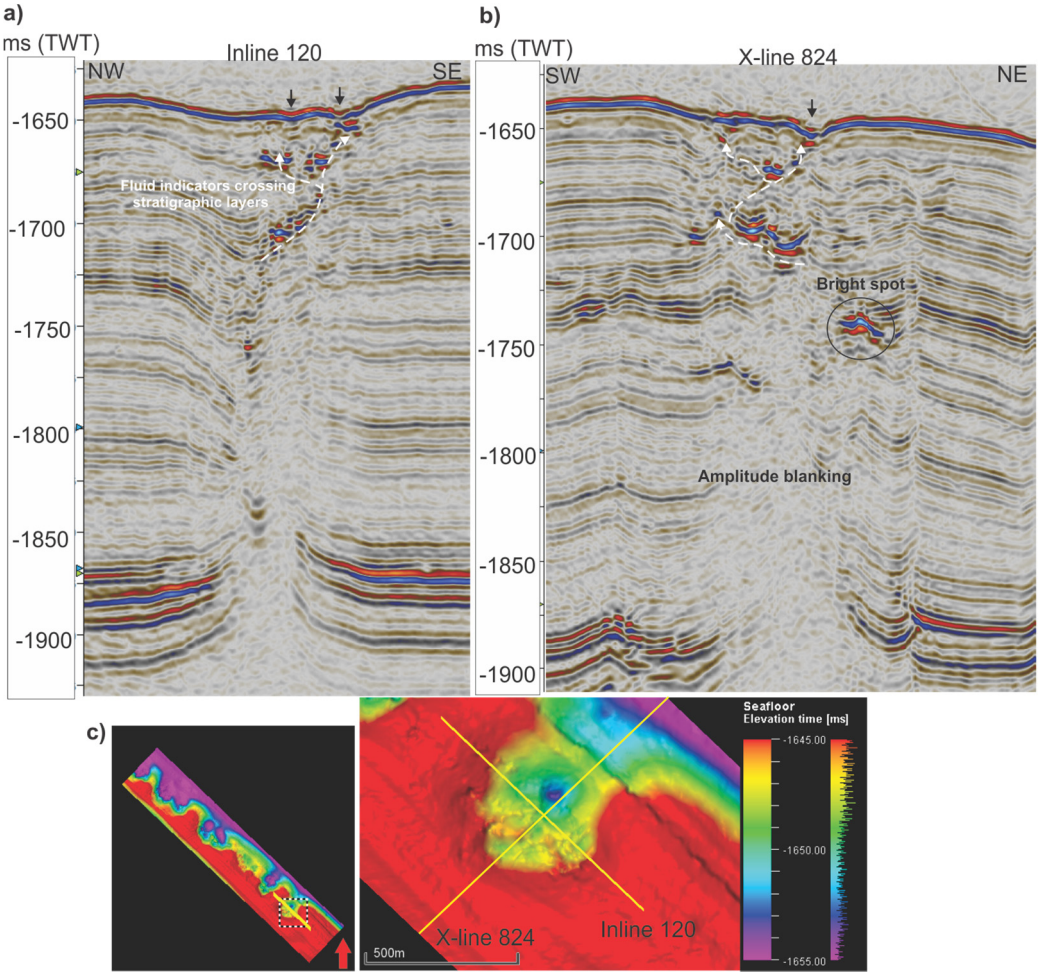

Figure 21 a) seismic inline 120. B) Seismic x-line 824. C) Overview map, showing location of seismic slices in a) and b).

4.2 4D processing

The full processing workflow conducted on the Vestnesa 3D surveys with the belonging QC estimates will now be presented. The 2012 survey are used as a base survey and the 2013 and 2015 surveys are monitors. The threes surveys will give out two "repeats", repeat one is the difference 2013-2012 and repeat two is the difference 2015-2012. The two repeats are processed side by side, but different degrees of correction will be applied to the two different sets based on the calibrations made in each of the processing steps. For each 4D processing step, the improvement in matching baseline and monitor data is shown as seismic difference. In addition, the 4D attributes measures NRMS, PRED, x-correlation and time-shifts are presented to quantitatively track the time-lapse matching.

Inline 30 from each of the three seismic surveys is displayed below (Figure 22). By examining the seismic no particular indifferences can be spotted, except the fact that the 2013 surveys seems to be phase reversed relative to the 2012 and 2015 surveys, this is quite apparent on the seabed reflector, and 2012 and 2015 surveys seem to contain more noise than the 2013 survey.

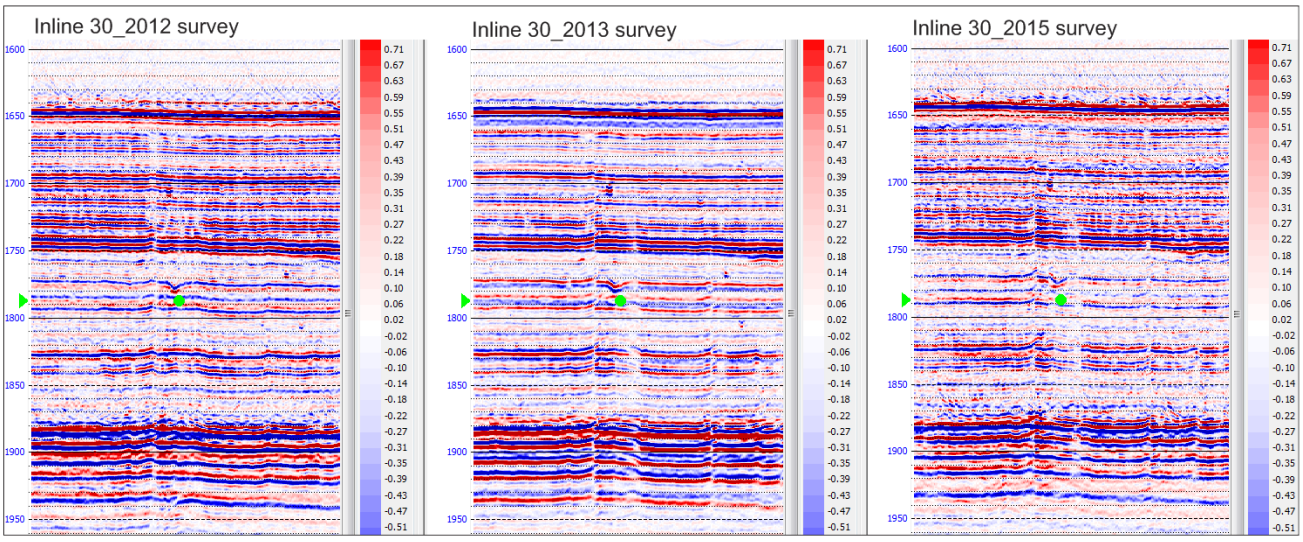

Figure 22 seismic Inline 30 from the three surveys acquired in 2012, 2013 and 2015, initial state.

The amplitude spectrums (Figure 23) displays the distribution of the amplitudes in relation to frequency for the three surveys. The graphs for the different surveys follow each other fairly good with the most deviation in the higher range, between 200-350 HZ. All surveys have a peak frequency at 175 Hz. The fact that the graphs follow each other fairly good indicates that the

tow depth of source and receiver array have not had any significant variation between each survey.

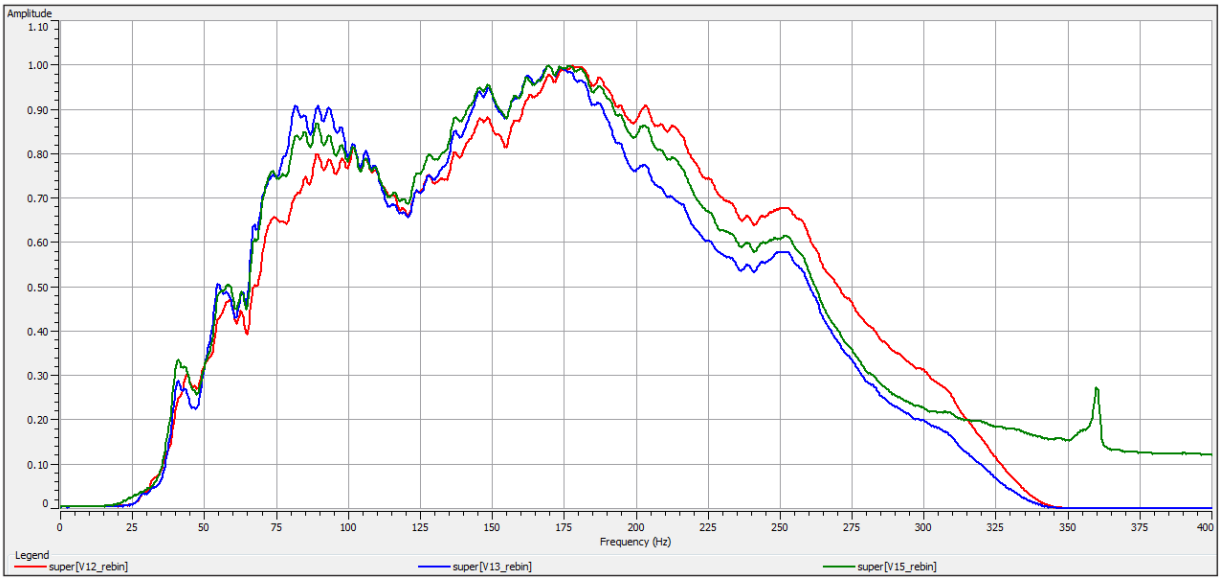

Figure 23 Amplitude spectrum of the three different surveys: 2012 (Red), 2013 (Blue) and 2015 (Green).

Before any 4D processes are applied to the data it is important to measure the initial 4D attributes or QC metrics. This is to make sure that the data is not wrongly processed, hence that actual changes become obscured. This is done by estimating several QC-metrics like the cross correlation, NRMS, predictability and phase- and time-shifts between the two seismic surveys in each repeat.

Figure 24 shows the cross-correlation of repeat 1 and repeat 2 with the baseline survey. Both repeat surveys show particular poor correlation values over the areas where the interpreted gas chimneys are located. It is also obvious that the 2015 survey is more similar to the base, 2012 survey, than the 2013 survey. The mean cross correlation between repeat 2 is at 0.697 while for repeat 1 only at 0.533, meaning that the traces correlate better in repeat 2 compared to repeat 1.

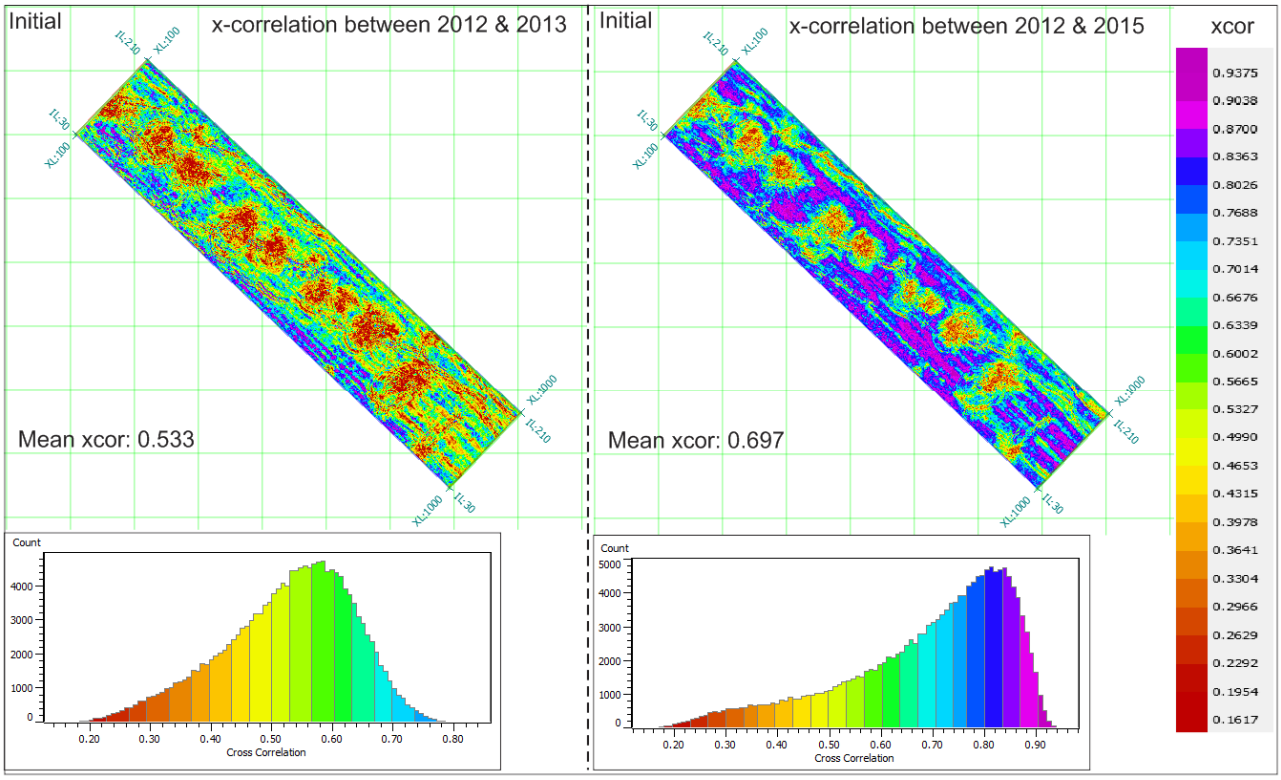

Figure 24 cross-correlation plots comparing repeat 1 and repeat 2, initial stage. The values are calculated over the time window: 1700-1900 ms (twt).

The slices in Figure 25 show the comparison between repeat 1 and repeat 2 in regards of time-shifts. The time-shifts between repeat 2 are less than between repeat 1, this was expected as the cross-correlation also was better on repeat 2. The fact that repeat 2 seems to match better with regards of time-shift and cross-correlation is a bit strange since the 2013 survey clearly has the best quality and overall the least noise (Figure 22). This could indicate that the acquisition or processing, or both of them, are more inconsistently done for the 2013 survey. Striping effect is apparent on both of the time-shift slices (Figure 25).

Both the cross-correlation values and time-shift were extracted over the time window: 1700 + 200 ms (TWT), where the chimneys are most evident in the seismic data.

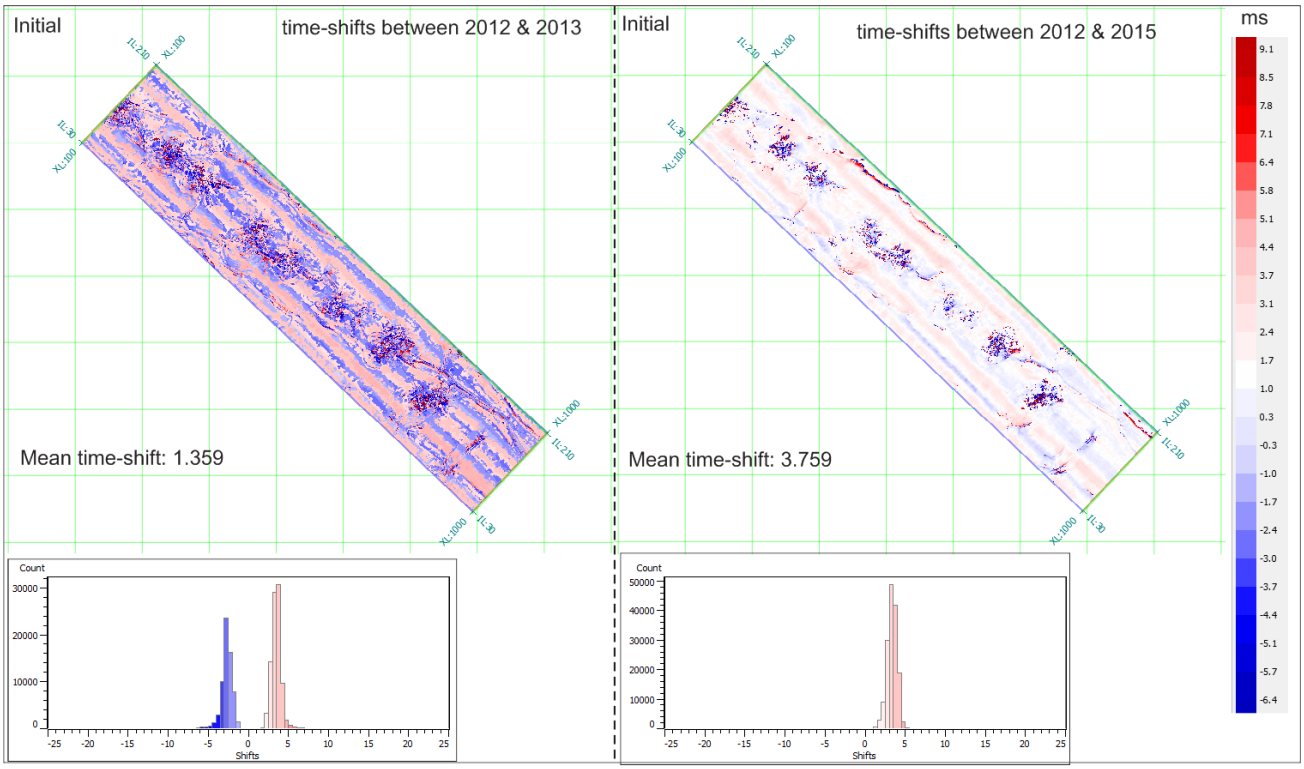

Figure 25 Time-shift plots comparing repeat 1 and repeat 2, initial stage. The values are calculated over the time window: 1700-1900 ms (twt).

The predictability measurements (Figure 26) shows that the predictability is better between repeat 1 than repeat 2. Repeat 2 has a mean predictability of 0.714, while repeat 1 has a mean of 0.752, hence 5.3% better than repeat 2.

However, predictability is more sensitive to noise and distortion, so even if the time shifts are larger between repeat 1, yielding poor correlation in regards of x-correlation and time-shifts, the predictability can still be better between these two surveys if there is more noise in the 2015 survey compared to the 2013 survey. Even so, the difference in regards of PRED is not that evident with a mean difference of 0.038 between the two differences, repeat 1 (2013-2012) and repeat 2 (2015-2012).

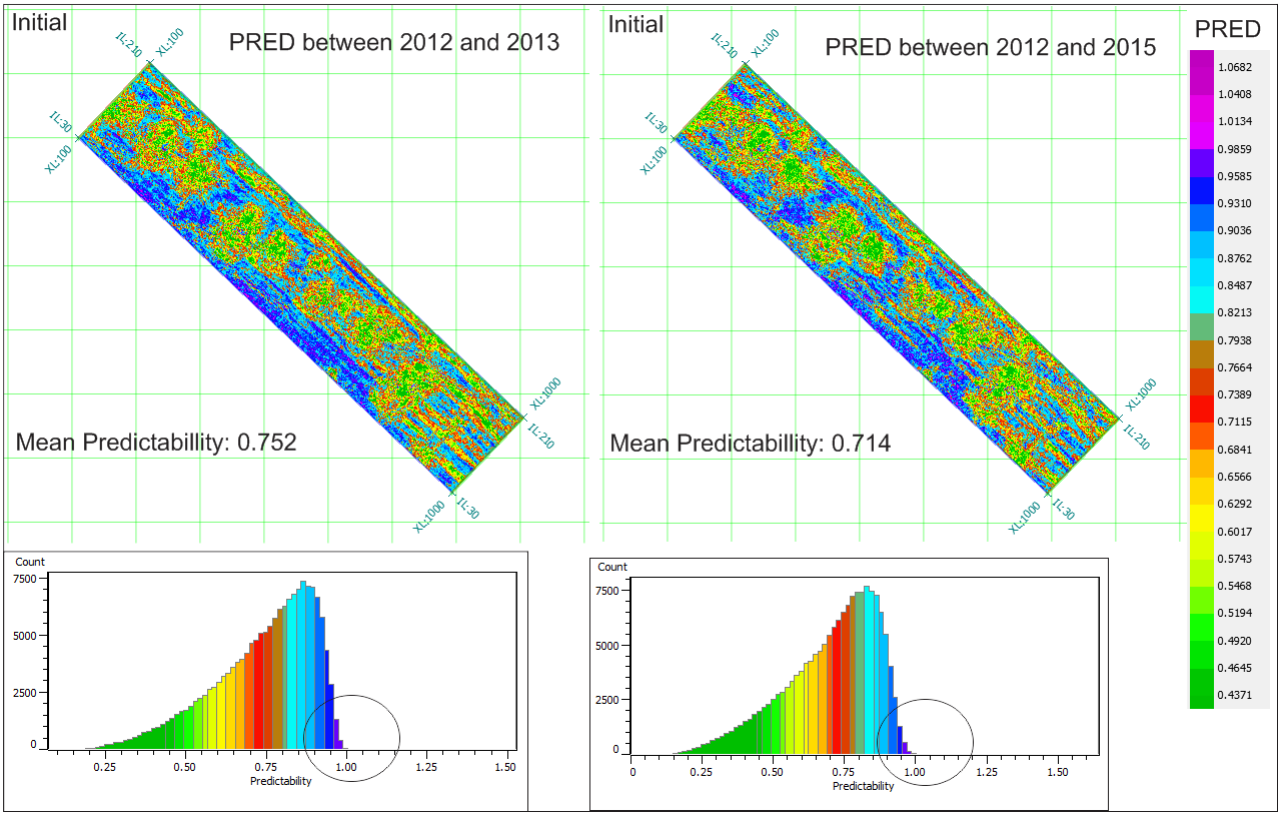

Figure 26 Predictability plots comparing repeat 1 and repeat 2, initial stage. The values are calculated over the time window: 1700-1900 ms (twt).

The initial mean NRMS values are quite high in both of the repeats (Figure 27). The mean NRMS value for the two repeats are quite similar. But the spatial distribution of the NRMS values for both repeat surveys is quite different. The trend in both of the plots are that both seem to be affected by acquisition/striping effect, meaning that adjacent inlines have time-shifts compared to each other. These striping is related with the highest NRMS values outside the area of the chimney conduits, especially in repeat 1. A reason for this could be because the two surveys have shifts in phase compared to each other or that static correction for tides were not applied properly.

The mean NRMS for repeat 1 are 1.651, while repeat 2 have a mean of 1.545, both of these values are quite high, but expected for unmatched surveys of high-resolution seismic data.

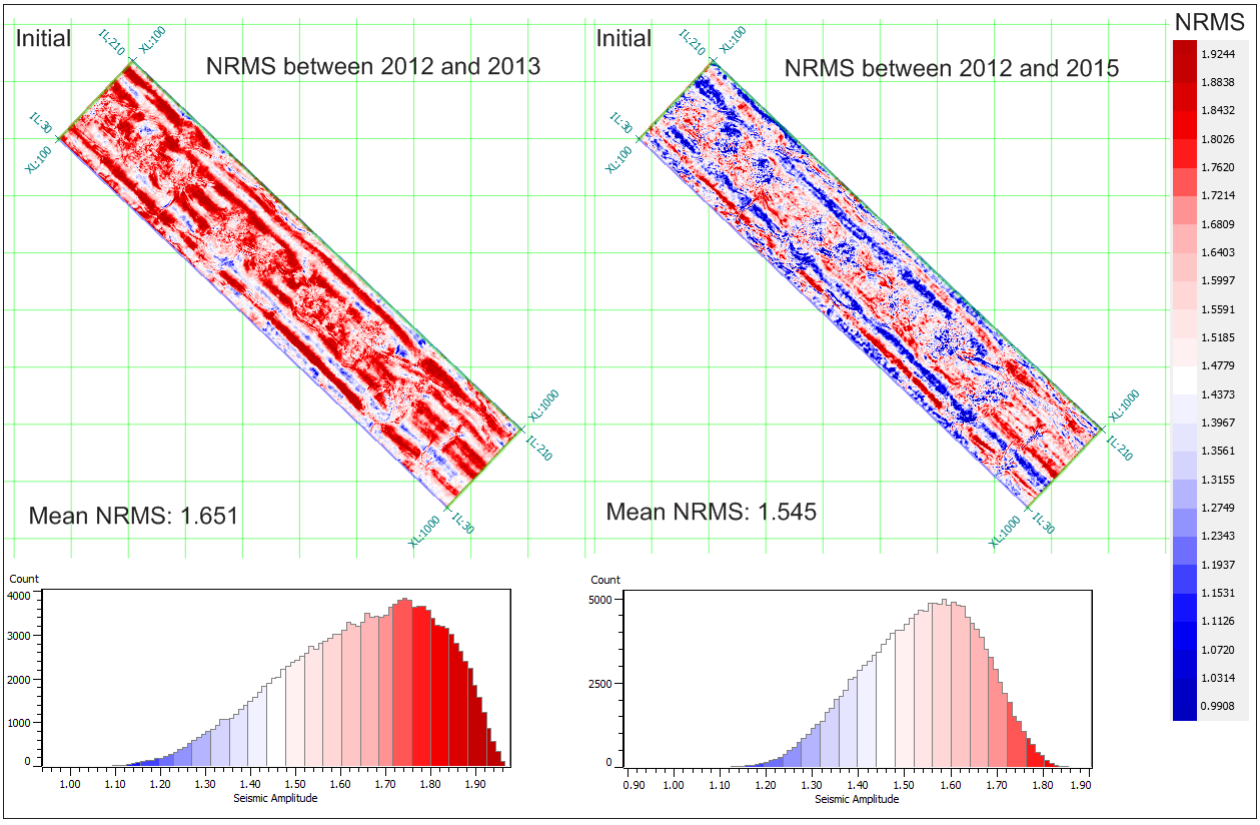

Figure 27 NRMS plots comparing repeat 1 and repeat 2, initial stage. The values are calculated over the time window: 1700-1900 ms (twt).

Phase and time-shift

The phase-shift plot (Figure 28, left) confirms that the 2012 and 2013 surveys have reversed polarities compared to each other as the phase-shift values are distributed on both sides of the phase-plot histogram, green and purple values. Also when comparing 2012 and 2015 surveys with regards of phase there are some small shifts that need to be corrected.

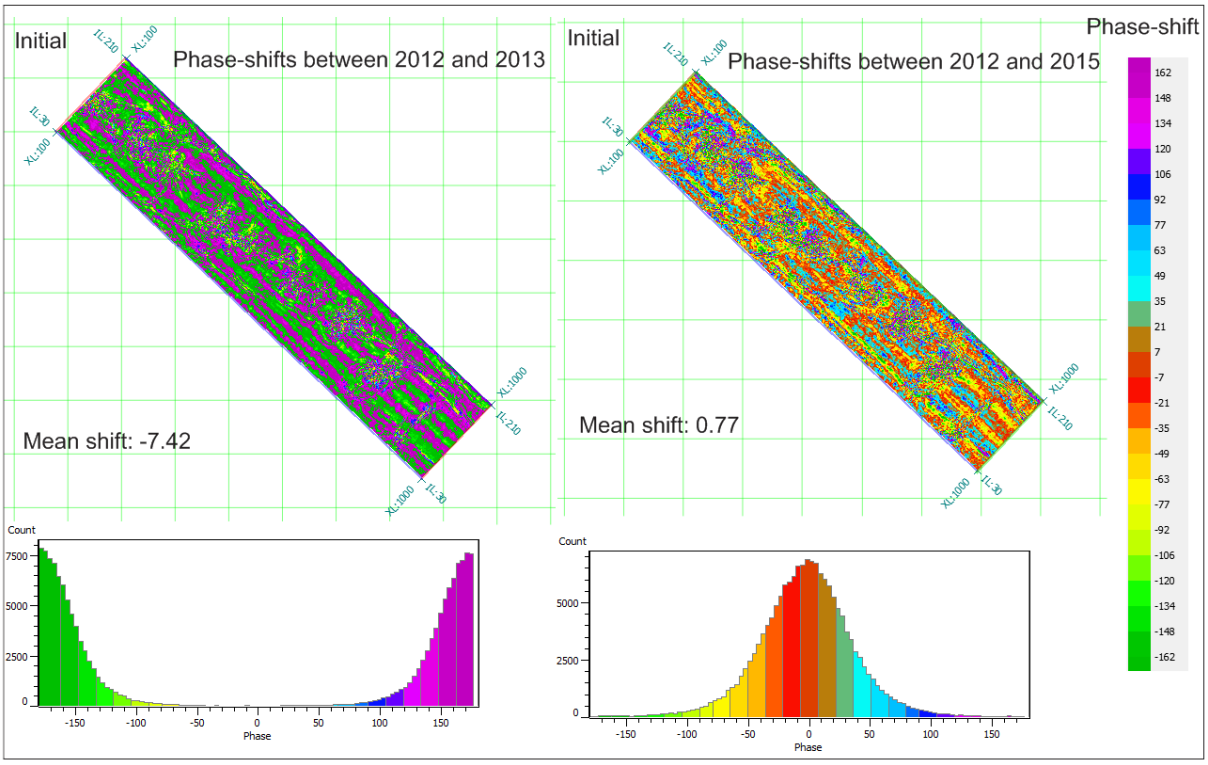

Figure 28 Phase-shift plots comparing repeat 1 and repeat 2, initial stage. The values are calculated over the time window: 1700-1900 ms (twt).

The phase- and time-matching process applied to the data was a global correction applied to the whole analysis window. For the 2015 survey, a bulk time shift of 3.75ms and a bulk phase shift of -2.76 degrees was applied and for the 2013 survey a bulk time shift of 1.09ms and a bulk phase shift of -15.23 degrees was applied. The improvements in the seismic data are shown below (Figure 29).

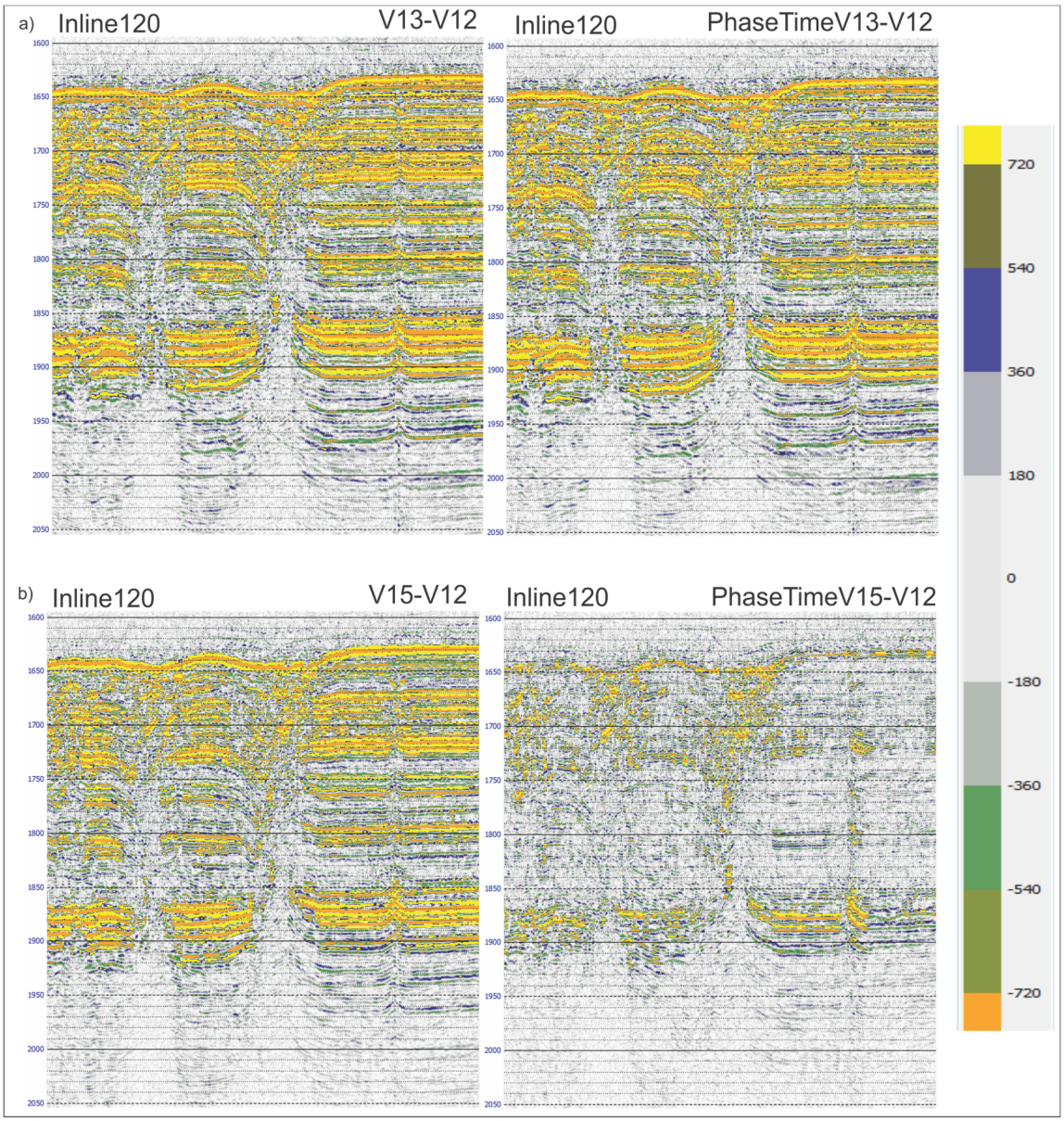

Figure 29 seismic slices showing initial difference and differences after phase- and time-shifts was applied of repeat 1 and repeat 2. a) Repeat 1, before (left) and after (right) phase- and time-shifts. b) Repeat 2, before (left) and after (right) phase- and time-shifts.

The improvements done during phase- and time-shift was significantly larger in repeat 2 compared to repeat 1 (Figure 29). A cross correlation threshold of 0.6 and a time shift threshold of 5ms was used in this process. This means that only the traces that have higher cross-correlation values than 0.6 and smaller time-shift than 5ms were used to calibrate the adjustment done in this process. These thresholds were chosen based on the cross-correlation and time-shifts values calculated prior to the process (Figure 24, Figure 25).

The mean NRMS of repeat 1 after the phase- and time-shift (Figure 30) shows a mean value of 1.78, which is higher than initially and it is surprising to see that the lowest values actually are in the areas where the interpreted chimneys are located (Figure 30, left).

While repeat 1 had an increase in mean NRMS, the mean NRMS value of repeat 2 has gone significantly down. Repeat 2 now has a mean NRMS of 0.924, this is a reduction of 0.621 from before the process was applied. The best/lowest values are outside the areas of where the interpreted chimney conduit are located (Figure 30, right).

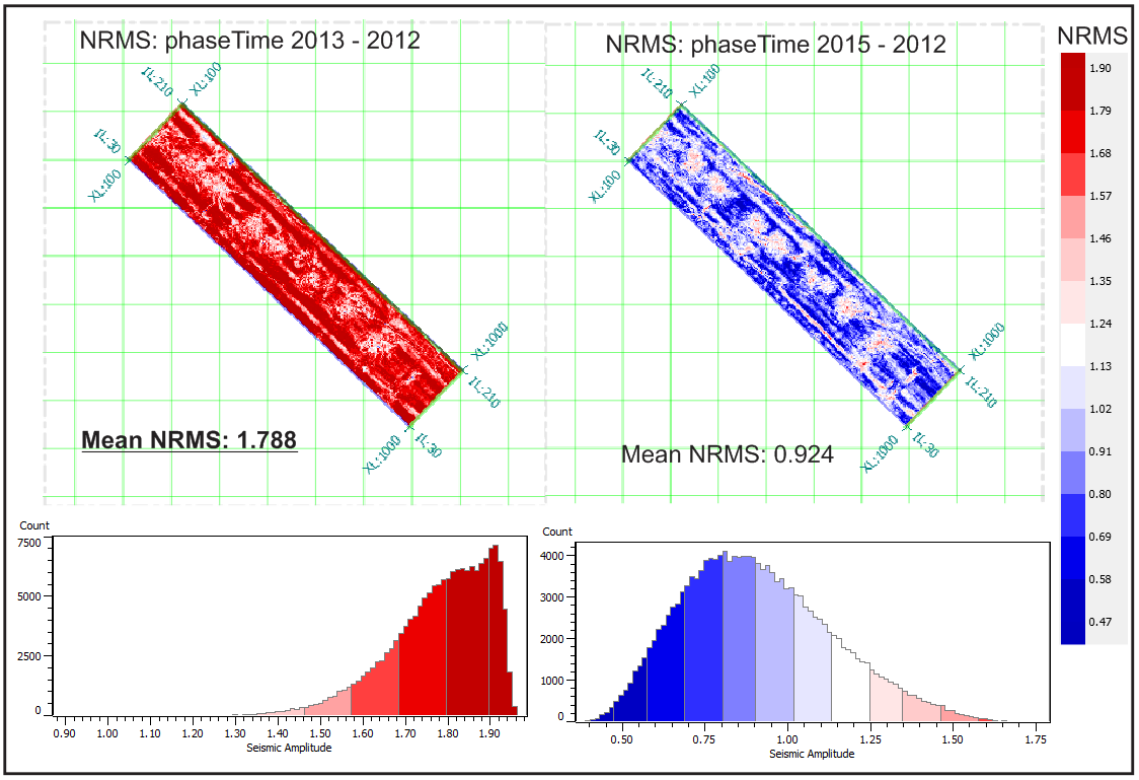

Figure 30 NRMS plots comparing repeat 1 and repeat 2, after phase- and time-shifts. The values are calculated over the time window: 1700-1900 ms (twt).

The mean predictability metric, on both repeats, has not changed any after the phase- and time-shifts was applied (Figure 26, Figure 31).

Repeat 1 has a mean PRED of 0.752, while repeat 2 has a mean PRED of 0.712.

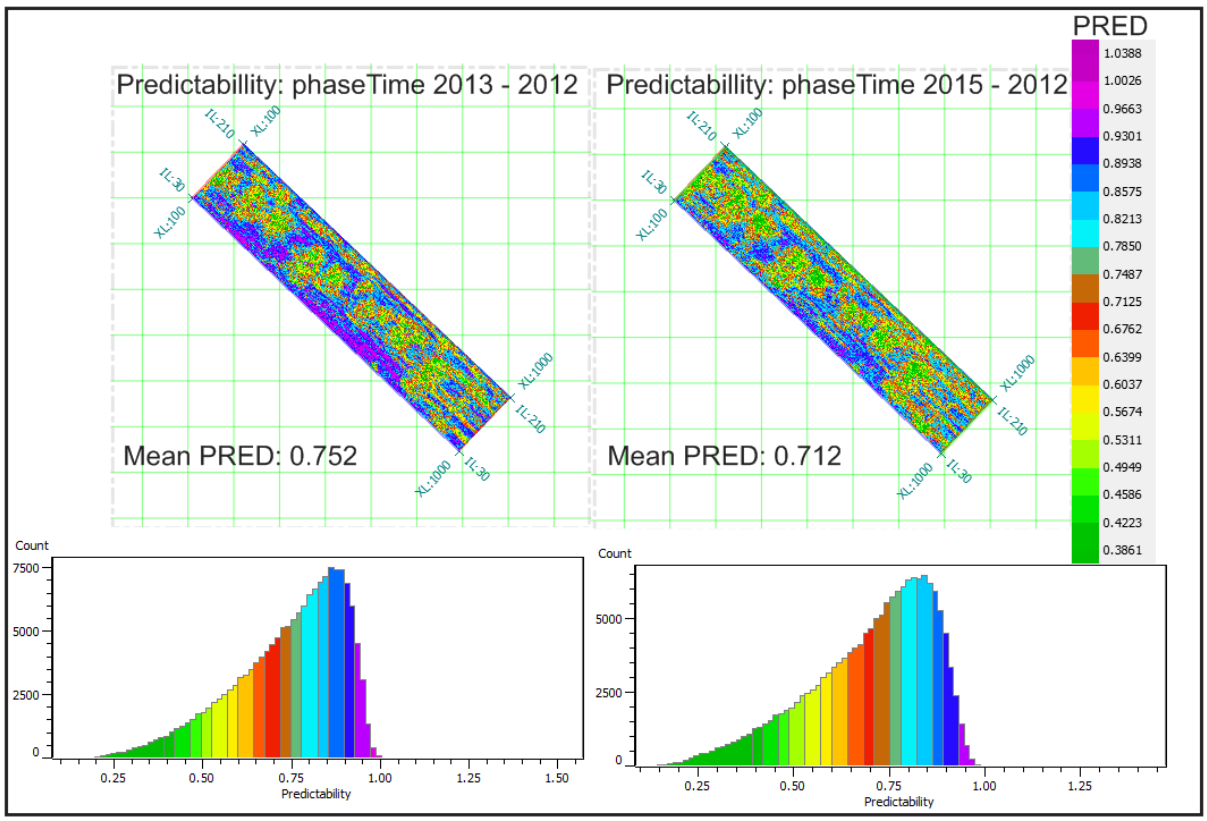

Figure 31 Predictability plots comparing repeat 1 and repeat 2, after phase- and time-shifts. The values are calculated over the time window: 1700-1900 ms (twt).

Shaping filter

The threshold used for the shaping filter process was: correlation threshold 0.5 and maximum correlation shift threshold 2ms. After the phase- and time-shifts was applied the cross-correlation has increased and the time-shifts have decreased, so the threshold are set a bit stricter on the shaping filter calibration. After the shaping filter was applied repeat 1 (Figure 32, top) have significantly improved, the strongest reflectors are becoming less evident.

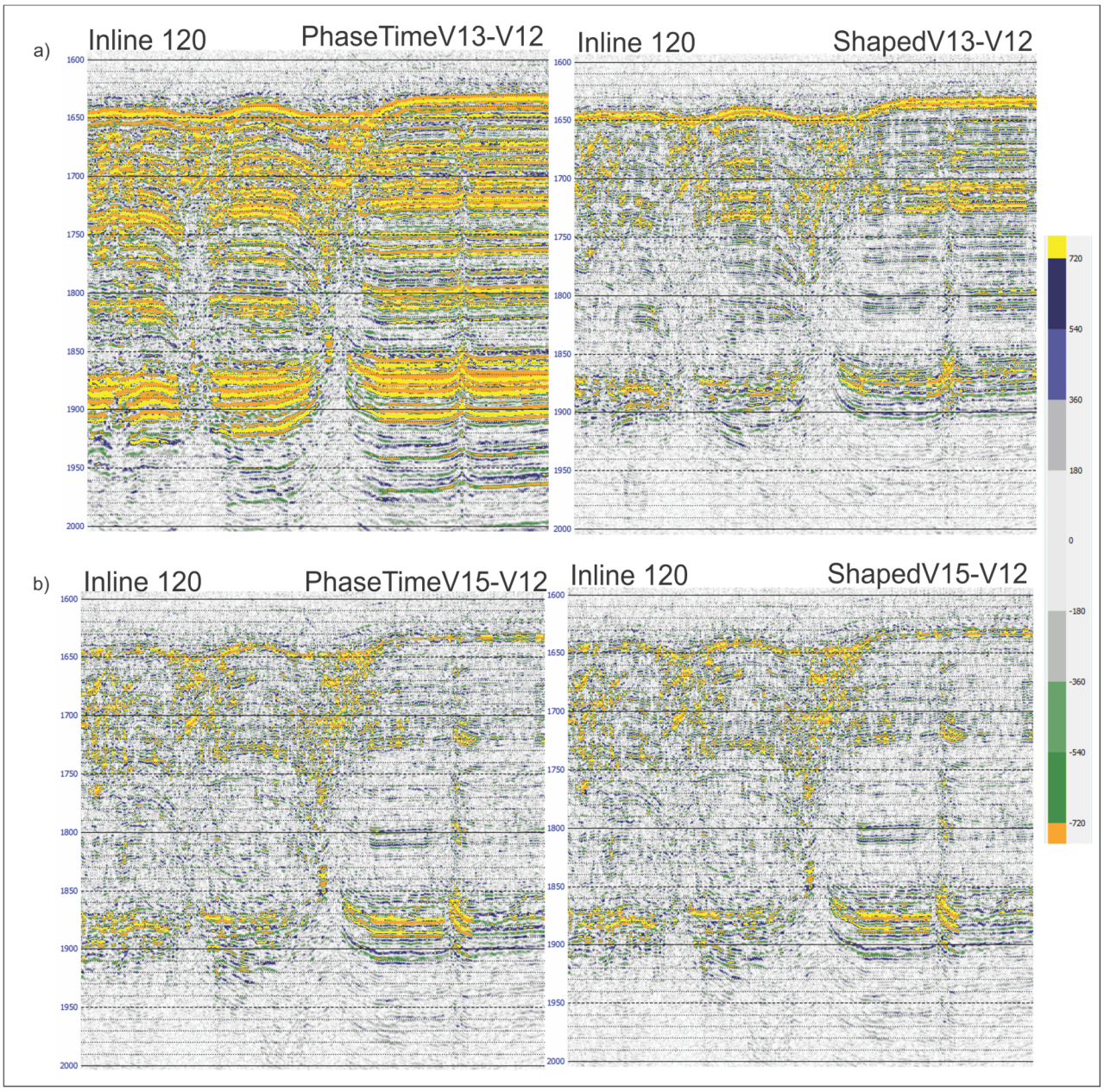

Figure 32 a) Repeat 1, seismic inline 120, before (left) and after (right) shaping filter was applied on the monitor. b) Repeat 2, seismic inline 120, before (left) and after (right) shaping filter was applied on the monitor.

The maximum correlation value found during shaping filter was 0.88 for repeat 1 and 0.954 for repeat 2.

After the shaping filter was applied to the monitor surveys the mean NRMS values for repeat 1 and repeat 2 where 0.865 and 0.924, respectively (Figure 33). The window size used was: 1700 + 200 ms (twt). The mean NRMS value for repeat 2 has not changed, while for repeat 1 the mean NRMS value has gone significantly down, from 1.78 to 0.865.

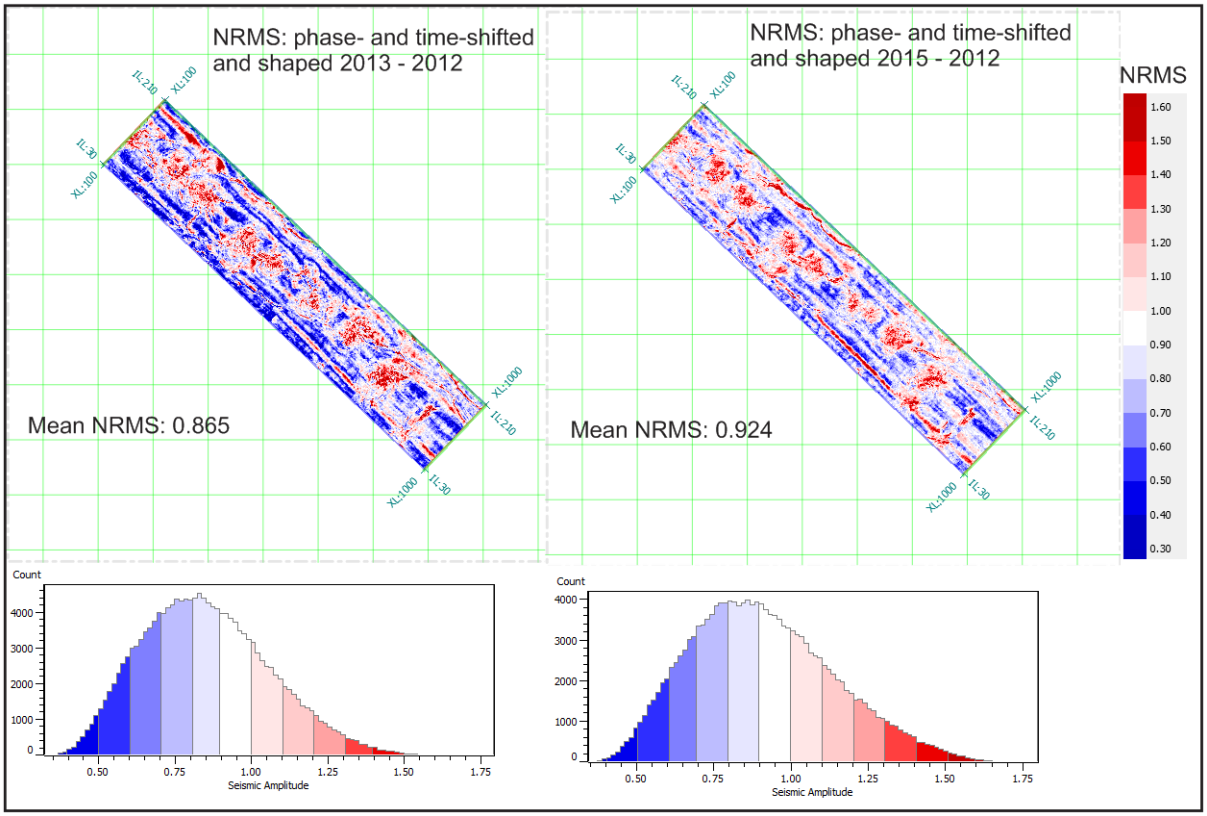

Figure 33 NRMS plots comparing repeat 1 and repeat 2, after shaping filter was applied on the monitors. The values are calculated over the time window: 1700-1900 ms (twt).

A small decrease in mean predictability is seen in both of the differences after the shaping filter was applied (Figure 34). This is not an improvement as the desired PRED is as close to 1 as possible, meaning that the difference are perfectly repeatable.

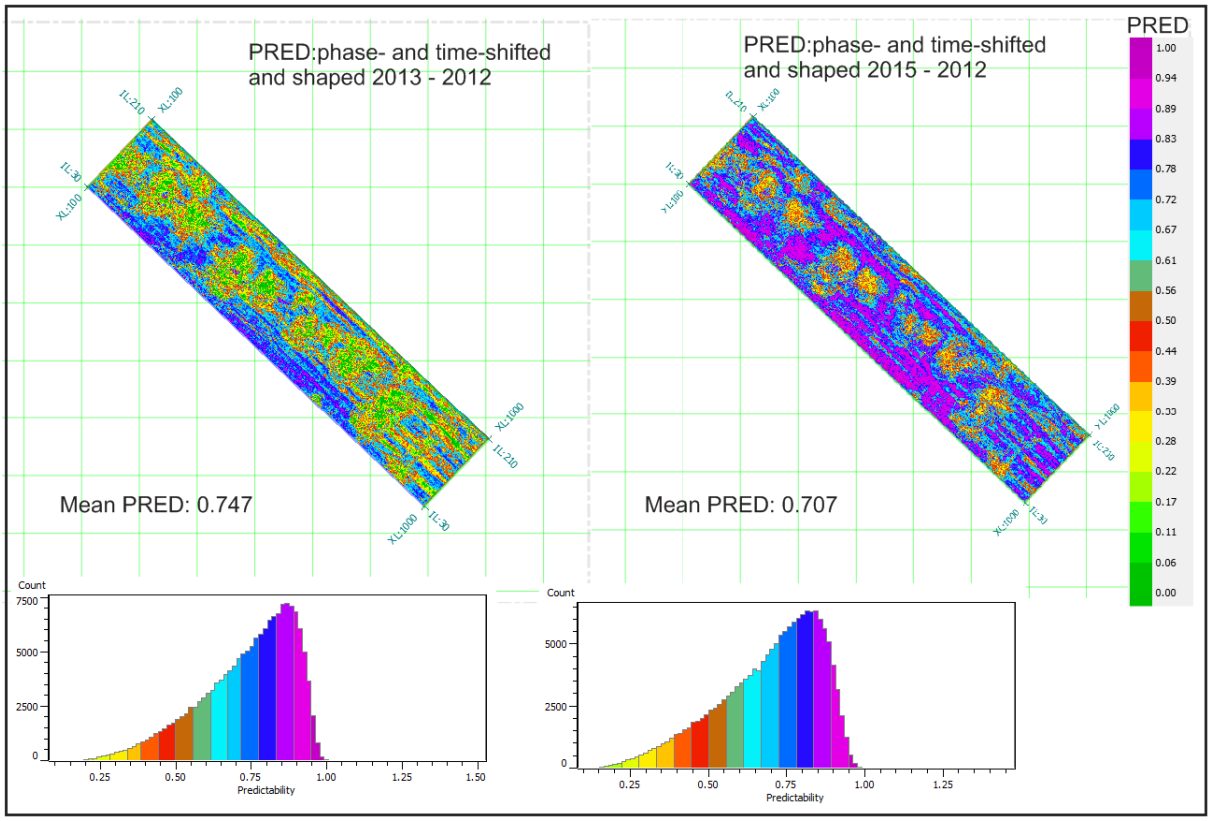

Figure 34 Predictability plots comparing repeat 1 and repeat 2, after shaping filter was applied on the monitors. The values are calculated over the time window: 1700-1900 ms (twt).

Shallow statics

When applying shallow statics the aim is to remove some of the time-shifts caused by near surface effects, and the shifts will be done trace by trace instead of globally, as in the previous steps applied. In this process a time window covering the entire seafloor was used, the window was from -1600 ms and 100 ms (twt) down, to calibrate the adjustment needed to correct for near surface effects.

After the shallow statics correction has been applied (Figure 35) it is clear that the seafloor reflector has become less evident, especially on repeat 1. Another change that is clear after this processing step is that, especially on repeat 1, some reflectors around -1900 ms (twt) have become more pronounced. Repeat 2 only shows small changes in the seismic expression after the shallow static correction was applied, the seafloor has become less pronounced in some areas (Figure 35, bottom).

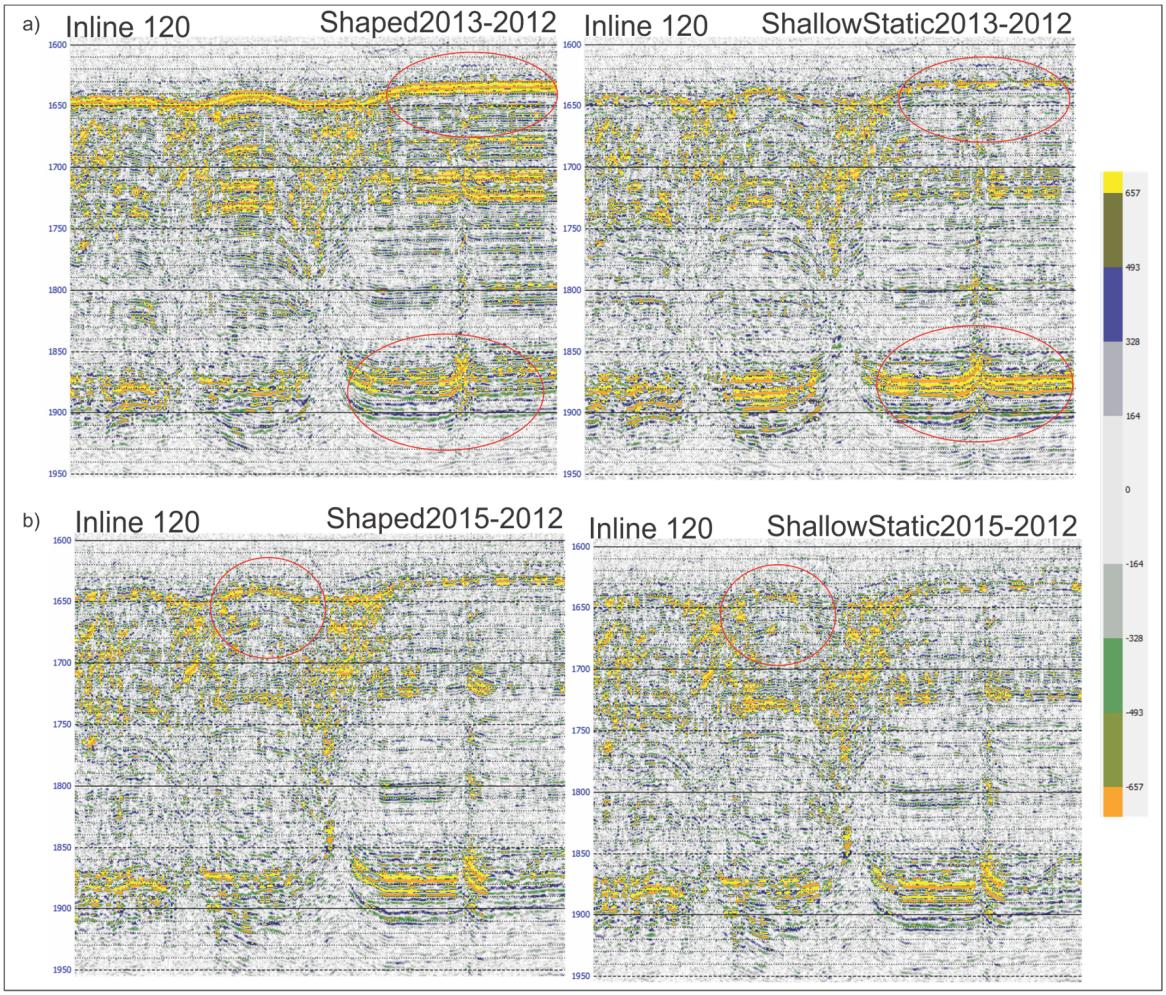

Figure 35 a) Repeat 1, seismic inline 120, before (left) and after (right) shallow static correction on the monitor. b) Repeat 2, seismic inline 120, before (left) and after (right) shallow static correction on the monitor.

After the shallow static correction process was applied the mean NRMS values for repeat 1 and repeat 2 where 0.853 and 0.894, respectively (Figure 36). The window size used was: 1700 + 200 ms (twt).

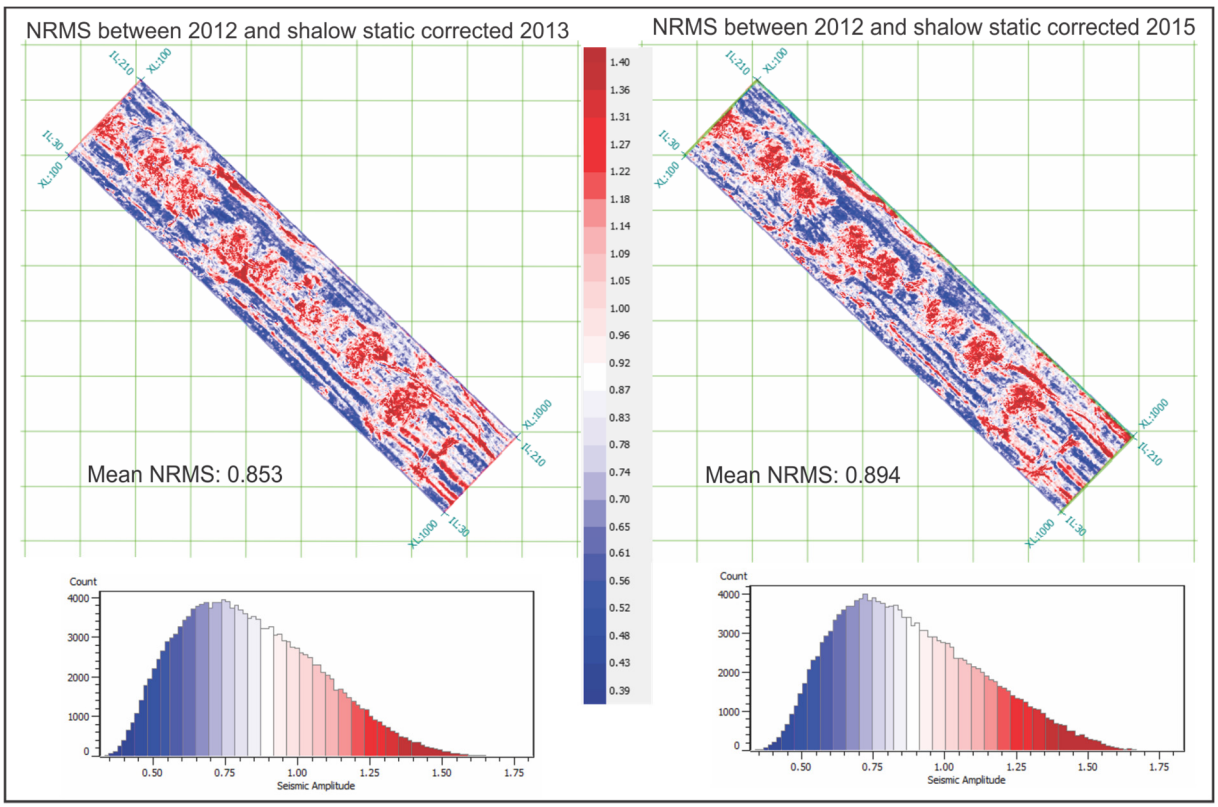

Figure 36 NRMS plots comparing repeat 1 and repeat 2, after shallow static correction on the monitors. The values are calculated over the time window: 1700-1900 ms (twt).

The NRMS values are still moderate to high, but the poorest values >1 occur in the areas where the gas chimneys are located. NRMS values around 0.5, which is quite good (colored blue on the plot) represent the areas where no major gas chimneys are present. All in all the NRMS values are quite high, but over 50% of the 3D survey area are affected by fluid flow features.

The predictability in repeat 1 and repeat 2 has not changed after the shallow static correction was applied (Figure 34, Figure 37). Still, the predictability is significantly better in the zones outside of where the gas chimneys are located compared to the predictability values right above the chimney conduits.

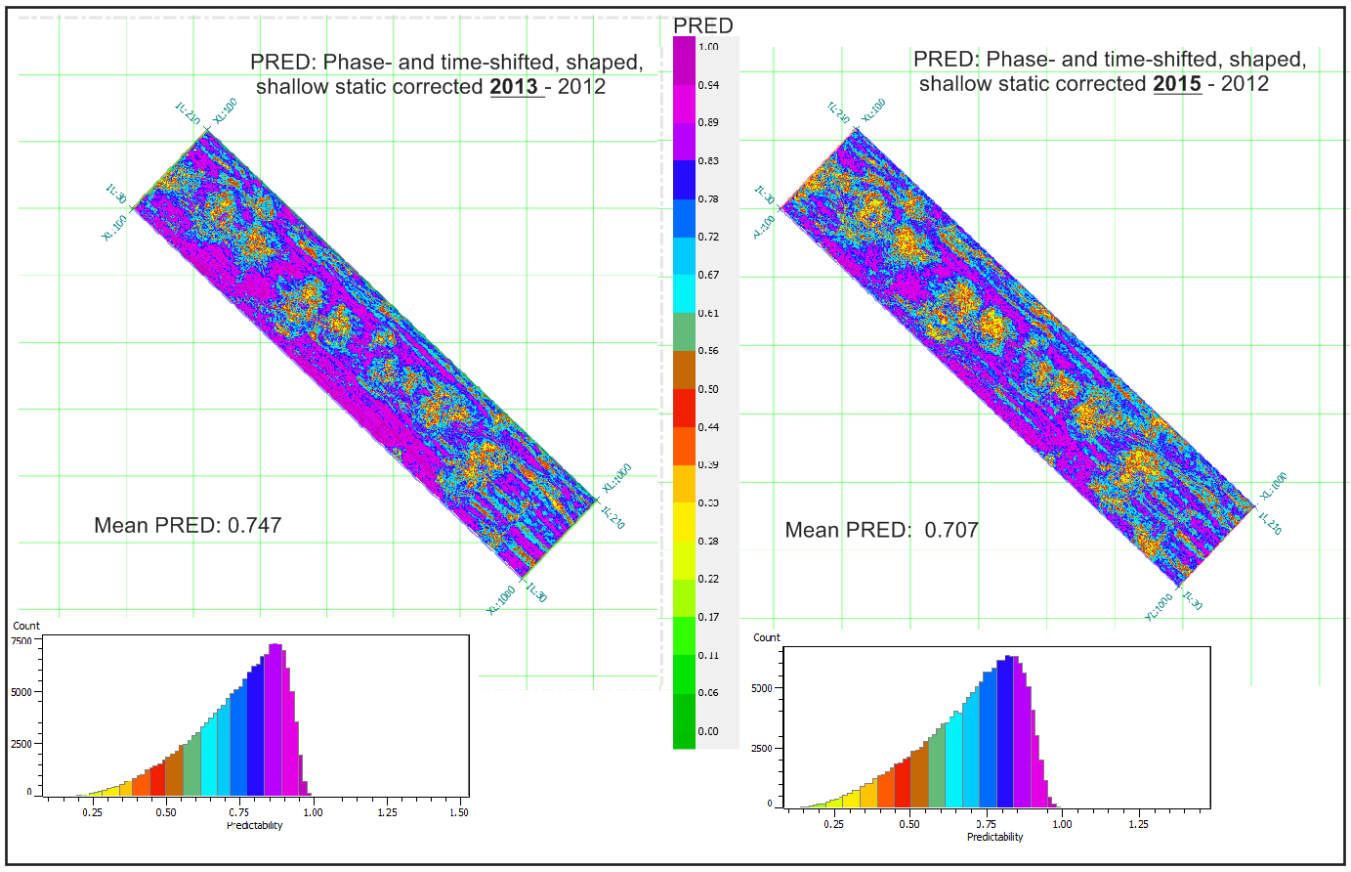

Figure 37 Predictability plots comparing repeat 1 and repeat 2, after shallow static correction on the monitors. The values are calculated over the time window: 1700-1900 ms (twt).

Time-variant shift (Repeat 1)

For calibrating the time-variant-shift a window from -1700 and 200 ms (TWT) down was set and several correlation windows was used in the calibration, the parameters used was as followed: Correlation window length: 20, correlation window step: 0.25 and maximum shift 5 ms.

The area around the BSR reflector that became more pronounced after the shallow static correction was applied (Figure 38) is now significantly reduced on the difference data.

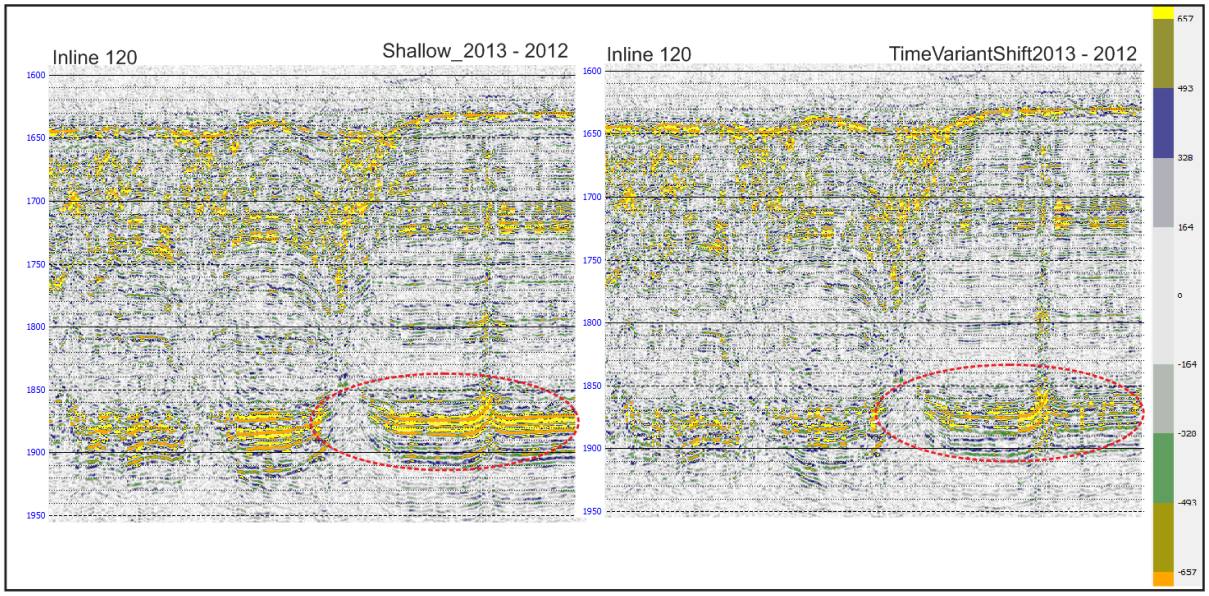

Figure 38 Repeat 1, seismic inline 120, before (left) and after (right) time-variant-shifts was applied on the monitor.

After the time-variant shift, which is supposed to remove the time-shifts due to fluid flow in the subsurface, the mean NRMS value of repeat 1 is now 0.718 (Figure 39), this is an improvement of 0.135 in mean NRMS value since before this process was applied (Figure 36). It is important to state that the time-variant shift processing step ideally uses, on conventional seismic used in the oil industry to calculate a reservoir depletion, a certain time-window based on a horizon linked to the reservoir to calculate the required time-shift needed to put reflections back in proper time and to correct for pull-up and push-down effects, but in this case, with abundant fluid flow features, this is impossible. Still, hopefully the time-variant shift applied on the 2013 data helped to increase the repeatability of repeat 1.

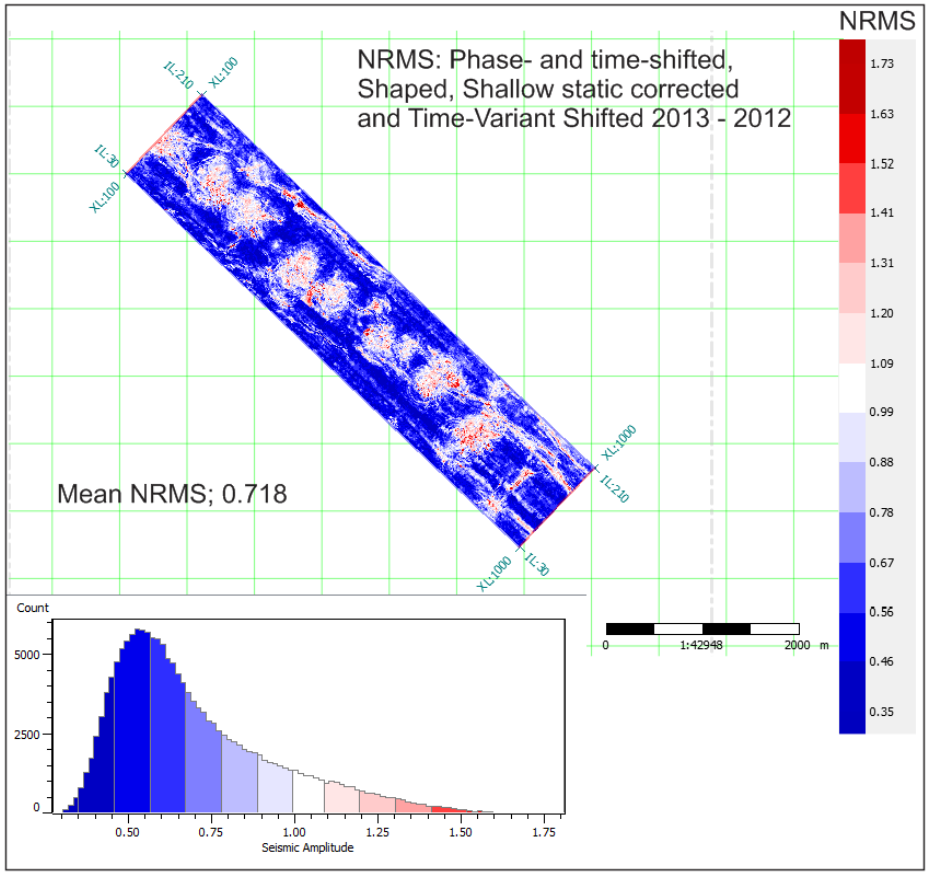

Figure 39 NRMS plot of repeat 1, after time-variant-shift was applied to the monitor. The values are calculated over the time window: 1700-1900 ms (twt).

The program, Hampson-Russel Pro4D, was not able to perform a time-variant shift on repeat 2. Despite several tries the error could not be resolved. The time-variant shifts improved matching of repeat 1 slightly, so we assume that this might have also happened for repeat 2. So unfortunately, this error might give a slight limitation for comparison between the two final time-lapse dataset which includes the 2013-2012 difference, repeat 1, and the 2015-2012 difference, repeat 2.

Final result

The final processed seismic represent:

- 2012 survey, base survey, unchanged.
- 2013 survey that has been processed with the following corrections; phase- and time-shift, shaping filter, shallow static correction and time-variant shift.
- 2015 survey that has been processed with the following correction; phase- and time-shift, shaping filter, shallow static correction.

The distribution of the highest NRSM values fits well with the location of the gas chimneys (Figure 40). NRMS values above 1.5 is detected above some of the chimneys, while in the regions that are not so much affected by the fluid flow have NRSM as low as 0.35. This shows the effect the complexity of the chimneys have on the NRSM value. The final mean NRMS values are: 0.718 for repeat 1 and 0.894 for repeat 2 (Figure 40).

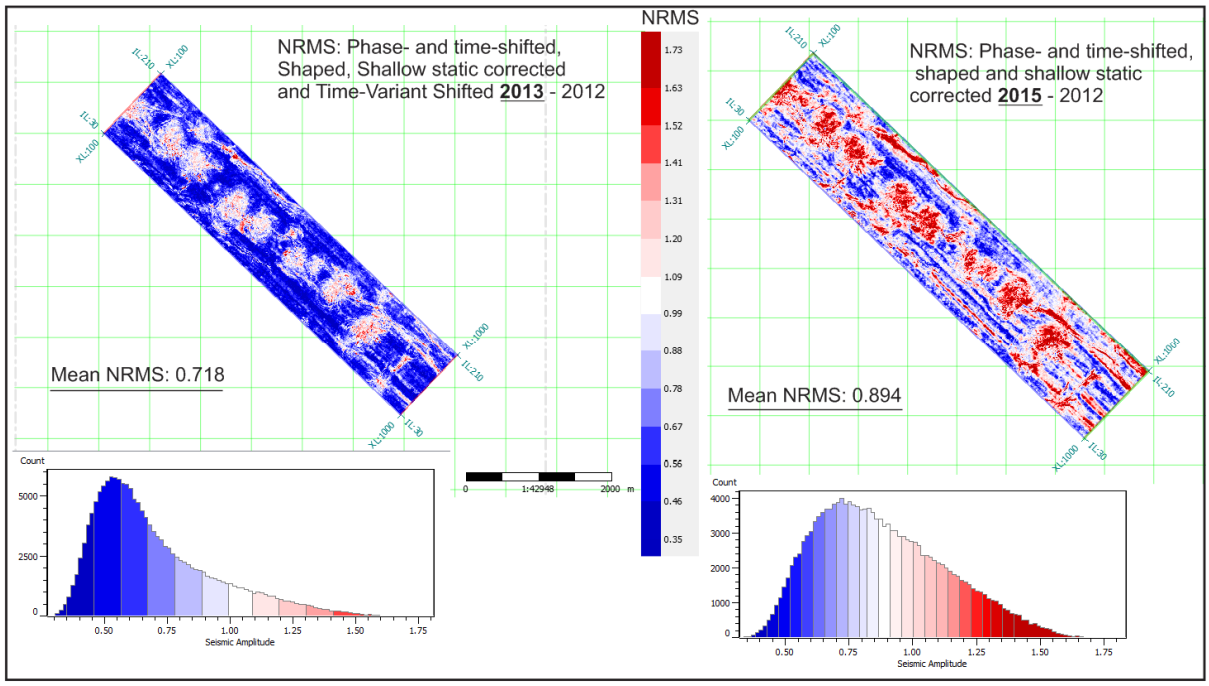

Figure 40 Final NRMS plots comparing repeat 1 and repeat 2. The values are calculated over the time window: 1700-1900 ms (twt).

The predictability, in both of the differences, has not changed significantly from initial to final result. Predictability is more sensitive to noise and distortion than to time-shifts, so even after big corrections in time-shift, the predictability is not expected to have changed a lot if there is a lot of noise in the data. Final predictability values are 0.788 for repeat 1 and 0.707 for repeat 2 (Figure 41).

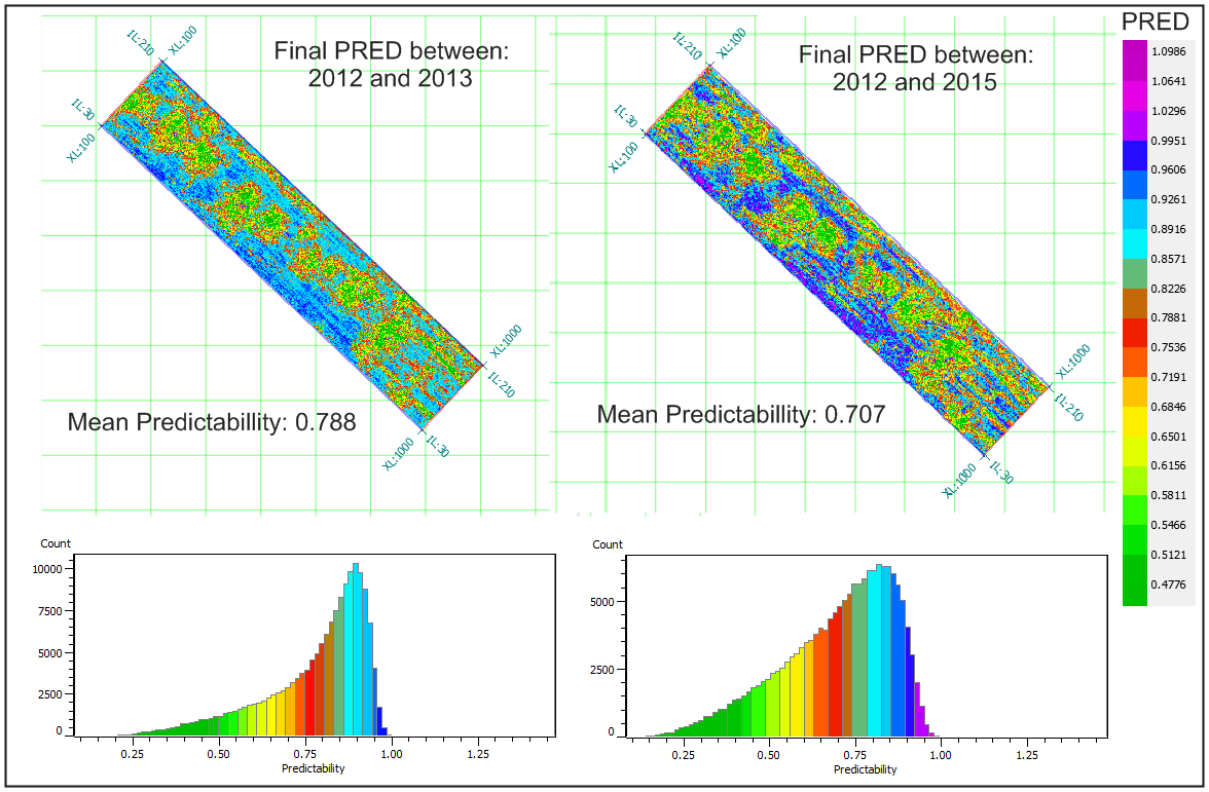

Figure 41 Final Predictability plots comparing repeat 1 and repeat 2. The values are calculated over the time window: 1700-1900 ms (twt).

The time-shifts present in the two repeats after the 4D processing are significantly less than initially (Figure 25,Figure 42). Some striping effect is still to be seen (Figure 42), especially on repeat 2, but these have been drastically reduced, representing only small shifts, less than 1 ms. The greatest time-shifts are over the areas of where the gas chimneys are located. Repeat 1 has a mean time-shift of 0.0097, while repeat 2 has a mean time-shift of -0.097.

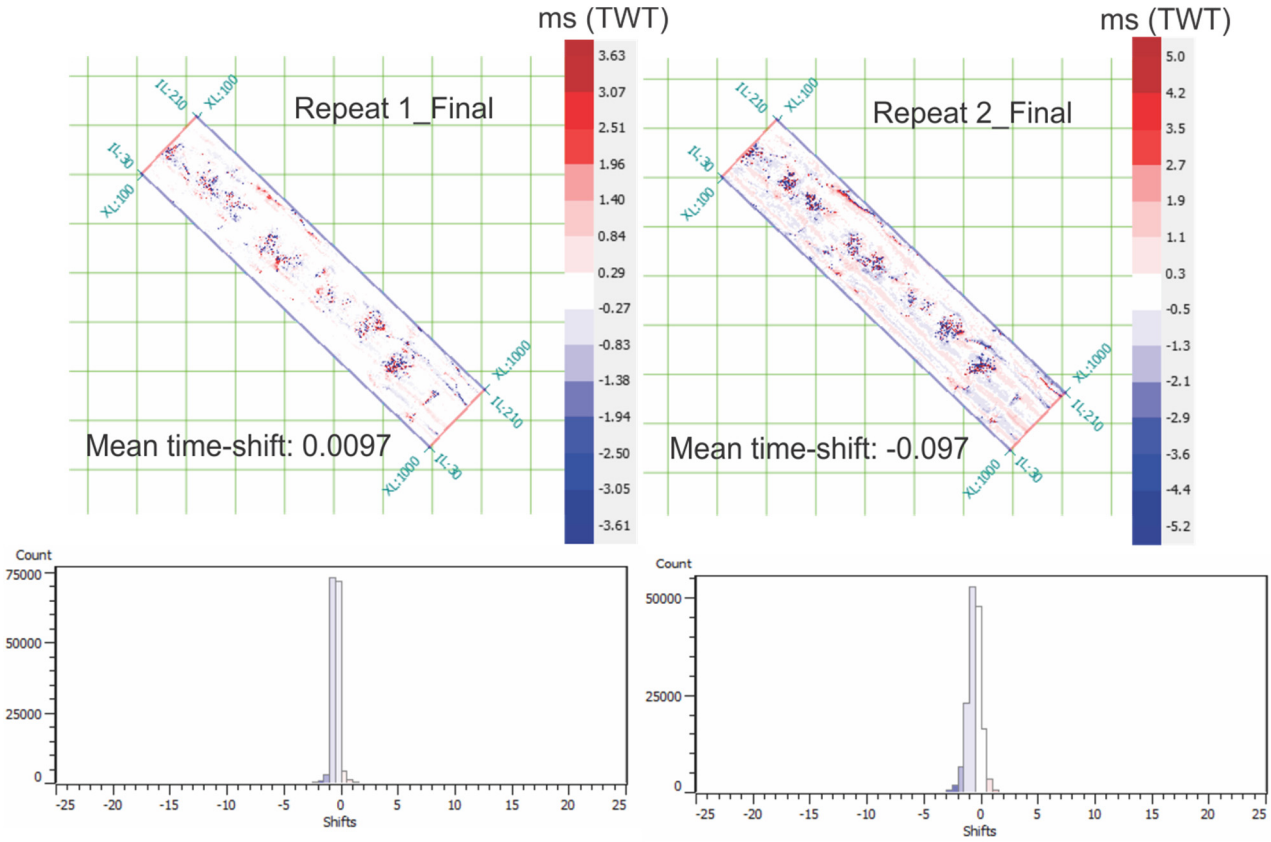

Figure 42 Final Time-shift plots comparing repeat 1 and repeat 2. The values are calculated over the time window: 1700-1900 ms (twt).

Cross-correlation Values as high as 0.9 is observed outside the area of chimney conduits, while the poorest values over the chimneys are below 0.2 (Figure 43). Repeat 2 have a lower mean cross-correlation value than repeat 1, and the reason for this seem to be the poor values in the areas of the chimneys.

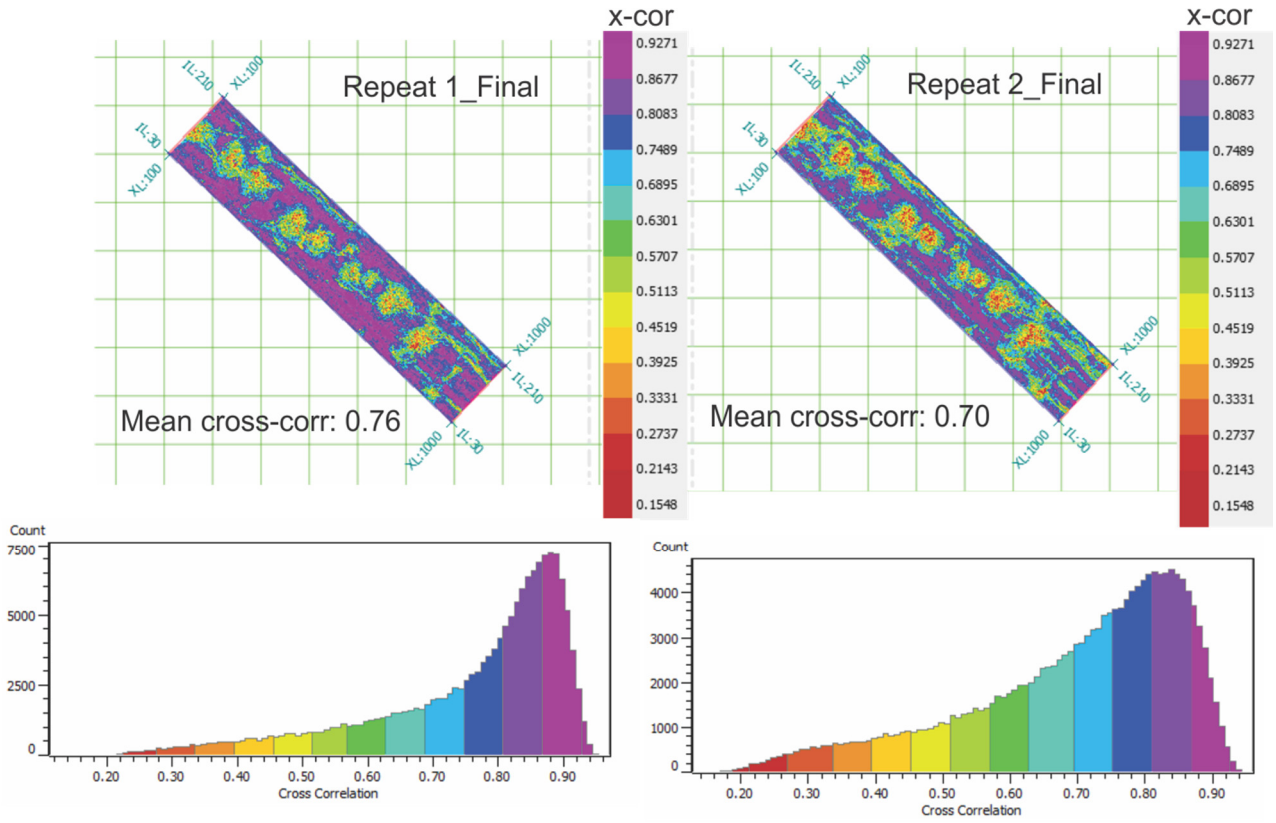

Figure 43 Final cross-correlation plots comparing repeat 1 and repeat 2. The values are calculated over the time window: 1700-1900 ms (twt).

To sum up the whole processing sequence all the QC metrics for each step and the threshold used during the processing are presented in table 1.

Tabell 1 QS metrics and threshold used in the full processing workflow. All QS metrics are calculated from the time window: 1700+200 ms (TWT).

	NRMS	PRED	X-correlation	Time-shift	Threshold
Initial	Rep1: 1.651 Rep2: 1.545	Rep1: 0.752 Rep2: 0.714	Rep1: 0.533 Rep2: 0.697	Rep1: 1.359 Rep2: 3.759	
Phase- & time-shift	Rep1: 1.788 Rep2: 0.824	Rep1: 0.752 Rep2: 0.712	Rep1: 0.545 Rep2: 0.696	Rep1: 1.03 Rep2: 0.057	X-corr: 0.6 Time-shift: 5 ms
Shaping filter	Rep1: 0.865 Rep2: 0.924	Rep1: 0.747 Rep2: 0.707	Rep1: 0.728 Rep2: 0.700	Rep1: -0.14 Rep2: 0.056	X-corr: 0.5 Time-shift: 2 ms
Shallow static	Rep1: 0.853 Rep2: 0.894	Rep1: 0.747 Rep2: 0.707	Rep1: 0.728 Rep2: 0.700	Rep1: 0.043 Rep2: -0.097	Trace by trace. Calibration window: 1600 + 100 ms (TWT)
RMS-Factor	-	-	-	-	The repeats were amplitude balance.
Time-variant shift	Rep1: 0.718 Rep2: -	Rep1: 0.788 Rep2: -	Rep1: 0.76 Rep2: -	Rep1: 0.0097 Rep2: -	X-corr: 0.8 Time-shift: (-1,1)
Final	Rep1: 0.718 Rep2: 0.894	Rep1: 0.788 Rep2: 0.707	Rep1: 0.76 Rep2: 0.700	Rep1: 0.0097 Rep2: -0.097	

4.3 4D interpretation

In the next section the 4D results are presented. The 2012 survey are used as a base and the 2013 and 2015 surveys are monitors. This means that all the corrections done during the processing workflow was done on the 2013 and 2015 surveys, based on the similarities/dissimilarities compared to the base, 2012 survey. The 4D data will represent the monitor surveys subtracted from base survey.

RMS volume attributes are used in the presentation of the 4D data, the strength of the amplitudes are highlighted independently of signal of the reflection.

Both repeats (2013-2012 and 2015-2012) have abundant of signals left after the 4D processing. The general trend is that most of the seismic reflections are present around the BSR, around and inside the conduits of the gas chimneys and within layers connected to the chimneys. There are still some non-fluid related changes in the 4D data, this will be discussed later on. Still, it is quite easy to see that most of the strongest reflections, that bright up from repeat 1 to repeat 2, are inside and around the interpreted chimneys and beneath the BSR (Figure 44).

However, the 4D matching was most difficult in the areas where a gas chimney occurs in the subsurface with NRMS values above 1 and PRED values below 0.7. These results might not allow interpreting detailed small-scale 4D changes in the subsurface that relate to actual changes in fluid content. In order to achieve that, more care has to be taken in the principal 3D seismic processing of the data (e.g. seismic phases, migration velocities) as well as improvements and parameter testing in the 4D processing, focusing on individual structures, that may lead to a better overall match between baseline and monitor. Such 4D processing focusing on a specific chimney structure was beyond the time frame for this thesis. Nonetheless, this thesis tries to explain some of the gross changes in the time-lapse data mentioned above.

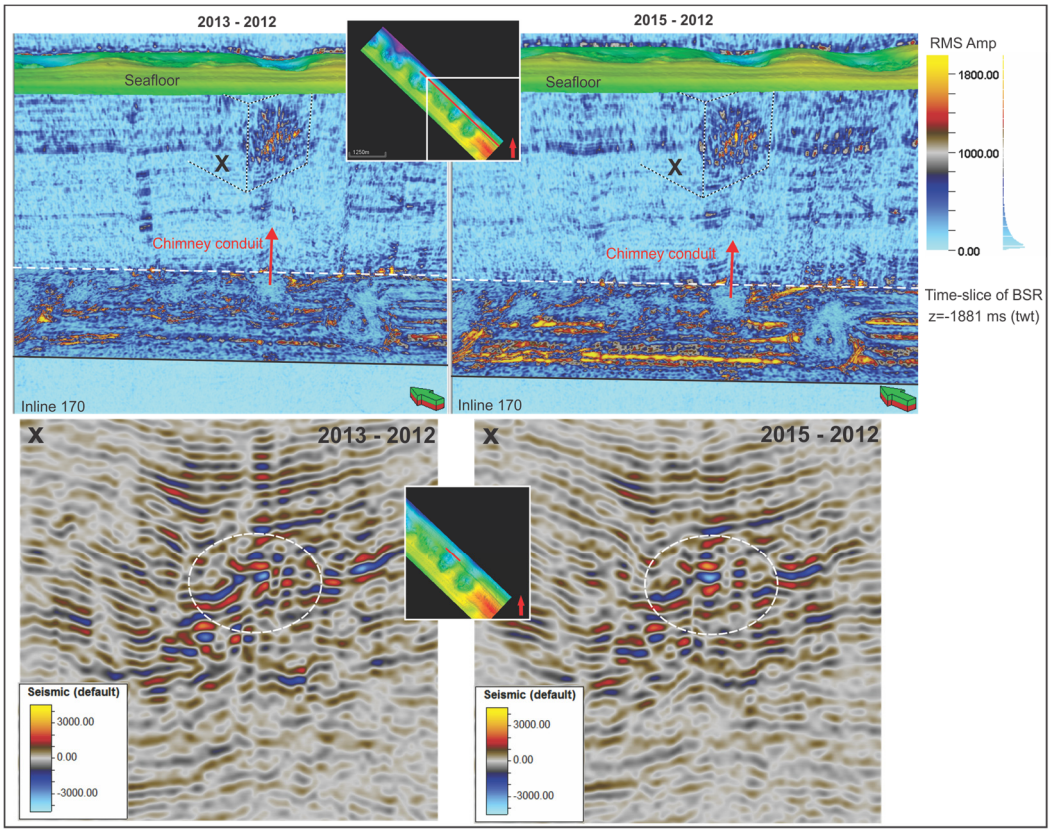

Figure 44 Top: RMS amplitude seismic of repeat 1 (left) and repeat 2 (right), inline 170, time-slice at -1881 ms (twt) and seafloor surface. Bottom: seismic slice of repeat 1 and repeat 2 over zoomed in area X.

From Figure 45 the amplitude distribution in the difference volumes over the shallowest part are displayed. The window used to calculate the RMS amplitude attribute map is from 1650 to 1750 ms (TWT). Simply assuming a seismic velocity of 1500 m/s, this is approximately a depth window from 0 to 70-80 meter below seafloor. The shallower parts of the seismic are the most confident areas to interpret as it less affected by attenuation and scattering effects in the chimney structures and therefore also less noisy compared to the deeper parts. The strongest amplitudes are concentrated around and within the chimneys, indicated by red and yellow colors on figure 42. All of the chimneys bright up in all of the repeats. The most chaotic patterns are observed on the two easternmost chimneys, the amplitude distribution have a larger extent and the amplitude values are higher, especially on repeat 2.

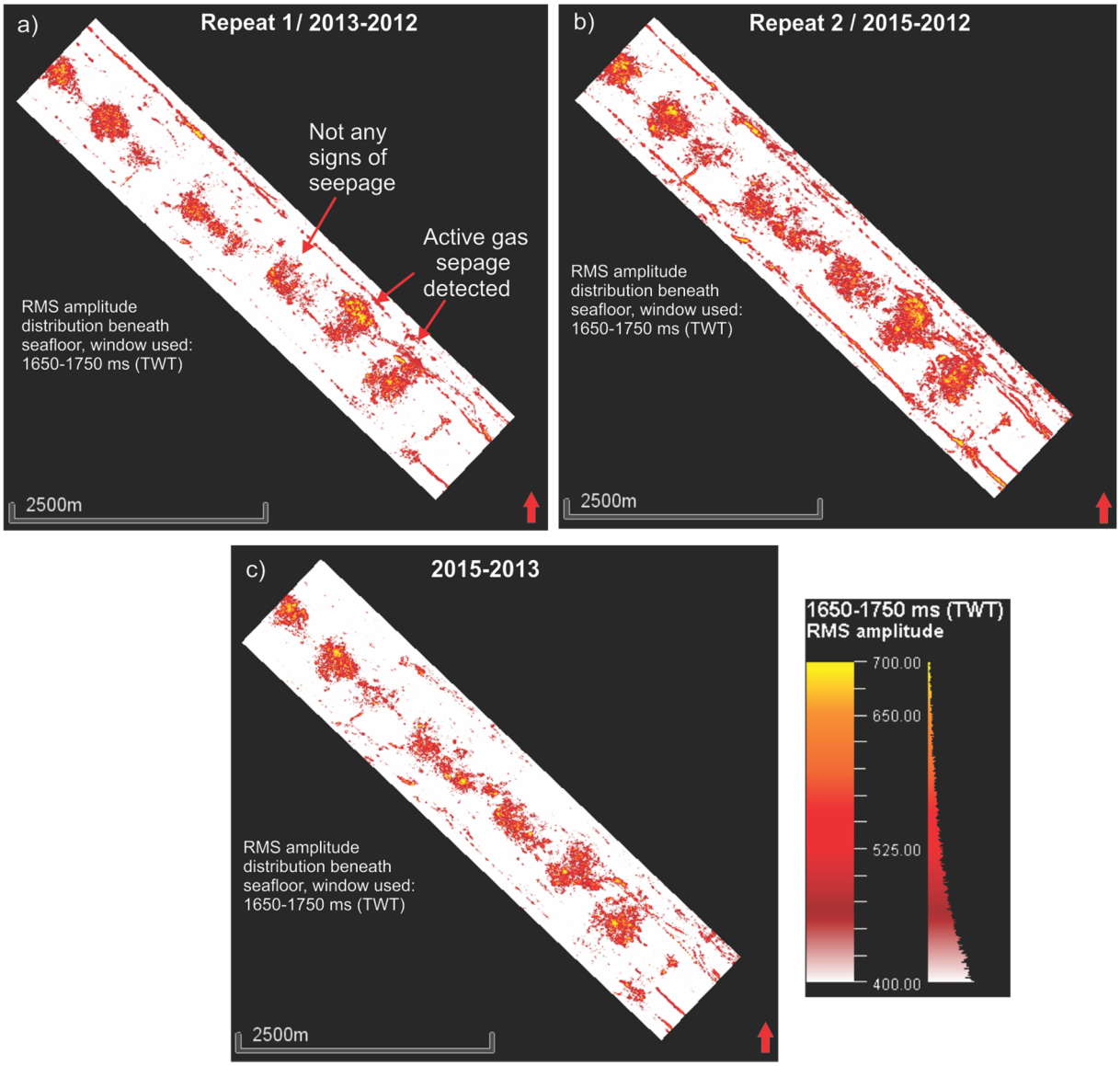

Figure 45 RMS amplitude map calculated over the time window: 1650-1750 ms (TWT). a) Repeat 1 / 2013-2012 difference. B) Repeat 2 / 2015-2012 difference. C) 2015- 2013 difference

The anomalously high amplitudes that are crossing the disrupted, stratigraphic layerings within the easternmost chimney (Figure 21) are also very noticeable in the time-lapse data (Figure 46). The bright spots occur along the same path as for the interpreted fluid pathways in the 3D seismic (Figure 20). From repeat 1 to repeat 2 there is no evident changes in the architecture of the gas conduits in the upper part of the chimney. The seafloor reflector and most of the other continuous reflectors have been drastically reduced, enabling an emphasis on 4D changes.

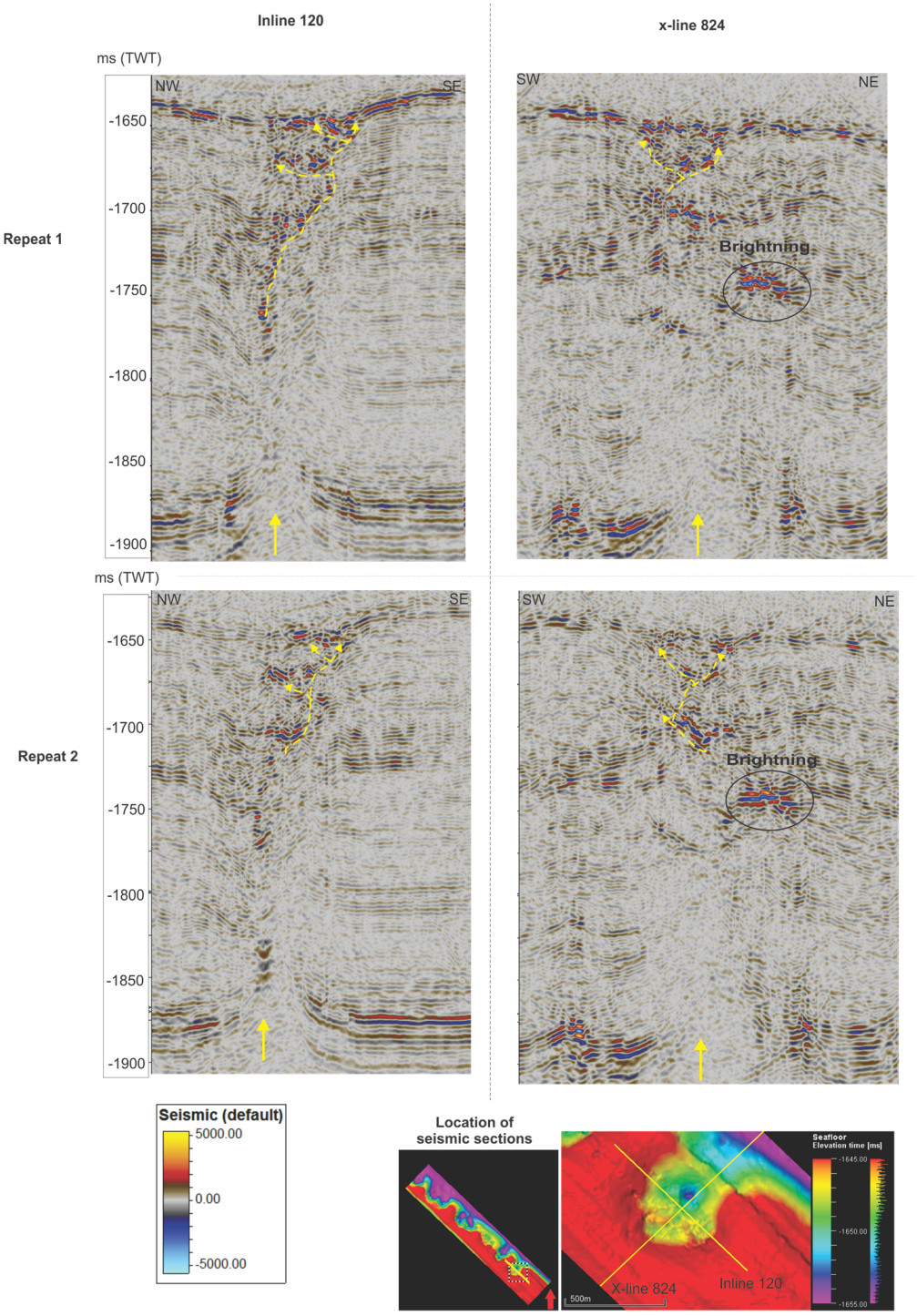

Figure 46 seismic slices, inline 120 and x-line 824, over the easternmost chimney. Both repeat 1 and repeat 2 are represented. Yellow arrows represent fluid migration pathways.

The bright amplitudes, shown on image above, terminate right beneath small depressions on the seafloor. A cluster of anomalously bright amplitudes are also detected on x-line 824 (Figure 46).

The similarities between the 4D data (Figure 46) and the 3D data (Figure 21) are the bright amplitude anomalies, while the reflectors representing the seafloor and other stratigraphic layers present in the 3D data have been drastically reduced by the 4D processing. This can be an indicator that the strongest amplitudes present in the seismic data are due to actual fluid related changes and that movement of gas in the time between 2012 and 2015 are the reason for several of the amplitudes detected. Some noise is expected to be present, but these have a more chaotic and random distribution and not as strong as the amplitudes observed, meaning that the amplitude anomalies can be interpreted as actual changes due to fluid flow.

The third chimney, from southeast (Figure 45), has not shown any signs of being active from previous studies done on the eastern segment of the Vestnesa Ridge (Bunz et al., 2012; Smith et al., 2014a). Still, also in this chimney the amplitudes bright up beneath the seafloor reflector on all of the 4D differences (Figure 45).

Figure 47 displays the internal structure of the third chimney from southeast. The seafloor and the BSR reflector are more present on repeat 1 than repeat 2, this is not considered as an actual 4D response. Stacking of bright amplitudes that terminate below the seafloor, like the ones detected on the easternmost chimney (Figure 46), is not present within this chimney conduit. The amplitudes present are a bit patchy and more chaotic compared to the amplitudes detected in the easternmost chimney (Figure 46). There are none anomalously high amplitudes right beneath the seafloor reflector (Figure 47). It appear as the repeat surveys contains more noise than the 2013 survey initially did (Figure 47) and therefor makes it difficult to interpret the small amplitudes present in the repeats as true 4D responses.

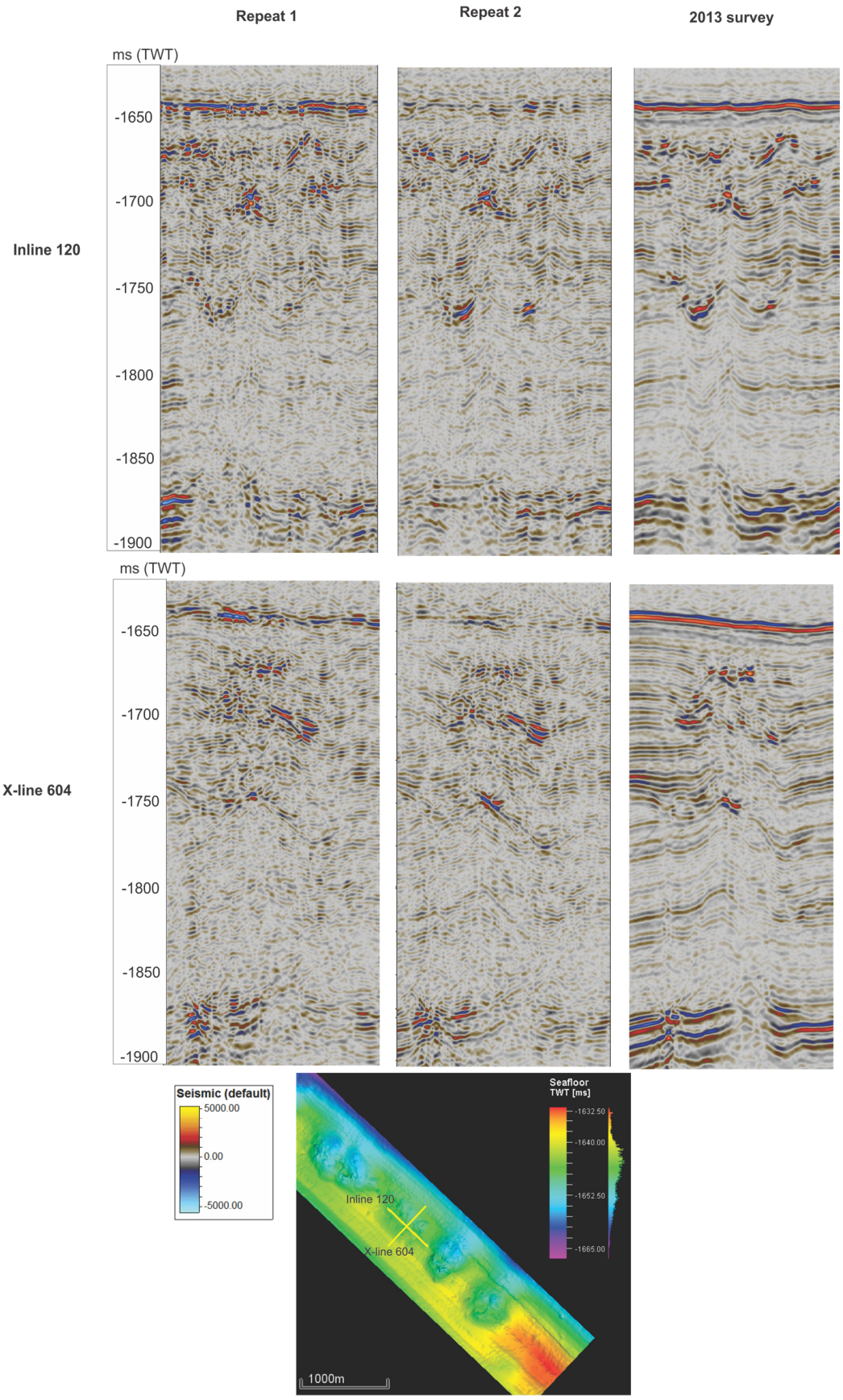

Figure 47 seismic slices, inline 120 and x-line 604, over the third easternmost chimney. Repeat 1, repeat 2 and 2013 survey. Overview map showing location of seismic lines

It is a trend in two repeats, 2013-2012 and 2015-2012 , that the amplitudes present in the shallower part of the chimneys (Figure 48, red circles) and beneath the BSR (Figure 48, white circles) bright up from repeat 1 to repeat 2. The seafloor reflector is more pronounced on repeat 1 compared to repeat 2. The amplitude anomalies are distributed mainly above the black arrows (indicating the location of where the chimneys pierce the BSR on Figure 48).

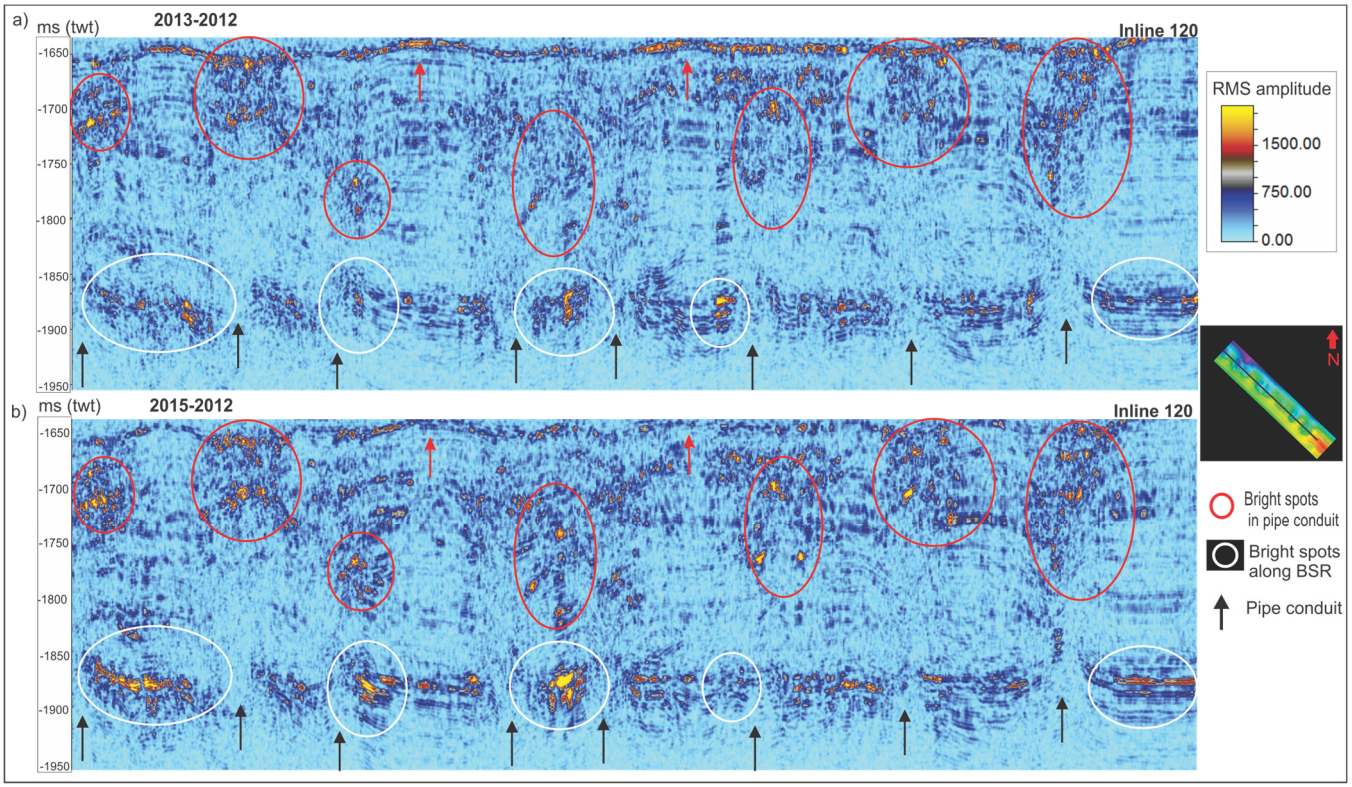

Figure 48 a) RMS volume of Repeat 1, 2013-2012. b) RMS volume of Repeat 2, 2015-2012. Red circles highlight bright spots in and around the interpreted chimneys conduits, white circles highlight changes/bright spots in the BSR region, black arrows indicate chimney conduits.

Figure 49 shows a seismic section located on the northeast margin of the survey area. This seismic section, inline 180, is chosen as an example because it is outside the zones that are under the most influence by the fluid flow since no major gas chimneys are detected. There seem to be only a small interruptance in the continuity of the BSR reflector, inside the box A-B. There is a brightening of amplitudes from repeat 1 to repeat 2 (Figure 49). The seafloor reflection and stratigraphic boundaries are fairly diminished on the difference data suggesting that 4D processing worked well in this part of the survey and that the brightening beneath the BSR originates from actual fluid induced changes and is not due to acquisition or processing

artifacts present in the repeats. Other amplitude anomalies are also present but these are not as strong as the amplitudes detected beneath the BSR.

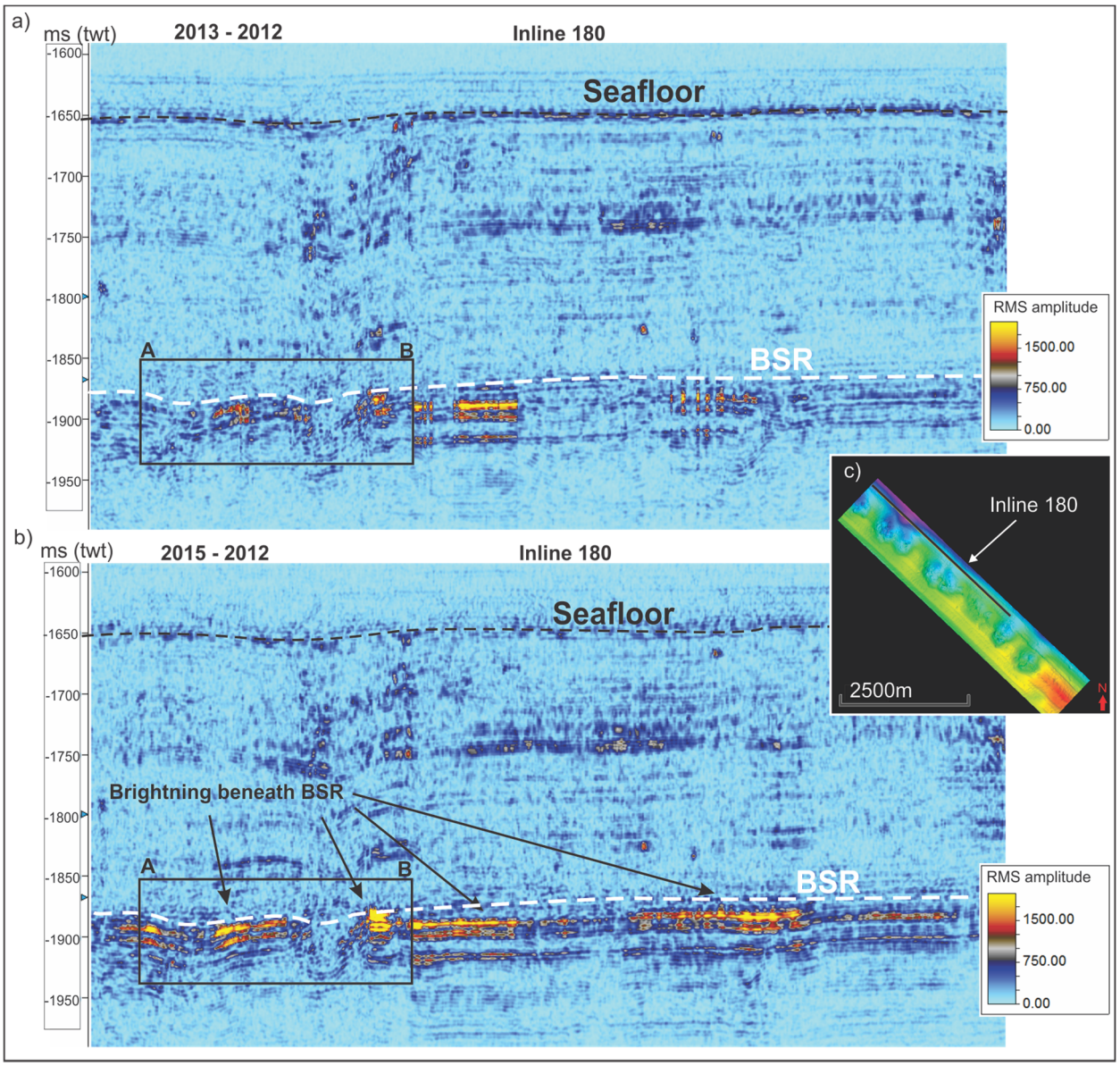

Figure 49 a) seismic 4D, 2013-2012, inline 180. b) Seismic 4D, 2015-2012, inline 180. Black arrows indicate areas of brightening beneath the BSR. c) Overview map over seismic line on the 3D survey area. A-B : zoomed in seismic section displayed in next figure

The strength and continuity of the seismic reflections are stronger on repeat 2 compared to repeat 1 (Figure 49, Figure 50). The thickness of the layer over which the amplitude anomaly occurs is quite significant and may indicate the extent/thickness of the free-gas zone beneath

the BSR. The fact that the amplitudes within the layer bright up from repeat 1 to repeat 2 may point towards further accumulation of free gas beneath the BSR.

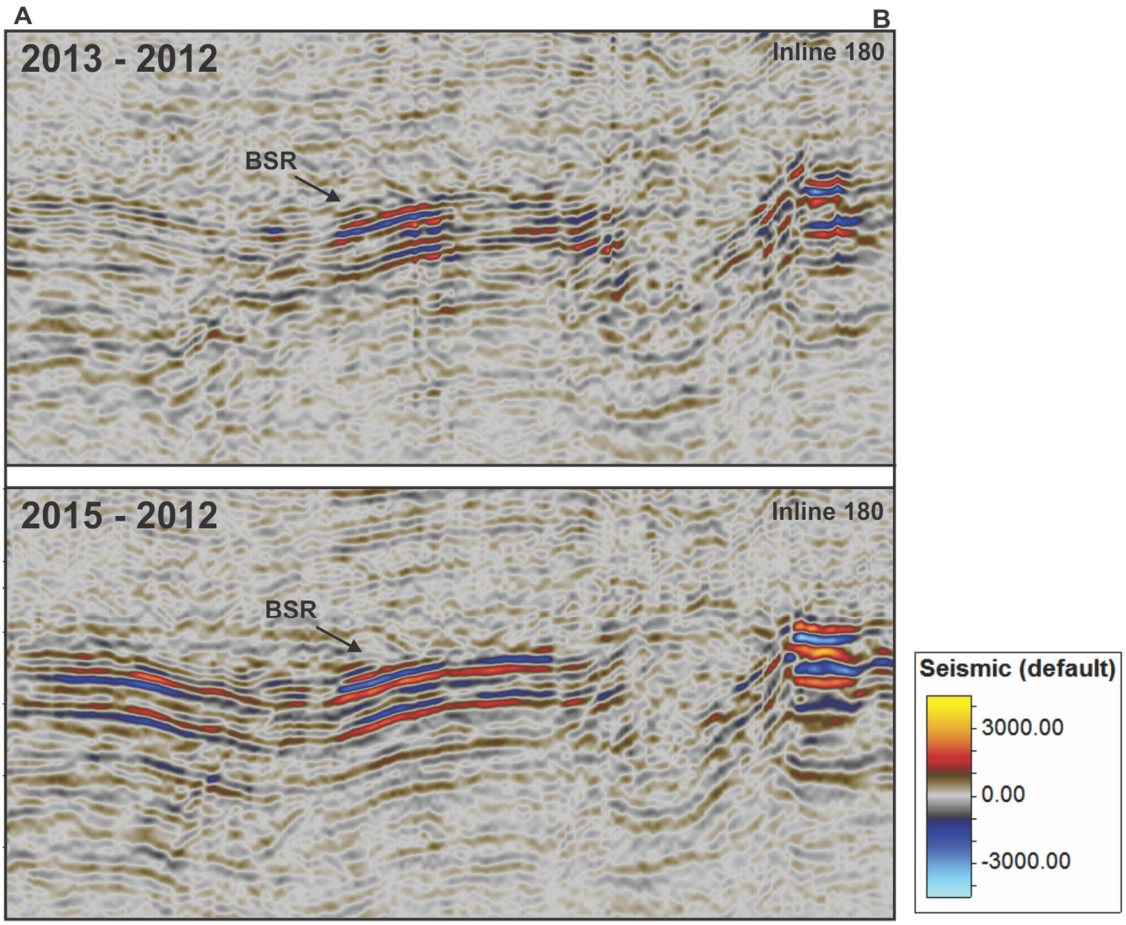

Figure 50 zoomed in area, A-B, Inline 180. Top: Repeat 1, 2013-2012. Bottom: Repeat 2, 2015-2012.

5 Discussion

5.1 Discussion of the 4D processing result

A lot of effort has been put into obtaining the best possible 4D result. The 4D processing is an iterative process, as it requires a lot of try and failing. Before interpreting the final 4D results it is important to discuss the different circumstances affecting the result as not every residual signal is believed to be a genuine 4D difference. Factors than can contribute to obscure the 4D result are inadequate 3D processing, as we have observed large phase differences initially for the base and monitors. In addition, there are some inconsistencies in the reflection strength between the base and the two monitors. Because this is high frequent seismic, containing frequencies up to 350 Hz, it is believed that the surveys contain high amounts of initial noise that will affect the final repeatability. There are also uncertainties to what kind of changes that is expected to occur between the different repeats and how detectable these changes are.

By use of high frequency P-Cable data we cannot expect the same final results in regards of NRMS, predictability and correlation values as seen in conventional seismic processing of time-lapse. The frequency bandwidth are much wider and the high frequencies are very sensitive to small changes in the subsurface. The peak frequency at 175 Hz (Figure 23) will lead to well mapping of small structures, and hence the difference between the surveys will be quite apparent in the final time-lapse. High frequencies are also very sensitive to non-fluid related changes such as acquisition parameters and other degrading effects originating from conditions during acquisition (Johnston 2013). The results achieved in regards of mean NRMS is 0.718 for repeat 1 and 0.894 for repeat 2 (Figure 40). This is most likely not solely due to actual changes in the subsurface, but also originates due to inconsistencies in acquisition and frequency related noise. During acquisition of the base (2012), the weather conditions were rougher compared to conditions in 2013 and 2015 (Stefan Bünz, pers. Com.). From Figure 51 we can see that here is in general more energy and more noise in the 2012 survey compared to the 2013 and 2015 surveys, the figure shows that the stratified layers for the base (2012 survey) have generally stronger reflection strength, and the energy looks a bit more aggressive compared to the monitor surveys (2013 and 2015). It is important to be aware of the initial condition of the 2012 survey as it was used as a reference volume for the processing, and the monitors were corrected based on similarities/dissimilarities to the 2012, base survey.

The fact that the mean NRMS value is lower/better for repeat 1 than for repeat 2 (Figure 40) could be because the 2013 survey clearly has the best quality and overall the least noise (Figure 22).

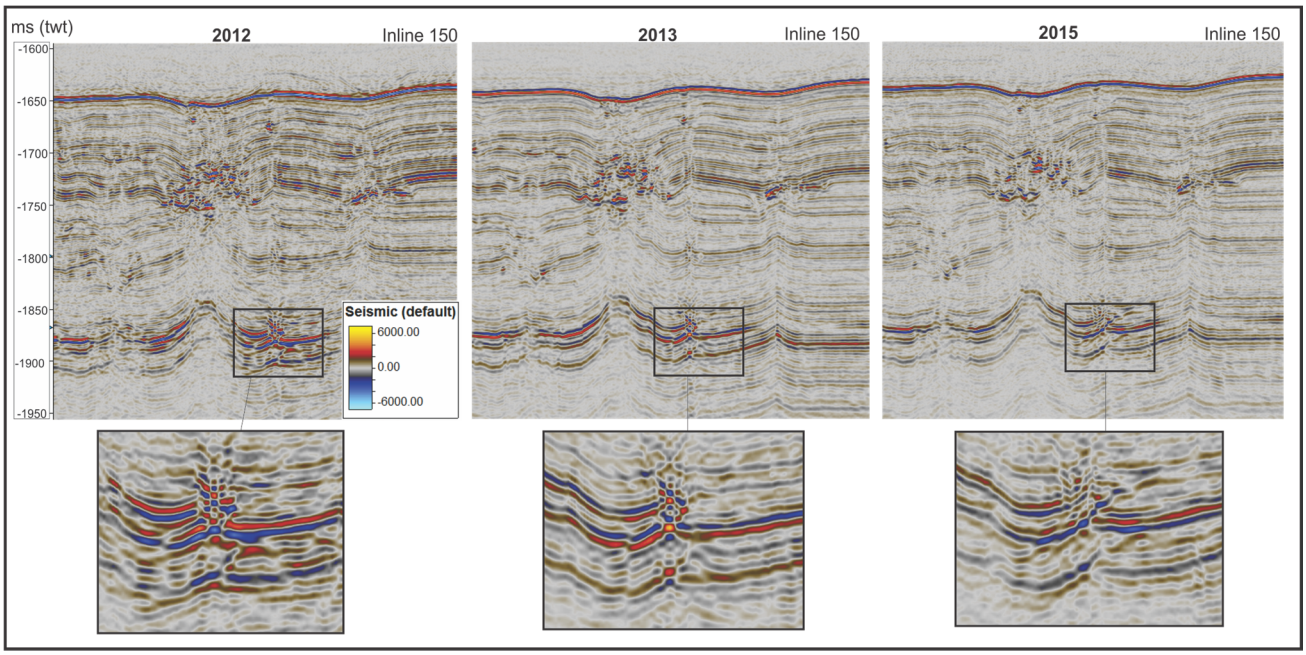

Figure 51 seismic slices of the initial state of the 3D seismic acquired in 2012, 2013 and 2015. Zoomed in areas highlight the difference in general energy of the reflections and noise within the seismic in the three different surveys.

Acquisition effects are present on the initial NRMS plots (Figure 27). These acquisition effects can originate from different factors: the temperature of the water can change over time, the tidal forces or weather conditions may influence the depth of the source/streamer. This acquisition effect represented by the striping detected on several QC-plots indicate that different Inlines have a shift in time compared to adjacent lines. If these acquisition striping effects are present in the 2012, base survey, they will still be present after the final processing have been conducted. These acquisition/striping effects on the seismic data should ideally be processed away in the 3D processing because they may make it more demanding to achieve repeatable 4D data.

The striping effect is not visible on repeat 1 after 4D processing, but on repeat 2 this effect is still present. The time-variant-shift correction is the process that removed the striping effect on repeat 1. It was not possible to run the time-variant-shift correction on repeat 2 due to some

complications in the software (that was not possible to solve). Time-shifts that are necessary to put reflections in their right location in repeat 2 may have been lost due to this error. It is inferred that a more repeatable result would be obtained for repeat 2 if the time-variant process was properly conducted on this repeat as well.

It is important to be aware of that within the survey area there are at least 8 major gas chimneys that interrupts the stratigraphic layers in the entire vertical column, and over half of the total 3D survey area are affected by these dynamic systems. It is difficult to achieve a god repeatable result in areas with complex geology, which is the case with the Vestnesa surveys. By looking at the final NRMS plot (Figure 40) it is evident which areas that are most affected by fluid flow, it is also evident that the areas that does not seem to be affected by fluid flow has significantly lower NRMS, as low as 0.5, while the NRMS estimate over the chimneys goes up to 1.5.

The predictability is more sensitive to noise and distortion than to time shift. So even if the time shift is big, the predictability can still be good (Johnston 2013). It is interesting to notice that the initial predictability of 0.752 in mean for repeat 1 and 0.714 in mean for repeat 2 is quite good values, these values does not change a lot during the processing workflow. In repeat 1 the mean PRED value increases a bit, from 0.752 to 0.788, while the mean PRED value in repeat 2 decreases a bit, from 0.714 to 0.707, during the full processing workflow (Figure 26, Figure 41). The fact the PRED value is so high to start with and changes little from initial to final, and the fact that the NRMS decreases significantly during the processing, can indicate that the overall similarities between the datasets are quite good on the final 4D data, but that the result is affected by high noise-levels. By running an initial quality check on the three different seismic datasets used in this thesis (Figure 51), it is quite easy to detect that the 2012 survey, which is also used as a reference volume, contains a lot more noise than the two monitor surveys: 2013 and 2015, this could be the main contributor for not getting an even higher initial PRED and for not achieving even lower NRMS in the end. The small change in PRED from initial to final result can indicate that the noise that was present in the differences, still are present after the processing workflow was conducted, which is quit logic if the main source for noise was in the 2012 survey and as this survey is not changed during the processing.

There are still many seismic reflections that does not originate from actual changes in the subsurface in the 4D data (Figure 52). The seafloor reflector are quite strong and continuous in some inlines, it was desired to remove as much as possible, but it turned out to be challenging. The fact that the seafloor reflector are present indicates that the 4D seismic also contains other

signals that does not originate due to actual changes produced by fluid flow. A theory could be that the seafloor reflector are present due to time-shifts between the different surveys, and if these time-shifts where to be completely removed by processing, other signals may become more evident.

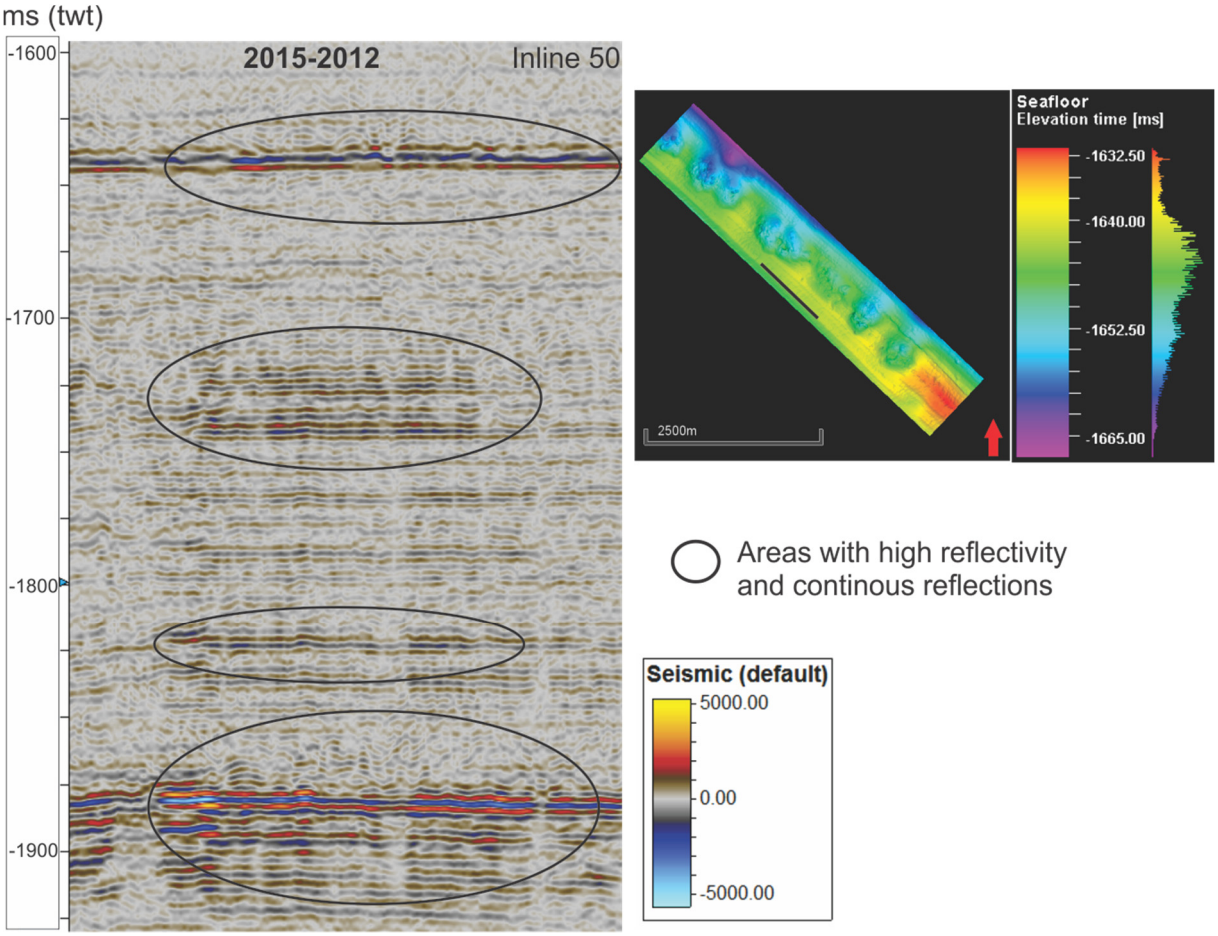

Figure 52 seismic inline 50, final difference 2015-2012, and areas with high reflectivity and continuous reflections are highlighter inside black circles.

Most of the residual 4D signals are within and around the chimney conduits and beneath the BSR. Though there are also signals left in areas expected to be static, like the stratified layers around the chimneys. The chimney conduits are the most complex geological features within the 3D survey area. It is natural to expect a 4D result with the most anomalously high amplitudes along the chimney conduits, both because these are areas that are difficult to compare in the processing flow and because we know that gas are flowing through these systems.

There are several pockmarks present on the seafloor. This makes the seafloor reflector complex as the pockmarks are the termination of the fluid flow. This can be a contributor to the fact that the seafloor reflector are present to some extent in the 4D result. It could be inferred that the architecture of the pockmarks have changed during the short time between each repeat, making it difficult to match the surveys in these zones. Though the rate of pockmark formation is not well understood.

For repeat 2, the process that caused the largest increase in the data repeatability was the phase- and time-shift process. The phases were initially well matched in repeat 2, but with a bulk time-shift of 3.75 ms applied in this process resulted in a significant reduction of amplitudes. While for repeat 1, there was significant differences in phase initially, and the phase- and time-shifts in this process did not manage to correct for this, hence the large amplitude difference left here (Figure 29). It might have been advantages to run a second phase-match on repeat 1.

For repeat 1, the process that caused the largest increase in the data repeatability was the shaping filter. The shaping filter process managed to remove a lot of the amplitudes in repeat 1, while repeat 2 remained unchanged (Figure 32). This indicates that the filter applied on repeat 1 managed to correct for the phase-time-differences that was still present after the phase- and time-shift.

The two repeat surveys reacted differently to the different processes applied, this shows that there are several approaches to obtain a repeatable result.

Figure 53 shows a comparison of repeat 2 before and after processing, from the figure we can see that a significant amount of amplitudes have been processed away. Despite all the uncertainties regarding the 4D result, as discussed above, this gives a visual impression of the reliability of the 4D data. In the processed repeat almost all of the stratified layers, the seafloor and to some extend the BSR have been removed and most of the residual signals are inside and around the chimney conduits.

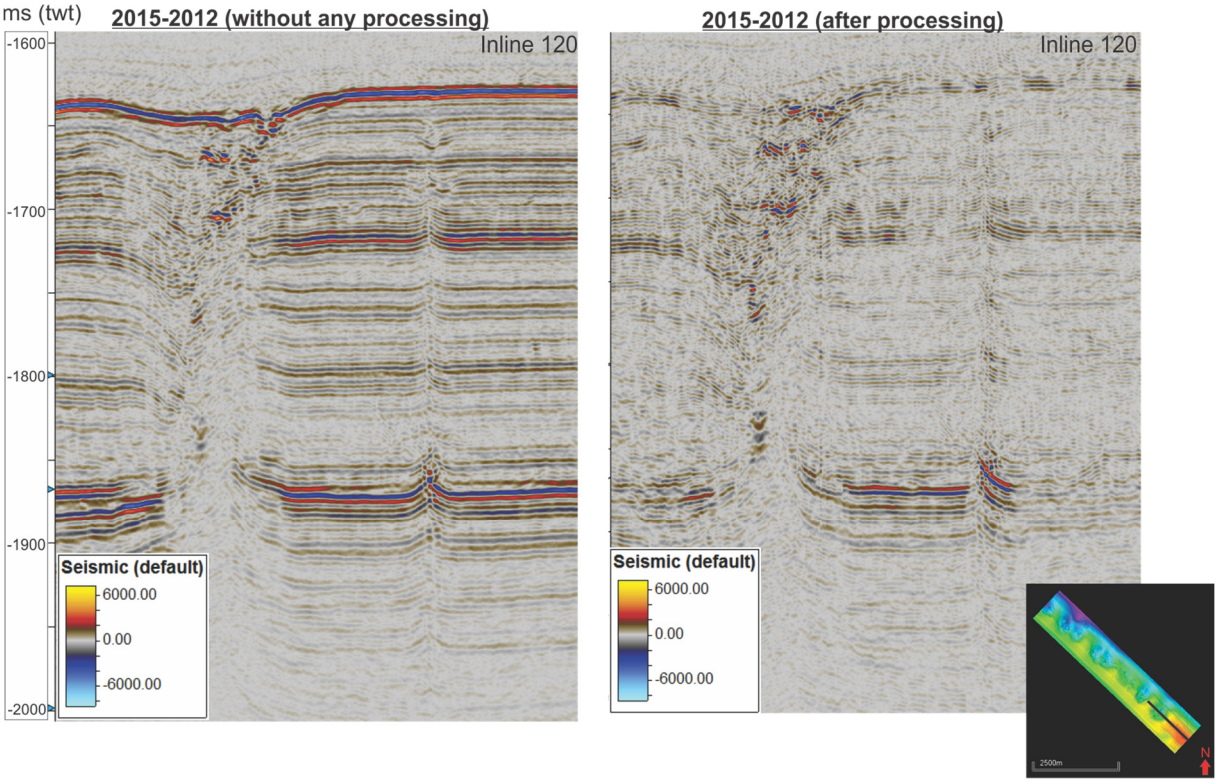

Figure 53 Difference in seismic response on the difference 2015 -2012, inline 120, before and after processing was conducted on the 2015 survey.

To end the discussion regarding the processing of the 4D data, and to some degree the reliability of it, it is important to state that most seismic lines within the 4D data appear reliable to a certain degree in the way that the seafloor reflector and the stratified layers have been drastically reduced in amplitude, while the reflections originating from the chimneys and the BSR bright up in some areas. The zones of the BSR and the chimney conduits also proved to be particularly challenging to match in the 4D processing, so not all changes must be considered as actual 4D responses.

5.2 Discussion of the 4D interpretation

Only a few percentage of gas saturation in the sediment pore spaces will cause a drastically reduction in compressional wave velocity (Andreassen, 2009). The most significant change in compressional wave velocity are found with gas concentrations up to 4% (Figure 54), after this point an increase in concentration will not add to further reduce the V_P significantly. This infers that if gas already has accumulated within a sedimentary sequence, further accumulation will not yield major changes in the seismic response, unless the extent and thickness of the gas charged sediments have changed. There are several bright spots detected on the 4D data and several of these bright up further from repeat 1 to repeat 2 (Figure 45, Figure 48, Figure 49), whether these are solely due to actual fluid induced changes caused by further accumulation of gas or influenced by noise present in the data is uncertain, especially since the areas that bright up the most, right beneath the seafloor reflector and beneath the BSR, proved to be particularly challenging to match in the 4D processing.

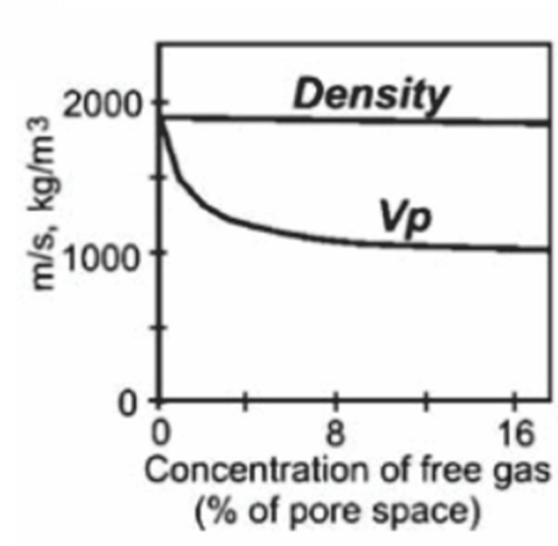

Figure 54 Velocity and bulk density as a function of gas saturation. The curves are calculated for sediments with porosity of 0.4 and a compressional wave velocity of 1900 m/s, using equation from (Gregory 1977) and assuming a uniform distribution of gas in the sediments. Modified from (Andreassen et al. 2007).

Cruises during 2006 and 2007 did not detect any gas seepage from the crest of the Vestnesa Ridge, the first discovery of active seepage out of one of the pockmarks was made in 2008. In 2010 gas flares out of three of the pockmarks on the eastern segment of the ridge were imaged by use of single-beam echo sounding (Bunz et al., 2012). Smith et al. (2014a) show that the

hydroacoustic response of gas flares in the water column above the pockmarks varies during two surveys in 2010 and 2012 (Figure 14). This indicates that the seepage activity can increase or decrease over short periods time, either during a 3-day 3D seismic survey over the chimneys or in between multiple years.

High amplitude anomalies in the easternmost active gas chimney stack and align vertically, cutting across disrupted strata and terminating in small depressions at the seafloor. The small seafloor depressions are the locations of gas seepage at the seafloor. Hence, it is most likely that the amplitude anomalies are related to the presence of gas and indicate the pathway of gas within the upper part of the chimney. Other potential causes for the amplitude anomalies, i.e. gas hydrates and/or carbonates seem less conceivable. The alignment of amplitude anomalies points towards a migration pathway through a specific self-enhanced and complex fracture system favoring a hydraulic system driven by overpressure (Cartwright et al., 2007; Hustoft et al., 2007). Deviation of the pathways might be simply due to overburden stress but might also result from hydrate formation clogging the fracture network (Liu et al., 2007; Smith et al., 2014). Any major changes in the architecture of the chimney have not been observed.

In an actively leaking system, changes might be expected along the migration pathways. Such changes are indicated in the 4D seismic data. However, due to the relatively poor repeatability metrics inside the chimney structures, the confidence in the observed time-lapse changes is still low. It may suggest that the time span between the base and repeat surveys are too short to detect possible changes. Fluid flow features and their rate of development are not well understood, so it is difficult to know how significant the changes can be over a relatively short period of time. As opposed to other 4D time-lapse application like CO2 storage monitoring, we do not know how much gas exists in the chimney and at what rates gas might migrate. This might become possible by tracking the amplitude anomalies over several years. Hence, several additional repeat surveys would be required.

The third chimney, from southeast (Figure 47), has not shown any signs of being active during previous studies on the eastern segment of the Vestnesa ridge (Bunz et al., 2012; Smith et al., 2014a), still, there are a lot of amplitude anomalies present in the 4D data. However, amplitude anomalies within this chimney conduit do not exhibit the same pattern as for the easternmost chimney structure where they are stacked and vertically aligned. Within this third chimney the amplitudes are more chaotically distributed and no amplitude anomalies are detected right beneath the seafloor reflector. The bright amplitudes detected within the chimney conduit might

indicate that changes are occurring in the subsurface due to fluid flow, but that the gas has not reached the seafloor yet. However, amplitude anomalies in both repeats of this chimney are much more similar (Figure 46) compared to both repeat surveys for the active, easternmost chimney (Figure 45). This might suggest that gas migration is reduced or absent at present, supporting the interpretation based on hydro-acoustic data that this chimney is inactive (Smith et al., 2014). Nonetheless, one has again to underline that amplitude anomalies might also be due to difficulties in matching this area in the 4D processing. It is evident that the two repeats on Figure 47 contain a lot of noise when comparing it to the initial state of the 2013 survey. This makes it difficult to interpret the amplitudes as true 4D response.

Gas hydrates ability to reduce the permeability of sediments often lead to accumulation of free gas beneath hydrate bearing sediments (Nimblett and Ruppel, 2003). Enhanced reflections directly below BSR`s are common features related to gas hydrate provinces, and strong reflections of this kind have been interpreted to represent free gas beneath sealing gas hydrates (Shipley et al., 1979; Bouriak et al., 2000; Vanneste et al., 2001). Figure 49 displays a seismic section on the northeast margin of the 3D survey area, the seafloor reflector and stratigraphic boundaries have been drastically reduced, indicating that the 4D processing worked well in that area. Yet, the time-lapse seismic contains a lot of anomalously high amplitudes beneath the interpreted BSR at around -1900 ms (twt) (Figure 49,Figure 50) and this could be due to a change in gas accumulation beneath the BSR over the 3 year time-span. The 4D changes in amplitudes are significant such that there is more confident that these changes actually resemble real changes in fluid content in the subsurface in this area. Fluid migration and gas generation is an ongoing process in this area (Plaza-Faverola et al., 2015; Dumke et al., 2016) and it is conceivable that more gas has been accumulated and trapped beneath sealing hydrate-bearing sediments above.

6 Conclusion

Active seepage of gas occurs on the Vestnesa Ridge on the western Svalbard margin. Gas seeps from pockmarks and underlying chimney structures that connect at least as deep as the free-gas zone beneath hydrate-bearing sediments. Three P-Cable 3D seismic data sets have been acquired over this area in 2012, 2013 and 2015 and are used in this thesis for developing time-lapse seismic studies of natural, focused fluid flow systems.

The feasibility of high-resolution 3D seismic data with high frequency content of up to 350 Hz for 4D time-lapse studies has not yet been established. In this thesis, a 4D processing workflow is developed in order to match the seismic data from the three aforementioned surveys. The 4D processing steps included re-binning of geometry, time- and phase-matching, shaping filter, shallow static correction and time-variant shifts.

The mean NRMS value of the final 4D data is not as low as would be desirable compared to conventional 3D seismic data. The NRMS values for both repeats changed drastically from start to end of the processing workflow, while the predictability measurement only changed minimal. Predictability is more sensitive to noise and distortions than to time-shift, so the fact that the predictability only changed minimal is believed to be due to high amounts of noise in the data, and that this noise is also pushing the NRMS towards a higher value. By running an initial quality check on the three surveys it appear as the reference volume, 2012 survey, is the main reason for the residual noise in the repeats.

The results achieved with regards of mean NRMS is 0.718 for repeat 1 and 0.894 for repeat 2, while the mean predictability measure values of 0.788 for repeat 1 and 0.707 for repeat 2. The biggest improvement with regards of NRMS value for repeat 1 was seen during the shaping filter process, the reason for this is likely that the filter added on the monitor managed to correct for the difference in phase on this repeat as it had significant differences to start with. Repeat 2 had the most improvements with regards of NRMS during the phase- and time-shift. This repeat only had a small difference in phase, but a mean time shift higher than 3 ms initially. The time-shift applied with a bulk shift of 3.75 ms managed to increase the repeatability of this repeat significantly.

The poorest NRMS values of up to 1.5 are observed over the areas of the gas chimneys, while outside of these structures the NRMS measures lower than 0.4 showing very good repeatability. The 4D processing is less confident where a chimney is present because chimneys represent

very inhomogeneous structures where seismic energy rapidly attenuates or is scattered away, which manifests itself in poorer repeatability measures.

High resolution P-Cable seismic data can be used for time-lapse studies if the effort made during acquisition and principal 3D processing is done with 4D in mind. Such that the ground for comparison between each repeat is good before a 4D processing workflow can be conducted. Some non-fluid related changes must be expected in the final 4D result, but these changes should be quite easy to extract from the actual fluid related changes and a confident 4D interpretation can be achieved.

The time-lapse seismic data from 2012 to 2013 and from 2013 to 2015 indicate a brightening and/or localized change of amplitudes in the subsurface. The most evident brightening occurs in a zone beneath the BSR away from chimney structures where the 4D attributes indicate good repeatability. This brightening might be due to increased accumulation of gas beneath hydrate-bearing sediments. 4D changes are also occurring inside an active chimney where a clear gas migration pathway could be mapped out. However, due to poorer repeatability metrics in the area of the chimneys, it is difficult to conclude whether these time-lapse amplitude anomalies are due to actual fluid induced 4D responses or affected by noise. In contrary, 4D interpretation of an inactive chimney shows clearly fewer time-lapse changes indicating that gas migration is currently reduced or absent in this specific structure.

The time-span of 3 years, from 2012 to 2015, might prove to be too short to detect any major structural changes in the architecture of the chimney conduits.

7 Recommendation for further work

- A 3D processing using the same phase-convention for the all the three surveys should be conducted. The 2012 and 2015 surveys have the same convention, but the seafloor reflector, which is a hard event, have negative amplitude values, while the 2013 survey have positive amplitude values along the seafloor. It is difficult to detect weather this has been fully corrected for during the 4D processing.
- Acquisition striping effects should be removed prior to 4D processing, especially crucial in the base survey.
- The 2012 survey contains much more noise and in general more energy than the 2013 and 2015 surveys, removal of noise should be considered on the 2012 survey before using it as a reference volume for a 4D processing workflow. The main driver behind 4D processing is to make the monitors similar to the base, so that the 4D responses become evident, it is therefore crucial that the base is properly processed and reliable for this usage.
- After these corrections have been done a new 4D processing workflow can be conducted on the three surveys and a more reliable and confident result can be obtained.

8 References

Ambrose, W. G., G. Panieri, A., Plaza, A. Schneider, M. L. Carrol, and E. K. L. Åstrøm. 2015. "Bivalve shell horizons in the seafloor pockmarks of the last glacial-interglacial transition suggest a 1000 years of methane emissions in the Arctic Ocean." *Geochemistry. Geophysics. Geosystems.*

Andreassen, K. 2009. "Lecture notes for Geo-3123." In *Marine Geophysics*, 81-100. Tromsø: University of Tromsø.

Andreassen, K., E. Glad Nilsen, and C. Ødegard. 2007. "Analysis of shallow gas and fluid migration within the plio-pleistocene sedimentary sucession of the SW Barents Sea using 3D-seismic data." *Geo-Marine letters, 27* 155-171.

Arts, R., A. Chadwick, O. Eiken, S. Thibeau, and S. Nooner. 2008. "Ten years experience of monitoring CO2 injection in the Utsira Sand at Sleipner, offshore Norway." 68.

Berg, R. R. 1975. "Capillary pressure in stratigraphic traps." *Am. Assoc. Pet. Geol. Bull. 59* 939-956.

Berndt, Christian. 2005. "Focused fluid flow in passive continental margins."

Bertoni, C., and J.A. Cartwright. 2005. "3D seismic analysis of circular evaporite dissolution structures." *Eastern Mediterranean. J Geol. Soc. 162* 909-926.

Boetius, A., K. Ravenschlag, C. J. Schubert, D. Rickert, F. Widdel, A. Gieseke, R. Amann, B. B. Jørgensen, and U., Pfannkuche, O. Witte. 2000. "A marine microbial consortium apparently mediating anaerobic oxidation of methane." *Letters to nature 407* 623-626.

Bouriak, S., M. Vanneste, and A. Saoutkine. 2000. "inferred gas hydrates and clay diapirs near the Storegga slide on the southern edge of the Vøring plateau, offshore Norway." *Marine Geology, 163* 125-148.

Bryant, W. R., and L. B. Roemer. 1983. "Structure of the continental shelf and slope of the northern Gulf of Mexico and its geohazards and engineering constrains." In *CRC Handbook of Geophysical Exploration at Sea*, by R. A. Greyer and J. R. Moore, 123-184. Florida: CRC Press.

Bunz, Stefan, Sergey Polyanov, Sunil Vadakkepuliyambatta, Chiara Consolaro, and Jurgen Mienert. 2012. "Active gas venting through hydrate-bearing sediments on the Vestnesa Ridge, offshore W-Svalbard." 190-197.

Cartwright, J., M. Huuse, and A. Aplin. 2007. "Seal bypass systems." *Am. Assoc. Pet. Geol.* 1141-1166.

Cartwright, Joe, and Carlos Santamarina. 2015. *Seismic characteristics of fluid escape pipes in sedimentary basins: Implications for pipe genesis.* ELSEVIER.

Cathles, L.M., Zheng Su, and Duofu Chen. 2009. "The physics of gas chimney and pockmark formation, with implications for assessment of seafloor hazards and gas sequestration." *Marine and petroleum geology.*

CGGVeritas. 2008. "Time lapse seismic." 1-15.

Chadwick, R.A, D Noy, R Arts, and O. Eiken. 2009. "Lates time-lapse seismic data from Sleipner yield new insights into CO2 plume development."

Consolaro, C., T. L. Rasmussen, G. Panieri, J. Mienert, S. Bunz, and K. Sztybor. 2015. "Carbon isotope excursion suggest times of major methane release during the last 14 kyr in Fram Strait, The deep-water gateway to the Arctic." *Climate of the past* 669-685.

Cosgrove, J. 2001. "Hydraulic fracturing during the formation and deformation of a basin: a factor in the dewatering of low-permabillity sediments." *Am. Assoc. Pet. Geol. Bull. 85* 737-748.

Davies, R. J., and A. L. Clarke. 2010. "Methane recycling between hydrates and critically pressured stratigraphic traps, offshore Mauretania." *Geology 38* 963-966.

Dumke, I., E. B. Burwicz, C. Berndt, D. Klaeschen, T. Feseker, W. H. Geissler, and S. Sarkar. 2016. "Gas hydrate distribution and hydrocarbon maturation north of the Knipovich Ridge, western Svalbard margin." *J. Geophysics. Res. Solid Earth, 121* 1405-1424.

Eiken, Ola, and Karl Hinz. 1993. "Contourites in the Fram Strait." *Sedimentary Geology* 15-32.

Eriksrud, Morten. 2014. *Seabed permanent reservoir monitoring (PRM) -A valid 4D seismic technology for fields in the Nort Sea.* EAGE, 67-73.

Ferrè, B., J. Mienert, and T. Feseker. 2012. "Ocean temperature variabillity for the past 60 years on the Norwegian-Svalbard margin influences gas hydrate stability on human time scales." *J. Geophys. Res., 117.*

Flemmings, P. B., X. Liu, and W. J. Winters. 2003. "Critical pressure and multiphase flow in Blake Ridge gas hydrates." *Geology 31* 1057-1060 .

Gregory, A. R. 1977. "Fluid saturation effects on dynamic properties of sedimentary rocks." *Geophysics 41* 895-921.

Greinert, J., K.B. Lewis, J. Bialas, I.A. Pecher, A. Rowden, D.A. Bowden, M. De Batist, and P. Linke. 2010. "Methane seepage along the Hikurangi Margin, New Zealand: Overview of studies in 2006 and 2007 and new evidence from visual, bathymetric and hydroacoustic investigations." *Marine Geology 272* 6-25.

Hart, B. S., P. Flemings, and A. Deshpande. 1995. "porosity and pressure: role of compaction disequilibrium in the development of geopressure in a Gulf Coast Pleistocene basin." *Geology* 45-48.

Heggeland, R. 1998. "Gas seepage as an indicator of deeper prospective reservoirs. A study based on exploration 3D seismic data." *Marine and Petroleum Geology 15* 73-102.

Helal, A. E-N., A. M. S. Lala, A. S. S. Ahmed, and A. T. M. Mohamed. 2015. "The impact of gas chimneys on the reservoir characteristics, offshore Nile Delta, Egypt." *Arab J Geosci.*

Holbrook, W. S., H. Hoskins, W. T. Wood, R. A. Stephen, and D. Lizarralde. 1996. "Methane hydrate and free gas on the Blake Ridge from vertical seismic profiling." *Science 273* 1840-1843.

Hovland, M., and A. G. Judd. 1988. "Seabed pockmarks and seepages-impacts on geology, biology and the marine environment." *Marine and petroleum Geology.*

Hovland, M., and A. Judd. 2007. "Seabed fluid flow." *Cambridge university press* 475.

Hovland, Martin. 2005. "Gas Hydrates." In *Petroleum Geology*, 261-268. Stavagner, Norway: Elsevier Ltd.

Howe, J. A., T. M. Shimmield, R. Harland, and N. Eyles. 2008. "Late Quaternary contourites and glaciomarine sedimentation in the Fram strait." *Sedimentology* 179-200.

Hustoft, S., B. Dugan, and J. Mienert. 2009. "Effects of rapid sedimentation on developing the Nyegga pockmark field: constrains from hydrological modeling and 3D-seismic data, offshore mid-Norway." *Geochem. Geophys. Geosyst. 10.*

Hustoft, S., J. Mienert, S. Bunz, and H. Nouze. 2007. "High-resolution 3D-seismic data indicate focused fluid migration pathways above polygonal fault systems of the mid-Norway margin." *Mar. Geol. 245* 89-106.

Hustoft, S., S. Bunz, and J. Mienert. 2010. "Three-dimensional seismic analysis of the morphology and spatial distribution of chimneys beneath the Nyegga pock-mark field, offshore mid-Norway." *Basin Res.* 22, 564-480.

Hustoft, S., S. Bunz, J. Mienert, and S. Chand. 2009. "Gas hydrates reservoir and active methane-venting province in sediments on <20 Ma young oceanic crust in the Fram strait, offshore NW Svalbard ." *Earth planet Sci. Lett.* 248 (1-2), 12-24.

Huuse, M., C. A.- L. Jackson, P. V. Rensbergen, R. J. Davies, P. B. Flemings, and R. J. Dixon. 2010. "Subsurface sediment remobilization and fluid flow in sedimentary basins: an overview." *Basin Research.*

Hyndman, R. D., and G. D. Spence. 1992. "A seismic study of methane hydrate marine bottom simulating reflectors." *Journal of Geophysical research 97* 6683-6698.

Johnston, David H. 2013. *Practical Application of Time-lapse seismic Data .* Tulsa, USA : Society of Exploratin Geophysicists .

Kennicutt, M.C., J.M. Brooks, R.R. Bidigare, R.R. Fay, T.L. Wade, and T.J. McDonald. 1985. "Vent-type taxa in a hydrocarbon seep region on the Louisiana slope." *Nature 317* 351-353.

Knies, Jochen, Jens Matthiessen, Christoph Vogt, Jan Sverre Laberg, Berit O. Hjelstuen, Morten Smelror, Eiliv Larsen, Karin Andreassen, Tor Eidvin, and Tore O. Vorren. 2009. "The pli-pleistocene glaciation of the Barents Sea-Svalbard region: a new model based on revised chronostratigraphy." *Quaternary science reviews* 1-18.

Kunii, D., and O. Levenspiel. 1969. *Fluidisation Engineering.* Butterworth, London.

Kvenvolden, K. A., and T. D. Lorenson. 2000. "The global occurence of natural gas hydrates."

Leifer, I., B. P. Luyendyk, J. Boles, and J. F. Clark. 2006. "Natural marine seepage blowout: Contribution to atmospheric methane." *Global Biogeochemical Cycles.*

Liu, X., and P. B. Flemings. 2006. "Passing gas through the hydrate stability zone at Hydrate Ridge, offshore Oregon." *Earth Planet. Sci. Lett. 241* 211-226.

Lui, X., and P. B. Flemings. 2007. "Dynamic multiphase flow model of hydrate formation in marine sediments." *J. Geophys. Res. B Solid Earth 112.*

Løseth, H., L. Wensaas, B. Arntsen, N. Hanken, C. Basire, and K. Graue. 2011. "1000m long gas blow out pipes." *Mar. Pet. Geol.* 28, 1047-1060.

Løseth, H., L. Wensaas, B. Arntsen, N. Hanken, C. Basire, and K. Graue. 2001. "1000m long gas blow out pipes." *In. 63rd EAGE Conference and Exhibition, Extended Abstracts* p.524.

Løseth, H., M. Gading, and L. Wensaas. 2009. "Hydrocarbon leakage interpreted on seismic data." *Marine and Petroleum Geology .*

Magalhaes, Viktor H., Luis M. Pinheiro, Michael K. Ivanob, Elena Kozlova, Valentina Blinova, J. Kolganova, Crisogono Vasconcelos, et al. 2012. "Formation processes of methane-derived authigenic carbonates from the Gulf of Cadiz." *Sedimentary geology* 155-168.

McCallum, M. E. 1985. "Experimental evidence for fluidization processes in breccia pipe formation." *Econ. Geol. 80* 1523-1543.

McDonnel, A., R. G. Loucks, and T. Dooley. 2007. "Quantifying the origin ang geometry of circular sag structures in northern Fort Worth Basin, Texas: paleocave collapse, pull-apart fault systems, or hydrothermal alteration?" *Am. Assoc. Pet. Geol. Bull. 91* 1295-1318.

Moss, J. L., and J. Cartwright. 2010. "3D seismic expression of Km-scale fluid escape pipes from offshore Namibia." *Basin Res.* 22, 481-502.

Nermoen, A., O. Galland, E. Jettestuen, K. Fristad, Y. Podlachikov, H. Svensen, and A. Malthe-Sorensen. 2010. "Experimental and analytical modeling of piercement structures." *J. Geophys. Res. 115, B10202.*

Nimblett, J., and C. Ruppel. 2003. "Permeabillity evolution during the formation of gas hydrates in marine sediments." *Journal of Geophysical Research, solid Earth, 108.*

O'Brien, G.W., G.M. Lawrence, A.K. Williams, K. Glenn, A.G. Barrett, M. Lech, D.S. Edwards, and R. Cowley. 2005. "Yampi Shelf, Browse Basin, North-West Shelf, Australia: a test-bed for constraining hydrocarbon migration and seepage rates using combinations of 2D and 3D seismic data and multiple, independent remote sensing technologies." *Marine and Petroleum Geology 22* 517-549.

Oghenekohwo, Felix, and Felix Herrmann. 2013. "Assesing the need for repeatability in aquisition of time-lapse data." 1-5.

Panieri, G., R. H. James, A. Camerlenghi, G. K. Westbrooks, C. Consolaro, I. Cacho, V. Cesari, and C. S. Cervera. 2014. "Record of metahen emissions from the West Svalbard continental margin during the last 23.5 Ka revealed by δ^13C of benthonic foraminifera." *Global Planet. Change, 122* 151-160.

Petersen, Carl Jörg, Stefan Büenz, Steinar Hustoft, Jürgen Mienert, and Dirk Klaeschen. 2010. "High-resolution P-cable 3D seismic imaging of gas chimney structures in gas hydrates sediments of an Arctic sediment drift."

Plaza-Faverola, A, S Buenz, J.E Johnson, S Chand, J Knies, J Mienert, and P Franek. 2015. "Role of tectonic stress in seepage evolution along the gas hydrate-charged Vestnesa Ridge, Fram Strait ." 733-742.

Plaza-Faverola, A., Bunz, S., and J. Mienert. 2011. "Repeated fluid expulsion through sub-seabed chimneys offshore Norway in respone to glacial cycles." *Earth planet. Sci. Lett.* 297-308.

Plaza-Faverola, A., S. Bunz, and J. Mienert. 2010. "Fluid distribution inferred from p-wave velocity and reflection seismic amplitude anomalies beneath the Nyegga pockmark field on the mid-Norwegian margin. ." *Mar. Pet. Geol. 27* 46-60.

Prince, P. K. 1990. "Current drilling practice and the occurence of shallow gas." In *Safety in offshore drilling*, by D. A. Ardus and C. D. Green, 3-25. Dordrecht: Kluwer Academic Publisher.

Qiliang, S., J. Cartwright, S. Wu, and D. Chen. 2013. "3D seismic interpretation of dissolution pipes in the south China Sea: genesis by subsurface, fluid induced collapse." *Mar. Geol. 337* 171-181.

Qiliang, S., S. Cartwright, and D. Chen. 2013. "3D seismic interpretation of dissolution pipes in the South China Sea: genesis by subsurface, fluid induced collapse." *Mar. Geol. 337* 171-181.

Reilly, M., and P. Flemings. 2010. "Deep pore pressure and sefloor venting in the Auger Basin, Gulf of Mexico." *Basin Res.*

Ruppel, Carolyn D. 2011. *Methane Hydrates and Contemporary Climate Change.* Nature education Knowledge .

Sarkar, S., C. Berndt, D. Chabert, D. G. Masson, T. A. Minshull, and K. G. Westbrook. 2011. "Switching of a paleo-ice stream in northwest Svalbard." *Quat. Sci. Rev.* 30(13), 1710-1725.

Shipley, T. H., R. T. Houston, F. J. Buffler, K. J. Shaub, K. J. McMillen, J. W. Ladd, and J. L. Worzel. 1979. "Seismic evidence for widespread possible gas hydrate horizons on continental slopes and rises. ." *AAPG Bull.; Vol. 63* 2204-2213.

Showalter, T. T. 1979. "Mechanisms of secondary hydrocarbon migration and entrapment. ." *Am. Assoc. Pet. geol. Bull. 63* 723-760.

Smith, A. J., J. Mienert, Bünz. S., and J. Greinert. 2014a. "Thermogenic methane injection via bubble transport into the upper Arctic Ocean from the hydrate-charged Vestnesa Ridge, Svalbard." *Geochemistry, Geophysics, Geosystems.*

Smith, Andrew J., Peter B. Flemings, Xiaoli Liu, and Kristopher Darnell. 2014b. "The evolution of methane vents that pierce the hydrate stability zone in the world`s oceans." *Journal of Geophysics research: Solid Earth.*

System, Hampson-Russel Help. 2014. *Time Lapse Analysis Concepts.*

Tjelta, T.I., G. Svanø, J.M. Strout, C.F. Forsberg, H. Johansen, and S. Planke. 2007. "Shallow Gas and its Mulitple Impact on a North Sea Production Platform." *6th International Offshore Site Investigation and Geotechnics Conference: Confronting New Challenges and Sharing Knowledge.* London: Society for Underwater Technology.

Vadakkepuliyambatta, S. 2014. "Sub-seabed fluid-flow systems and gas hydrates of the SW Barents Sea and North Sea margins." 1-21.

Vadakkepuliyambatta, S., S. Buenz, J. Mienert, and S. Chand. 2013. "Distribution of subsurface fluid-flow systems in the SW Barents Sea." *Marine and Petroleum Geology.*

Van Rensbergen, P., A. Rabaute, A. Colpaert, T. S. Ghislain, M. Mathijs, and A. Bruggeman. 2007. "Fluid migration and fluid seepage in the Connemara field, porcupine basin interpreted from industrial 3D seismic and well data combined with hig-resolution site survey data." *Int. J. Earth Sci.* 96, 185-197.

Vanneste, M., M. De Batis, A. Golmshtok, A. Kremlev, and W. Versteeg. 2001. "Multi-frequency seismic study of gas hydrate-bearing sediments in Lake Baikal, Siberia." *Marine Geology, 172* 1-21.

Vogt, P. R., K. Crane, Sundvor. E., Max. M. D., and S. L. Pfirman. 1994. "Methane-generated (?) pockmarks on young, thickly sedimented oceanic crust in the Arctic Vestnesa ridge, Fram Strait." *Geology, 22(3)* 255-258.

Watts, N. L. 1987. "Theoretical aspects of cap-rock and fault seals for single- and two-phase hydrocarbon columns." *Mar. Pet. Geol. 4* 274-307.

Widess, M. B. 1973. "How thin is a thin bed? ." *Geophysics, 38* 1176-1180.